Exploring the metabolism of the signaling lipid lysophosphatidylserine in mammalian physiology and developing LC-MS-based lipidomics platforms

विद्या वाचस्पति की
उपाधि की अपेक्षाओं की आंशिक पूर्ति में प्रस्तुत शोध प्रबंध

A thesis submitted in partial fulfillment of the requirements of the degree of Doctor of Philosophy

द्वारा / By
अर्नब चक्रवर्ती / Arnab Chakraborty

पंजीकरण सं. / Registration No.: २०१९३६३८/ 20193638

शोध प्रबंध पर्यवेक्षक / Thesis Supervisor:
डॉ. सिद्धेश एस कामत/ Dr. Siddhesh S Kamat

भारतीय विज्ञान शिक्षा एवं अनुसंधान संस्थान पुणे
INDIAN INSTITUTE OF SCIENCE EDUCATION AND RESEARCH PUNE

2025

To

Ma and Baba, who have made me capable of this today…

Declaration by Student

Name of Student: **Arnab Chakraborty**

Reg. No.: 20193638

Thesis Supervisor(s): **Dr. Siddhesh S Kamat**

Department: Biology

Date of joining program: **1st August 2019**

Date of Pre-Synopsis Seminar: **29 Jan 2025**

Title of Thesis: **Exploring the metabolism of the signaling lipid lysophosphatidylserine in mammalian physiology and developing LC-MS-based lipidomics platforms**

I declare that this written submission represents my idea in my own words and where others' ideas have been included; I have adequately cited and referenced the original sources. I declare that I have acknowledged collaborative work and discussions wherever such work has been included. I also declare that I have adhered to all principles of academic honesty and integrity and have not misrepresented or fabricated or falsified any idea/data/fact/source in my submission. I understand that violation of the above will be cause for disciplinary action by the Institute and can also evoke penal action from the sources which have thus not been properly cited or from whom proper permission has not been taken when needed.

The work reported in this thesis is the original work done by me under the guidance of
Dr. Siddhesh S Kamat
Date: 02 Apr 2025

Signature of the student

Certificate

Certified that the work incorporated in the thesis entitled ("Exploring the metabolism of the signaling lipid lysophosphatidylserine in mammalian physiology and developing LC-MS-based lipidomics platforms") submitted by Arnab Chakraborty was carried out by the candidate under my supervision. The work presented here or any part of it has not been included in any other thesis submitted previously for the award of any degree or diploma from any other University or institution.

Date: 2nd April 2025

Dr Siddhesh S Kamat

Supervisor
IISER Pune

Acknowledgments

I am deeply indebted to those who have provided invaluable support and guidance throughout the course of my research and the completion of this thesis.

First and foremost, I would like to express my deepest gratitude to my supervisor, **Dr. Siddhesh Kamat**, for his invaluable guidance, constant support, and encouragement throughout my PhD journey. His experience, patience, and knowledge regarding the field have been a great source of inspiration.

I sincerely thank my research advisory committee members, **Dr. Thomas Pucadyil, Dr. Girish Ratnaparkhi, and Dr. Sunil Laxman**, for their insightful feedback, constructive criticism, and unwavering support that greatly enriched my research work.

I am deeply grateful to **IISER Pune** and the **Department of Biology** for providing an excellent research environment and the necessary facilities that enabled me to complete my PhD. I would also like to thank **KVPY** (undergraduate fellowship)**, CSIR** (PhD fellowship), and **Infosys** (travel grant) for their financial support during this research journey.

To Ma (**Suchandra Chakraborty**) and Baba (**Col Soumyabrata Chakraborty**) – All my achievements will always be a testament to your parenting, and my gratitude cannot be explained in words. Thank you for everything.

My heartfelt thanks to my collaborators and co-authors: **Archit, Prajwal, Theja, Kundan, Arshdeep, Rohith, Yogita, Rashmi, Atanu, Vaishnavi, Sudipta, Shambhavi, Simran, Dr. Ullas Kolthur, Dr. Vinay Nandicoori, Dr. Rajesh Gokhale, Dr. Chandrima Das, Dr. Rajan Sankaranarayan, Dr. Harinath Chakrapani, and Dr. Sheetal Gandotra**, whose contributions and insights have been invaluable to my research.

To my family—**Dadun, Didun, Dadu, Ammu, Ma, Baba, Mamun, Mimi, Jethu, Mammam, Dada, Arjun, and Rik**—I owe my deepest gratitude for their unconditional love, patience, and support. You have been my pillars of strength throughout this journey.

Special thanks to my fiancée, **Atreyi**, and her family for their endless love, understanding, and encouragement. Your unwavering support has been a constant source of motivation for me. You have helped me cherish the highs and navigate the lows of my Ph.D. journey.

I am incredibly grateful to my friends—**Kaveri, Aakash, Apurba, Uma, Sonali, and Neeraj**—for their constant companionship, encouragement, and all the fun times.

A big thank you to all my lab members, both past and present, for creating a collaborative and supportive work environment. Your camaraderie and support made the long hours in the lab enjoyable.

To my batchmates—**Subhradip, Mukundan, Shivani, Akhilesh, Gauri, and Akansha**—thank you for the wonderful memories, friendship, and support inside and outside the lab.

I would like to acknowledge my gaming friends—**Pradyun, Dhruv, Ajay, Srijan, Anirban, Aravind, Jeyadharan, Runit, Kunal, Kaushik, Yash, Salman, Tushar, Rohan, and Anubhav**—for the fun and laughter that provided much-needed breaks from the rigors of research.

A special mention goes to my mentors, both on and off the field, Dr. Krishanpal and Dr. Diganta, for their invaluable guidance, support, and advice, which have helped shape my personal and professional growth.

Lastly, I extend my gratitude to my sports teammates and opponents—**Pradyun, Adrian, Aswin, Projjwal da, Ashani, Deep, Dhruv, Aakash, Mayank, Yash, Varaprasad, Mukta, Daksh, Kautik**, and many others—for the spirit of teamwork and healthy competition that taught me resilience and perseverance.

Thank you all for believing in me and for being an integral part of this journey.

-Arnab Chakraborty

TABLE OF CONTENTS

LIST OF FIGURES AND TABLES

Thesis abstract:

Lysophosphatidylserine (lyso-PS) is an essential signaling lysophospholipid in mammals, and deregulation in its metabolism has been directly linked to an array of human autoimmune and neurological disorders such as PHARC (polyneuropathy, hearing loss, ataxia, retinitis pigmentosa, and cataract), an early onset autosomal recessive neurological disorder caused by deleterious mutations to the lyso-PS lipase ABHD12. Biochemically, ABHD12 catalyzes the hydrolysis of lyso-PS (lyso-PS lipase) and controls the concentrations and signaling pathways regulated by this potent signaling lysophospholipid in the mammalian brain. Since over 30 mutations in ABHD12 have been observed in human PHARC subjects and the biochemical activity of these pathogenic mutants remains unknown, we performed a bioinformatics study to identify functionally relevant conserved residues in the ABHD12 protein sequence that are likely important for its enzymatic activity. To validate these in silico findings, we generated numerous mutants of murine ABHD12, including those associated with human PHARC subjects, assayed them for their enzymatic activity, and performed the first thorough sequence-function relationship for mammalian ABHD12.

Since lyso-PS has been extensively studied in the context of autoimmune and neurological disorders, our knowledge of lyso-PS metabolism is almost exclusively limited to the immune and central nervous systems (CNS) despite lyso-PSs being almost ubiquitously present in every tissue. Since lyso-PS levels are tightly governed by a lyso-PS lipase in the nervous system (ABHD12), we profiled the lyso-PS lipase activity associated with different mammalian tissues. We found that most tissues could degrade lyso-PS by virtue of membrane-associated metabolic serine hydrolase (mSH) enzymes; however, ABHD12 only influences lyso-PS metabolism exclusively in the brain. To bridge this gap, we used a repertoire of mSH inhibitors to screen the lipase activity reduction of tissue membrane fractions and identified the mSH lipase ABHD6 as a potential lyso-PS lipase in the liver and kidneys. Using specific pharmacological inhibitors in cell lines and mice, we functionally annotate ABHD6 as a lyso-PS lipase in primary hepatocytes and mouse liver and kidneys. We also validated the lyso-PS lipase activity of ABHD6 using an overexpression system in mammalian cells. These findings expand our understanding of lyso-PS metabolism in mammalian physiology and open up ABHD6 as a target for lyso-PS-mediated processes in the liver and kidneys.

Lipids such as lyso-PS are challenging macromolecules to study because of a lack of techniques to quantify them in biological samples. While lipids are a diverse class with total species in the order of 10000s, their coverage in a typical LC-MS/MS experiment is around 2-5%, in contrast to 80-90% for other metabolites. In an effort to identify and quantify lipids in a variety of biological samples, we first used a modified folch method to extract lipids. Subsequently, we developed methods to perform untargeted and targeted lipid analysis on quadrupole-time of fight (Q-TOF) and triple quadrupole (Q-Q-Q) mass spectrometers, respectively. Our methods enabled relative and absolute quantification of lipid species such as fatty acyls, glycerophospholipids, glycerolipids, and saccharolipids in extracts from organisms ranging from mycobacteria, bacteria, zebrafish to human plasma. Our lipidomics analyses were instrumental in assigning novel functions to different proteins and for looking at the effects of various drug treatments.

Chapter 1: An Introduction to the signaling lipid Lysophosphatidylserine (Lyso-PS)

Chapter abstract:

Lysophosphatidylserine (lyso-PS) has emerged as yet another important signaling lysophospholipid in mammals, and deregulation in its metabolism has been directly linked to an array of human autoimmune and neurological disorders. It has an indispensable role in several biological processes in humans, and therefore, cellular concentrations of lyso-PS are tightly regulated to ensure optimal signaling and functioning in physiological settings. Given its biological importance, the past two decades have seen an explosion in the available literature toward our understanding of diverse aspects of lyso-PS metabolism and signaling and its association with human diseases. In this section, I will comprehensively cover the current state of knowledge about lyso-PS and discuss open questions in the field I tackled as part of this thesis.

INTRODUCTION

Signaling lipids act as critical hormone-like biomolecules that regulate many facets of mammalian physiology, and deregulation in their metabolism is often linked to serious pathophysiological consequences and diseases in humans[1–3]. Examples of such well-studied signaling lipids in the context of mammalian physiological processes and diseases are the prostaglandins[4], endocannabinoids[5], and lysophospholipids[6,7]. Sphingosine 1-phosphate (S1P)[8] and lysophosphatidic acid (LPA)[9] are classical examples, and perhaps the best characterized members amongst the different lysophospholipids. Of note, drugs targeting the metabolic enzymes and/or cognate receptors for both S1P and LPA are currently in clinical use or in different stages of clinical trials for impending use in human autoimmune and neurological disorders[7,8]. Over the past two decades, the lysophosphatidylserines (lyso-PSs)[10–12] have emerged as yet another signaling lysophospholipid with many important physiological functions, and causative associations to an array of neurological and autoimmune genetic diseases in humans.

In the 1950s, extensive efforts were made to identify biological factors that are involved in blood coagulation, and during this time, studies showed that a lipid-rich fraction from the porcine brain enriched with phosphatidylserine (PS) was found to modulate the anticoagulation properties of blood[13]. Upon further analysis of this lipid fraction, a degraded

form of PS, that we now know is lyso-PS, was in fact shown to facilitate this activity, and this is perhaps the first description of lyso-PS in literature[13]. Interestingly, around the same time, in an independent study, high-dose injection of PS into rabbits led to severe hemolysis and respiratory failure that caused mortality of these animals, leading to the hypothesis that an "unknown histamine-like contaminant" in PS led to this phenotype[14,15]. Even though at the time, the contaminant responsible for this pathological outcome was not identified, we now know that it was most likely lyso-PS, that causes mast cell degranulation and in turn histamine release to produce the aforementioned immunological effects. Despite the identification of lyso-PS during the late 1950s and early 1960s, little remained known in terms of this lysophospholipid's metabolism and biological activities until the past two decades.

The upcoming sub-sections cover literature on different aspects of lyso-PS in mammalian systems such as its chemical structure, metabolizing enzymes and its biological roles.

CHEMICAL STRUCTURE OF LYSO-PS

Lyso-PSs are a singly deacylated form of PS lipids and are, therefore, classified as a lysophospholipid or lysoglycerophospholipid[16,17]. Specifically, lyso-PS is a combination of three simple biological building blocks: (i) a sugar (glycerol backbone), (ii) an amino-acid (phospho-*L*-serine head group), and (iii) a fatty acid (lipid tail) (**Fig 1.1**)[11]. While the glycerol backbone and the lipid tail are common to most other lysophospholipids, it is the phospho-*L*-serine that forms a phosphoester bond with the *sn-3* hydroxyl of (*R*)-glycerol to form the glycerophosphoserine head group, that is unique to lyso-PS, and distinguishes it from all the other lysophospholipids. It is hypothesized that this intricate combination of hydrophilic (glycerol and phospho-*L*-serine) and lipophilic (fatty acid) building blocks give lyso-PS an overall amphiphilic property and makes them potent signaling lipids. The overall structure of lyso-PS also has two stereocenters: (i) carbon atom at the *sn-2* position of the (*R*)-glycerol backbone and (ii) α-carbon atom of the phospho-*L*-serine head group (**Fig 1.1**)[18].

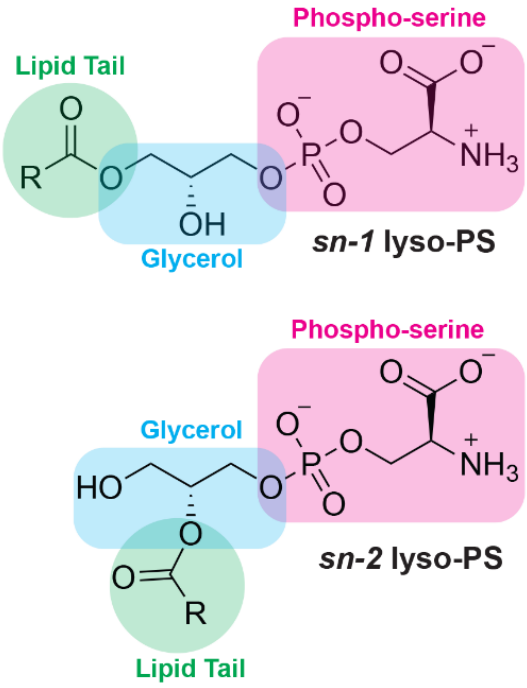

Fig 1.1 Structures of sn-1 and sn-2 lyso-PS.

The lipid tail (fatty acid) is attached to the glycerophosphoserine head group via an ester linkage, and depending on the site of esterification (*sn-1* or *sn-2* hydroxyl group), it can result in two forms of lyso-PS: (i) 1-(fatty acyl)-2-hydroxy-lyso-PS (*sn-1* lyso-PS); or (ii) 1-hydroxy-2-(fatty acyl)-lyso-PS (*sn-2* lyso-PS) (**Fig 1.1**). Of the two forms, at physiological pH (~ 7), only the *sn-1* lyso-PS is present, and the *sn-2* lyso-PS exists only at very low pH (< 4)[19], due to known spontaneous non-enzymatic acyl and/or phosphoryl-migration reactions that occur within lysophospholipids[20]. Hence, most of the biological studies done and/or described with lyso-PSs pertain almost exclusively to the *sn-1* lyso-PS form, given its predominance at physiological conditions of pH. Like most of the other lysophospholipids, within lyso-PSs, the glycerophosphoserine head group can be found esterified with a diverse range of lipid tails that span medium chain (C10 – C14), long chain (C16 – 20), and very long chain (C22 – C24) fatty acids, also possible with varying degrees of unsaturation (e.g. C18:1, C18:2, C20:4, C22:6). Short-chain fatty acid variants have not been reported for lyso-PSs yet. In most mammalian biological systems, the long-chain lyso-PS species are found to be the most abundant, with C18:0 and C18:1 being the highest in concentrations amongst them. Though it is not fully clear why nature chose to have many fatty acyl-variants of lyso-PSs, some possible individual roles for these fatty acyl-variants lyso-PS are only becoming apparent over the past couple of years.

DETECTION AND BIODISTRIBUTION OF LYSO-PS

Given its potency as a signaling lysophospholipid in mammalian systems, physiologically, lyso-PS is present at very low concentrations and, therefore, has been challenging to detect and quantify over the years. However, with the technological advances in liquid chromatography and mass spectrometry (LCMS) techniques, a few robust protocols have emerged, enabling reliable detection and quantification of lyso-PSs in different biological systems. In this section, we will summarize these different LCMS-based detection techniques for quantifying lyso-PSs in mammalian systems and discuss the distribution of this signaling lipid in various mammalian tissues and cells.

Methods for detecting lyso-PS

The advent of mass spectrometry-based LCMS technologies and their emerging applications in high-throughput measurements of small molecules in biological systems (e.g. lipidomics)[21–23], has greatly facilitated the detection and quantification of poorly abundant signaling lipids, including lyso-PS. This ability to detect and assess the physiological concentrations of the signaling lipids such as lyso-PS has tremendously advanced our understanding of the potential mechanisms by which these important biomolecules signal in different mammalian tissues and cells. The overall process of detecting and quantifying lyso-PS in biological systems has two major components. i.e., (a) the extraction (or enrichment) and chromatographic separation of lyso-PS from biological systems; (b) the downstream LCMS data acquisition and analysis (**Fig 1.2**).

The initial step in the enrichment of lyso-PSs from mammalian systems (e.g. tissues, cells, plasma/serum) is the organic extraction of the lipidome. Two established protocols have been reported for the enrichment of lyso-PSs from mammalian systems. The first method, which is also the more widely used method for lyso-PS extraction, is a modified version of the Folch extraction protocol for enriching lipids from biological systems[24]. Here, lipids from biological systems are extracted using a mixture of chloroform and methanol, with an additional extraction step that involves the acidification of the residual aqueous layer after a first organic solvent extraction (using chloroform-methanol), for enhancing the enrichment of phospholipids and lysophospholipids in the lipidome[25,26]. The eventual lipidomic extracts from this method are typically resolved on an octadecyl-carbon chain bonded silica matrix (C18) column using reversed-phase chromatography techniques for better separation and detection of lyso-PSs. The second method for lyso-PS enrichment is a polar metabolite (e.g.

lysophospholipid) enrichment strategy that involves the precipitation of proteins and debris from tissues/cells using acetonitrile as an organic solvent. The metabolite extracts from this method are typically further resolved using the hydrophilic interaction liquid chromatography (HILIC) via a normal phase separation strategy for better lyso-PS separation and detection[27].

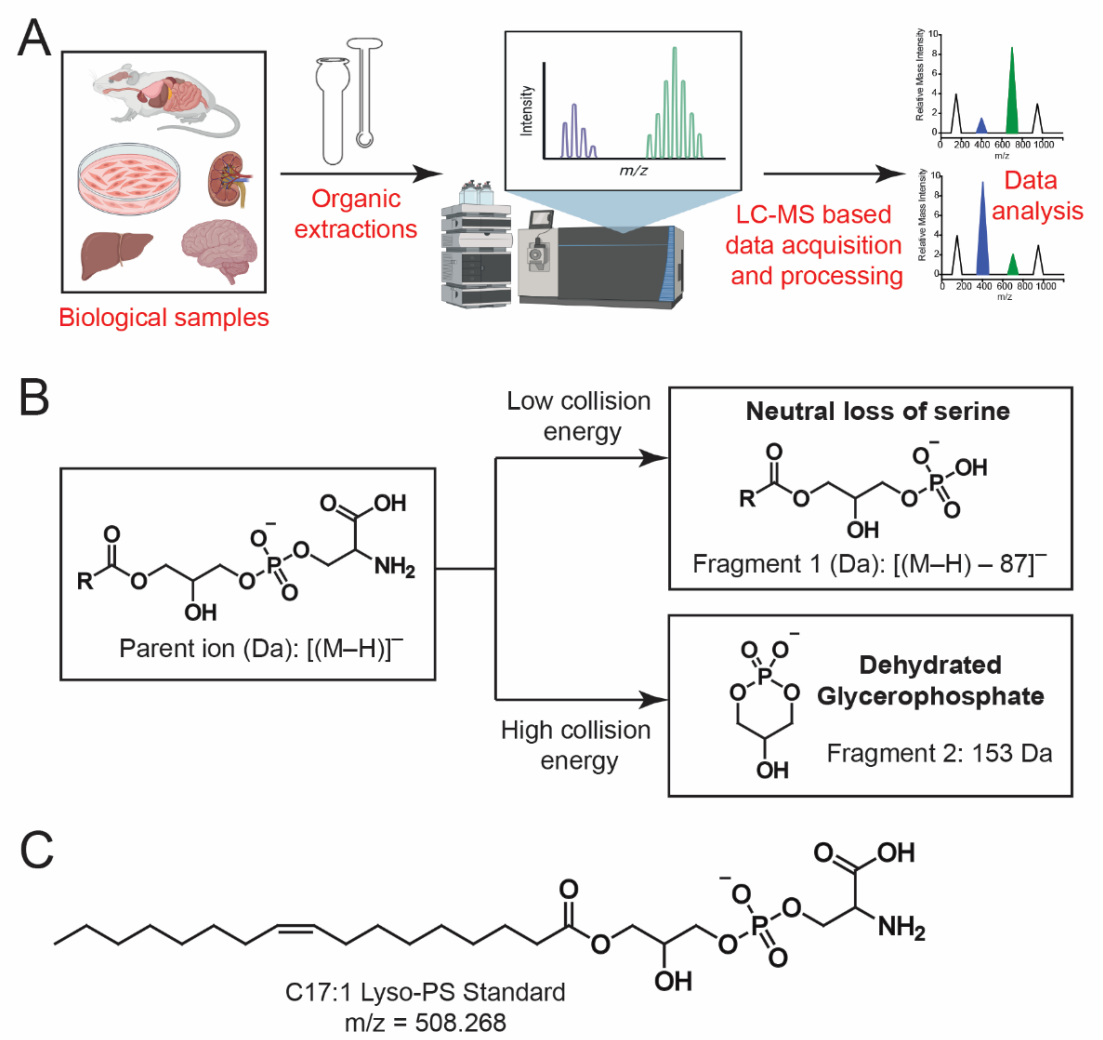

Fig 1.2 (A) A general workflow for analyzing lyso-PS lipids by LCMS. *(**B**) Fragments of lyso-PS detected by LCMS during an MS/MS analysis of a lyso-PS parent ion at different collision energies. (**C**) Structure of C17:1 lyso-PS used as an internal standard for LCMS lipidomic measurements of lyso-PS in biological systems.*

Following the aforementioned lipidomic enrichment and chromatographic separation, lyso-PS is best detected by LCMS analysis using multiple reaction monitoring (MRM) methods, typically on triple quadrupole mass spectrometers compatible with ultra-high-performance liquid chromatography (UHPLC) separations. Following UHPLC separation, lyso-PS is

detected by the electrospray ionization (ESI) technique in the negative ion mode, where, after fragmentation (MS/MS) of the parent ion, lyso-PS produces two signature daughter fragments: (i) a parent ion – 87 Da fragment, due to the neutral loss of the serine moiety from the head group (Fragment 1), and (ii) a fragment with m/z = 153 Da, that corresponds to the dehydrated form of glycerophosphate (Fragment 2) (**Fig 1.2 B**)[25]. Typically, Fragment 1 is the more dominant fragment of lyso-PS at lower collision energies (≤ – 15 V) while Fragment 2 is the predominant fragment at higher collision energies (≥ – 35 V). Transitions of the parent ion to either Fragment 1 or Fragment 2 (or in some cases both) have been reported in literature for MRM analysis towards quantitative detection of lyso-PS in mammalian systems. In almost all cases, the commercially available, unnatural C17:1 lyso-PS has been used as a reliable internal standard for the absolute quantitation of lyso-PS from different mammalian biological systems (**Fig 1.2 C**).

In this thesis, I have used a Modified Folch method to extract lipids (specifically enriching phospholipids) from biological systems using a C17:1 lyso-PS standard and a targeted MRM approach to detect lyso-PS species using a triple quadrupole HPLC-MS.

Biodistribution of lyso-PS

Using the lipid extraction and LCMS protocols discussed the previous section, quite some knowledge is now available for the distribution of lyso-PS lipids in various mammalian systems, largely from screening of tissues from rodent models (mostly mice) and cell lines. Different studies that report the quantitative profiling of lyso-PS in various rodent tissues have shown that this signaling lysophospholipid is present in the central nervous system (brain, spinal cord, eye), metabolic tissues (liver, kidney, heart, lungs, colon) tissues of the immune system (spleen, thymus, lymph node) and plasma/serum[25,26,28]. Of these tissues in mice, the anatomical distribution of lyso-PS has extensively been studied in the brain, and even though it is ubiquitously present throughout this tissue of the central nervous system, it is significantly enriched in the cerebellum and the olfactory bulb.

Table 1: Levels of C18:0 lyso-PS in different mammalian tissues

Tissue	18:0 Lyso-PS (nmol/g tissue)
Cerebellum	11.2
Hippocampus	37
Cortex	12.1

Heart	77.7
Kidney	15.3
Liver	18.9
Lungs	81.4
Eye	48.9

Studies from cultured mammalian cells have shown that lyso-PS is present in both the cells and secreted media of various primary immune cells (e.g. macrophages, mast cells, microglia, T cells) and several immortalized cell lines (e.g. cancer cell lines, macrophage cell lines, lymphoblast cell lines from human subjects)[26,29–32]. Amongst the rodent tissues and various cell lines profiled, C18:0 and C18:1 lyso-PSs seem to be the most abundant species, with C16:0, C20:4, and C22:6 being the other consistently detectable lyso-PS species in these mammalian biological systems.

While there are currently no extensive tissue-wide lyso-PS profiling studies available in humans, some recent lipid profiling studies from blood/serum/plasma, or tissue biopsies (e.g. cancer tissue), or tissues/feces of diseased patients or from post-mortem analysis, have shown that lyso-PS is present in several human tissues, especially in the context of diseases[33–36].

BIOLOGICAL FUNCTIONS OF LYSO-PS

Over the past two decades, numerous studies have shown that lyso-PS plays an important role in regulating a multitude of physiological processes in mammals, especially in the immune and central nervous systems[11,12]. Given this, the past few years have seen a significant increase in the number of reported mechanistic studies that causally relate lyso-PSs to diverse immunological phenotypes, and their association with human diseases.[37,38] This section includes a brief summary of the role and functions of lyso-PS in all the biological processes where significant mechanistic studies are available (**Fig 1.3**)

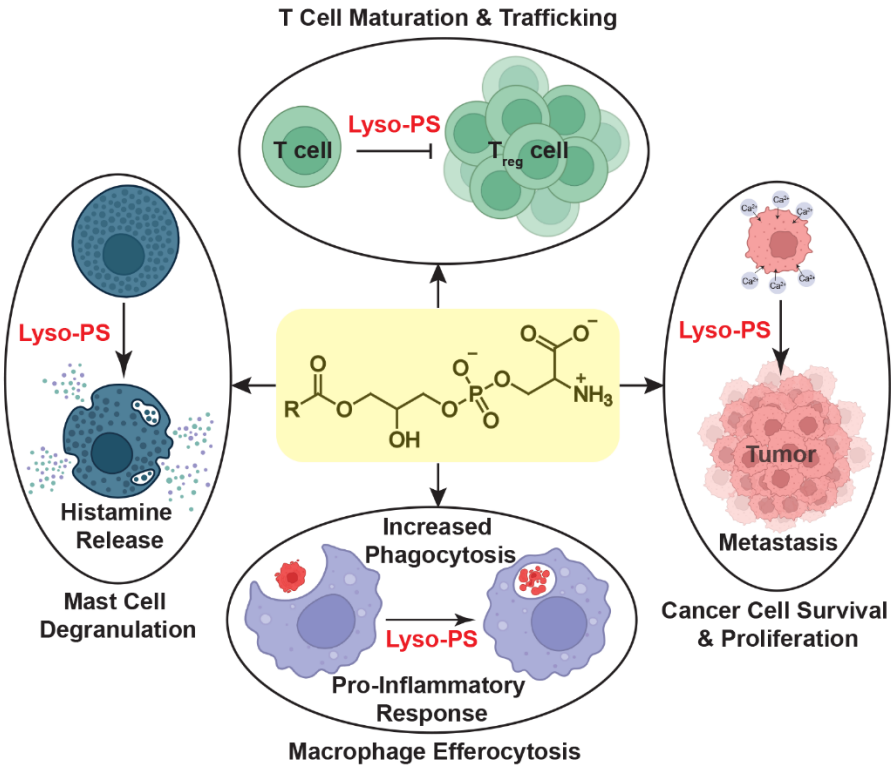

Fig 1.3: Biological functions regulated by lyso-PSs

Mast cell degranulation

Mast cells are tissue-resident immune cells derived from the myeloid lineage, that have important roles to play in both innate and adaptive immunity towards resolving infections and allergic reactions[39]. Early investigations during the 1950s showed that in response to inflammatory and/or allergic stimuli, mast cells secreted histamine, which in turn was responsible for regulating several downstream biological processes. Interestingly, around the same time, injection of a brain lipid fraction containing a degraded form of PS (now known as lyso-PS) was shown to elicit systemic "histamine-like substance" production in rabbits, which caused severe hemolysis and was responsible for the eventual death of these animals[14,15]. Two decades later, PS containing liposomal vesicles that were first incorporated in cellular membranes, and subsequently biologically degraded (presumably by lipases) to form lyso-PS, were shown to elicit histamine release from mast cells[40]. The same study also showed that this immunological phenotype was specific to PS being biologically converted to lyso-PS, and no other phospholipid (or lysophospholipid) could elicit the same response from mast cells. Combining these observations/results, this study established for the first time that

lyso-PS was indeed directly modulating the histamine release during the degranulation of mast cells. *In vivo*, both mast cells and basophils are known to release histamine in response to antigens, and cellular pharmacological studies on these immune cells have shown that lyso-PS has no effect on basophils, but robustly modulates the histamine release specifically from mast cells[41,42].

Macrophage efferocytosis

Macrophages are a class of phagocytic cells of the innate immune system derived from the myeloid lineage[43]. They are primarily responsible for clearing out apoptotic cells and/or cellular (or tissue) debris and/or pathogens by orchestrating pro-inflammatory responses via a process called efferocytosis[44]. During injury or infection, via efferocytosis, macrophages (either tissue-resident or systemically circulating) find "eat me" signals on damaged and/or apoptotic cells (or tissues) and, using these metabolic cues, clear such pathological conditions. While a few biochemical factors, including some lipid mediators (e.g. prostaglandins, leukotrienes)[45], are known to be involved during the process of efferocytosis, the role that lyso-PS plays during the resolution of infections and inflammation associated with this immunological process, has only come to light little over the past two decades[46].

The first evidence of the involvement of lyso-PS during efferocytosis was shown by activating neutrophils to upregulate its oxidative capacity via induction of NADPH oxidase enzymatic activity to physiologically simulate resolution of neutrophilia during tissue injury and acute inflammation[47]. Lipidomics measurements showed that upon increased NADPH oxidase activity, neutrophils secreted significantly more lyso-PS, presumably from the heightened activity of a hitherto unknown phospholipase that hydrolyzes exofacial PS precursors, and this increased secretion of lyso-PS from them was dependent on the NADPH oxidase activity[48]. Interestingly, besides lyso-PS, the cellular or secreted concentrations of no other phospholipid or lysophospholipid were found to be altered is such oxidatively stressed neutrophils[48]. Following up, it has since been shown that this NADPH oxidase dependent increased secretion of lyso-PS resulted in the uptake (or engulfment) of such oxidatively stressed activated and dying neutrophils by macrophages in cell culture based experiments. Further mechanistic studies on this topic have since implicated the generic lysophospholipid recognizing GPCR, GPR132 (also known as G2A), to be responsible for this lyso-PS dependent efferocytosis activity of macrophages[48,49].

T cell maturation and trafficking

In an effort to understand the effects that different phospholipids have on the trafficking and proliferation properties of lymphocytes (in particular T cells), initial cellular pharmacological studies showed that amongst the different phospholipids, only PS inhibited the synthesis of DNA of the lymphocytes from human peripheral blood mononuclear cells (PBMCs)[50]. While this effect was specific only to PS (even in the presence of chemical agents that facilitated DNA synthesis), interestingly, it was found from subsequent cellular studies done in serum depleted conditions, that PS in fact had a very minimal inhibitory effect on DNA synthesis in lymphocytes[51]. It was shown in another follow up study, that promiscuous phospholipases present in serum enzymatically converted PS to lyso-PS, and that lyso-PS (and not PS) hampered lymphocyte proliferation, specifically that of T cells[52].

Following up on these initial findings, elegant immunological studies have shown that lyso-PS acts through a GPCR, GPR174, and negatively influences the maturation and functions of T cells[53]. Specifically, *in vitro*, lyso-PS suppresses the proliferation of T cells and their maturation (or generation) into regulatory T cells, while *in vivo*, lyso-PS signaling via GPR174 was shown to regulate the accumulation of regulatory T cells in tissues of the central nervous system during an experimental autoimmune encephalomyelitis (EAE) model[53].

Cancer cell survival and proliferation

Several studies have reported important functions of different lysophospholipids in the survival and proliferation of cancers, and shaping their tumor microenvironment[6,54]. Not surprisingly, the past two decades have seen studies that implicate lyso-PS in various signaling pathways that promote cancer cell survival and their metastasis in humans. Amongst the different phenotypes, cellular pharmacological studies have shown that lyso-PS induces the influx of intracellular calcium in various immortalized (human) cancer cell lines[55,56], as well as primary human cancers (leukemia and colorectal cancer)[57,58], and by doing so, promotes the chemotactic (metastatic) and stimulatory properties on these cancer cells and their microenvironments.

Additionally, lyso-PS treatment also increases the levels of cytosolic cyclic adenosine 5'-phosphate (AMP) and phosphorylation of the nodal signaling protein Extracellular Signal-Regulated Kinase (ERK) in immortalized cancer cell lines[59,60]. This is not surprising, as lyso-PSs potentially signal through GPCRs, and all the aforementioned phenotypes are associated with signaling cascades downstream of GPCRs that most likely promote cell proliferation and

chemotaxis[61]. Of note, the past few years have seen numerous clinical reports that show causally how the dysregulation in the expression (or localization) or mutations to the lyso-PS receptor (GPCR) GPR34 results in tumor cell growth and metastasis of different human cancers, in particular lymphomas[62,63]. Interestingly, more recently, a few reports now show that different micro-RNAs target the expression of a lyso-PS receptor or metabolic enzyme, and by doing so, tune effective cellular lyso-PS levels to promote metastasis of human cancers[64]. While it is evident that lyso-PS regulates cancer cell survival and metastasis, detailed SAR studies with different lyso-PSs or its synthetic analogs have not been reported for this biological activity of lyso-PS.

Metabolic phenotypes

While the physiological role of lyso-PS in the regulation of metabolism has remained cryptic to date, there are a few reports suggesting a potential role for this lysophospholipid in the regulation of glucose metabolism. Initial studies have shown that systemic injection of lyso-PS in rodents results in an insulin-independent hyperglycemic phenotype, with lowered circulating blood glucose levels coupled to a significant accumulation of glucose in the brains of these animals[65]. These studies also suggested an insulin-type hormone-like behavior of lyso-PS in regulating this glucose metabolic phenotype. In an effort to mechanistically explain this, it has since been shown that lyso-PS increases the expression of the glucose transporter GLUT4[66,67] in myotubes and adipocytes, and thereby increases the systemic transport and absorption of glucose in muscles and stored fat in these animal models[68]. Further, systemic lyso-PS administration (like insulin) was found to significantly lower circulating blood glucose levels in diabetic or obese rodents[68].

ENZYMES METABOLIZING LYSO-PSs IN MAMMALIAN CELLS AND TISSUES

Given the potent biological activities modulated by lyso-PSs, their metabolism (biosynthesis, consumption, and degradation) in various mammalian cells and tissues is tightly regulated by the interplay of an ensemble of enzymes that make or break this signaling lipid. Lipases are known to biosynthesize lyso-PS from PS precursors, or degrade them to free fatty acids and the glycerophosphoserine head group, while acyltransferases consume lyso-PSs to re-make their PS precursors. A summary of the known lyso-PS metabolizing enzymes is shown in **Fig 1.4**. These are further discussed in detail in chapters 2 and 3 when we further discuss the metabolism of lyso-PS.

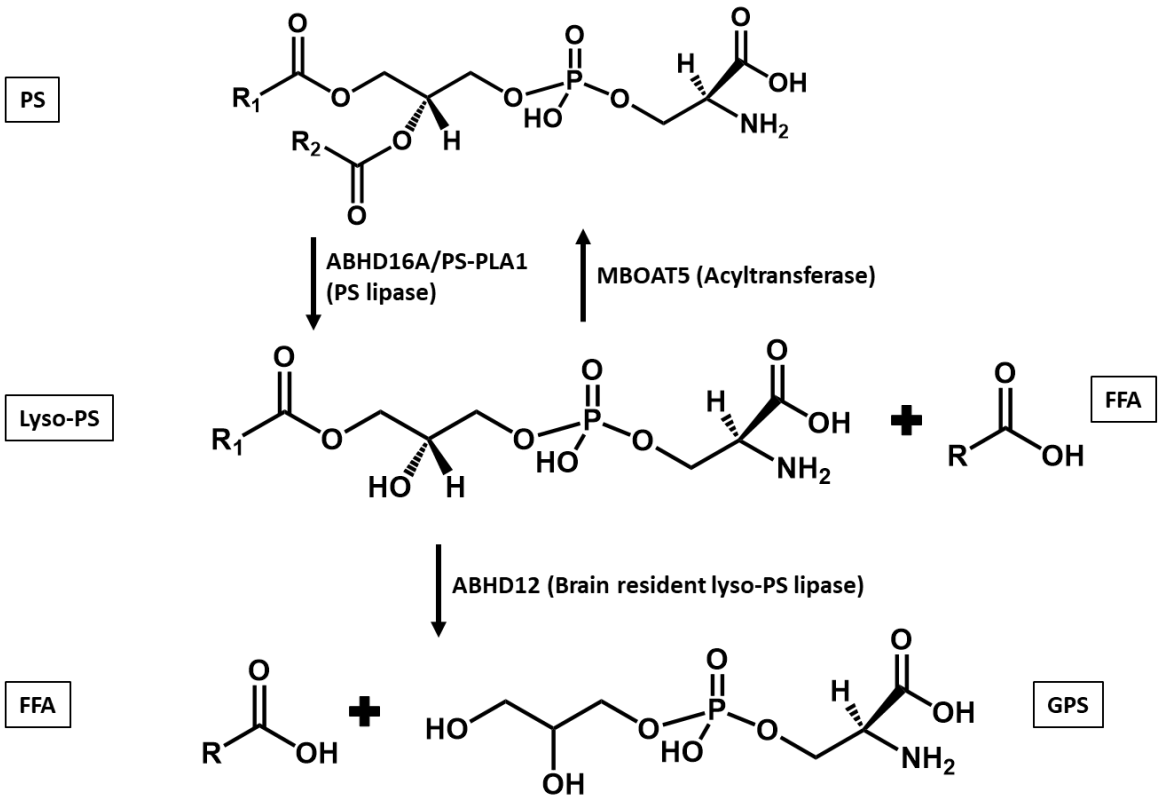

Fig 1.4 : Enzymes involved with lyso-PS metabolism

DISEASES ASSOCIATED WITH DYSREGULATED LYSO-PS METABOLISM AND/OR SIGNALING

Over the past decade, several studies, particularly those looking at focused population-level genome-wide association studies (GWAS), have shown that deleterious mutations and/or polymorphisms to the putative lyso-PS metabolic enzymes or receptors cause different diseases in humans. Since these proteins are almost exclusively localized to the central nervous and immune systems, most of the diseases associated with deregulated lyso-PS metabolism and signaling to date are neurological and autoimmune in their pathological manifestations. Briefly, lyso-PS is implicated in the following diseases:

Neurological diseases

Little over a decade ago, PHARC (***p***olyneuropathy, ***h***earing loss, ***a***taxia, ***r***etinitis pigmentosa, ***c***ataract) was first identified as an autosomal recessive neurodegenerative disease in humans caused by deleterious mutations in the *abhd12* gene[69,70] (Online Mendelian Inheritance in Man (OMIM) # 612674)[71]. The *abhd12* gene encodes the integral membrane

enzyme ABHD12, which is the major lyso-PS lipase in the mammalian nervous system, and is responsible for terminating lyso-PS signaling in the mammalian brain (further discussed in Chapter 3)[25]. To date, there are > 30 mutations mapped in the human *abhd12* gene that are responsible for PHARC, and human subjects that suffer from PHARC exhibit auditory and visual defects, and malfunctions in their sensorimotor system due to peripheral neuropathy and ataxia[72].

In the past couple of years, mutations to the *abhd16a* gene, which encodes the PS lipase ABHD16A (a major lyso-PS biosynthetic enzyme in the mammalian brain) have been mapped in humans that suffer from a complex form of hereditary spastic paraplegia (HSP) in humans[73–75] (OMIM # 619735)[71]. The mutations described in literature are either point mutations to important residues (catalytic residues or in the transmembrane region) of the proteins or missense mutations resulting in truncated catalytically incompetent forms of the protein, causing loss of PS lipase activity in both cases[73–75]. Human subjects harboring deleterious mutations to ABHD16A suffer from developmental delays, intellectual disabilities, progressive spasticity of their limbs, and have anatomical anomalies in the brain. In conjunction with studies from mice models[26,32], lipidomics measurements on fibroblasts derived from human subjects with ABHD16A mutations have shown that dysregulated PS-lyso-PS metabolism seems to be the likely causative factor for the pathology associated with this complicated form of HSP.

Besides PHARC and complex HSP that involve defective lyso-PS metabolism, the putative P2Y-family of lyso-PS receptors have also been implicated in the progression of cognitive defects and pathologies associated with Alzheimer's disease[36,76]. Since the connection of lyso-PS signaling or its receptors to this neurodegenerative disease is only speculative at this point, more mechanistic and/or validation experiments are needed to ascertain this causal relation.

Autoimmune diseases

Graves' disease is an autoimmune disease that affects the thyroid gland, where deregulated thyroid function is caused by autoantibodies generated to the thyrotropin receptor[77]. In humans, this autoimmune disease can occur at all ages but seems to mostly affect women in a reproductive age group. Initial GWAS studies on populations prone to this autoimmune condition suggested that the lyso-PS receptor, GPR174 was among the major risk factors that might lead to Graves' disease[78,79]. Since these initial findings, several

focused genomic studies on human subjects suffering from Graves' disease across the world have identified polymorphisms or mutations to GPR174 to be the causative factor for the pathology and progression of the dysregulated thyroid function associated with this autoimmune disease. Along similar lines, Addison's disease (also known as Adrenal Insufficiency) is another autoimmune condition marked by an inability of the adrenal gland to produce hormones (particularly cortisol)[80]. Genomic studies on populations suffering from Addison's disease suggest that polymorphisms to GPR174 might also have a causal role in the pathogenesis of this autoimmune disease.

Besides Graves' and Addison's disease, recent studies from preclinical animal models and patient-derived samples suggest that lyso-PS signaling may also perhaps have a role to play in the progression of other common autoimmune conditions involving lysophospholipid signaling such as ulcerative colitis, Crohn's disease, and multiple sclerosis[33,35,53,81–83]. While the association to these autoimmune conditions is only observational and fairly speculative currently, further studies are needed to conclusively establish a mechanistic connection of lyso-PS in this context.

OPEN QUESTIONS TACKLED IN THE THESIS:

While the past two decades have seen tremendous progress in our understanding of the physiological processes modulated by lyso-PS-dependent signaling pathways in humans, new outstanding questions and important thrust research areas have since emerged. I have explored some of these during my PhD.

While significant studies have been done to delineate how the biochemical activity of ABHD12 regulates lyso-PS metabolism and, the association of the ABHD12-lyso-PS signaling axis during PHARC, the absence of any experimentally solved three-dimensional structure has resulted in only a limited understanding of the protein sequence-activity relationship of ABHD12. This can be particularly important in the context of PHARC, as newer ABHD12 mutants are mapped in humans suffering from neurological symptoms via genetic sequencing efforts. A thorough bioinformatics survey on the ABHD12 sequence coupled with the now available Alphafold structure[84] could shed some light on the sequence-function relationship of residues that are mutated in PHARC patients. We addressed this question in **chapter 2.**

Since the known metabolic enzymes and receptors for lyso-PS are highly expressed in the nervous and immune systems, the focus of most of the biological studies associated with lyso-PS has been almost exclusively limited to these tissues. However, recent lipidomic measurements have shown that lyso-PSs are almost ubiquitously present in every tissue, including metabolically active tissues such as the liver and kidneys[25,32]. Yet, virtually nothing is known about the biosynthetic or catabolic pathways that homeostatically regulate lyso-PS metabolism in these tissues. In humans, a majority of the phospholipases and lysophospholipases belong to the metabolic serine hydrolase family of enzymes, and a significant portion of this enzyme family still lacks the assignment of a physiologically relevant biochemical activity and an *in vivo* biological function. Leveraging the repertoire of pharmacological and genetic tools available to interrogate the enzymes of the mSH family[85,86], it is possible to determine if certain tissue-specific lipases might, in fact, be metabolic regulators of lyso-PS. For example, the major lyso-PS lipase ABHD12 is highly expressed in the brain, and is known to regulate levels of lyso-PS only in the nervous system. Since lyso-PS is present in almost all tissues of the body, there must be hitherto unknown lyso-PS lipases that must regulate the levels of lyso-PS in tissues other than the nervous system. The identification of such lyso-PS lipases will certainly add new dimensions in our understanding of systemic lyso-PS metabolism, its effects in other tissue physiology, and if there is indeed any inter-organ crosstalk and signaling associated with this signaling lysophospholipid. We addressed this question in **chapter 3**.

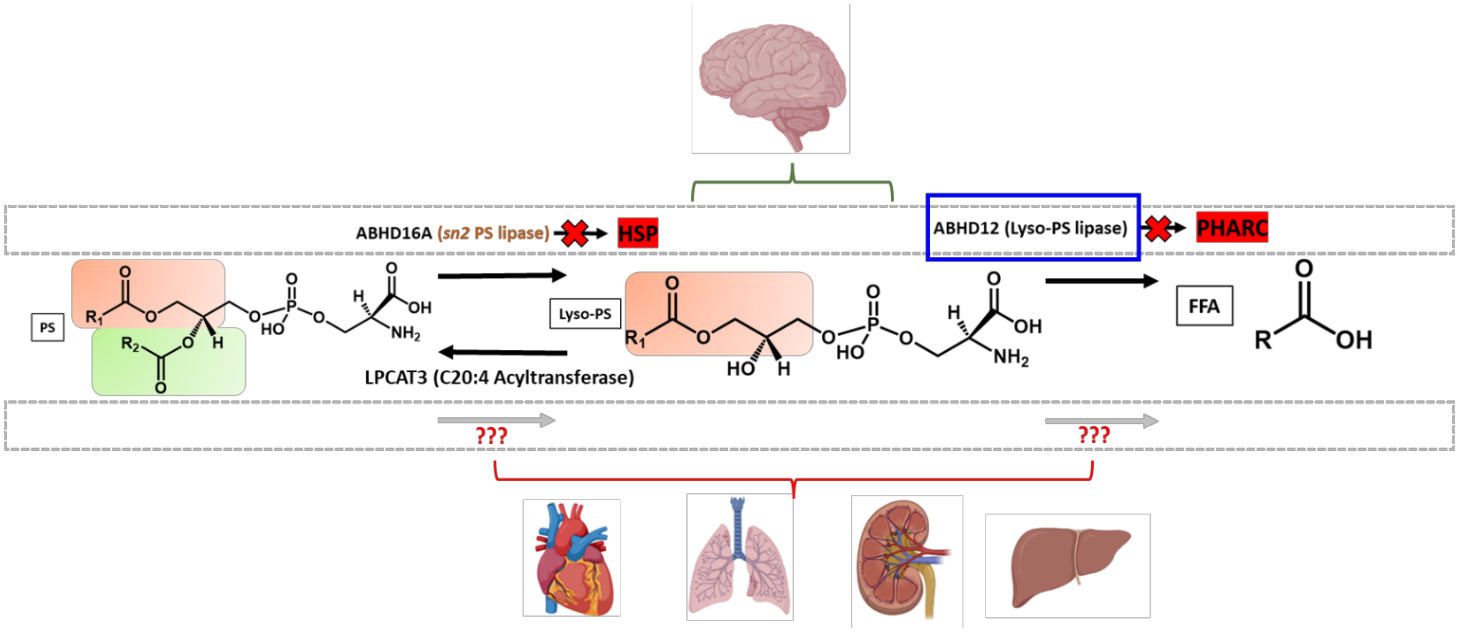

Fig 1.5 : Open questions tackled in the thesis *(Blue: Determining a sequence activity relationship for ABHD12 – Chapter 2; Red: Identifying enzymes capable of metabolizing lyso-PS in peripheral tissues – Chapter 3)*

Finally, for all the diseases discussed involving lyso-PS dysregulation (e.g. neurological and autoimmune diseases), besides expensive and time-consuming genetic mapping analysis, currently, there are no reliable biomarkers or rapid clinical diagnostics tests that can be used for an accurate early diagnosis of the disease. Therefore, moving forward, it might be useful to develop such rapid, yet reliable diagnostic tests (e.g. LCMS based lyso-PS measurements in bodily fluids, lyso-PS sensing rapid ELISAs) that may be used clinically for the early, accurate, and relatively inexpensive diagnosis of the diseases associated with dysregulated lyso-PS metabolism and signaling. We developed certain LCMS methods to identify and characterize other lipid species, discussed in **chapter 4**. These methods could be extended to detect lyso-PS species and other lipid species as biomarkers too.

PUBLICATION

Chakraborty, Arnab, and Siddhesh S. Kamat. "Lysophosphatidylserine: A Signaling Lipid with Implications in Human Diseases." ***Chemical Reviews*** 124, no. 9 (2024): 5470-5504.

Chapter 2: Characterization of ABHD12 sequence determinants

INTRODUCTION

Over a decade ago, an autosomal recessive genetic disorder named PHARC (acronym for all the symptoms associated with the disease: ***p***olyneuropathy, ***h***earing loss, ***a***taxia, ***r***etinitis pigmentosa, and ***c***ataract; OMIM: 612674) was reported in humans[69–71]. Clinically, human PHARC subjects show early onset visual disturbances (e.g. cataract or partial blindness) and auditory deficits (e.g. deafness), that are often coupled to polymodal sensory and motor defects caused by peripheral neuropathy (e.g. *pes cavus*)[70,72]. The symptoms associated with PHARC in human subjects manifest in early teenage years, and progressively worsen with age, and there seems to be no gender or race bias associated with this genetic disease[72]. In extreme cases, demyelination of sensorimotor neurons and cerebellar atrophy has also been reported in older human PHARC subjects, and yet, to date, there are no reported medical cures or therapies to treat this human genetic neurological disorder. Given the array of symptoms, PHARC was commonly misdiagnosed as possibly other neurological disorders, until genetic mapping confirmed that this neurodegenerative disease was caused by deleterious mutations in the *abhd12* gene on chromosome 20p11 in humans[70]. To date, over 30 reported pathogenic mutations have been reported in the *abhd12* gene, all causing PHARC in humans[72,87]. These mutations include deletion-insertion, nonsense, frameshift, splice site, and missense type mutations in the *abhd12* gene from samples that were genetically sequenced from human PHARC subjects[87].

The *abhd12* gene encodes an integral membrane associated lipase, α/β-hydrolase domain containing protein # 12 (ABHD12), which belongs to the metabolic serine hydrolase family of enzymes[88,89]. Untargeted lipidomics analysis on the brains of ABHD12 knockout mice (the murine model of PHARC) showed that relative to wild-type controls, the loss of ABHD12 activity resulted in a massive accumulation of different lysophosphatidylserine (lyso-PS) lipids[25]. Lyso-PSs are a class of signaling lysophospholipids, that have many important functions in mammalian physiology, and dysregulation in their metabolism is now causally linked to an array of human neurological and autoimmune disorders, including PHARC[10]. From a biochemical standpoint, mechanistic studies have since shown that via its enzymatic activity, ABHD12 catalyzes the degradation of lyso-PS lipids, and, by doing so, functions as the principal lyso-PS lipase (**Fig 2.1**) in the mammalian central nervous and immune systems[25].

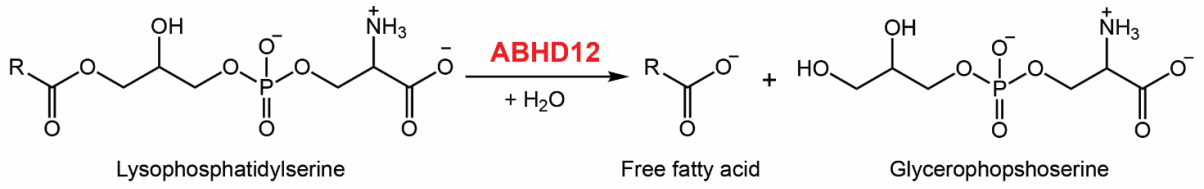

Fig 2.1: The lyso-PS lipase reaction catalyzed by ABHD12. *In this reaction, R denotes long or very-long chain fatty acids.*

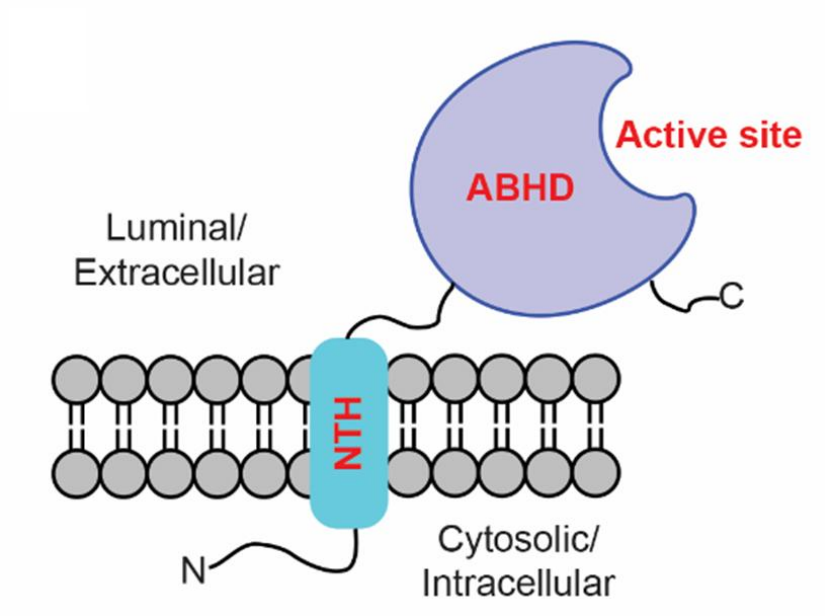

Fig 2.2: Schematic representation of the predicted protein structure and luminal/extracellular active site orientation of human ABHD12 *(NTH = N-terminal transmembrane helix; ABHD = α/β-hydrolase domain)*

Following up on these studies, our lab has previously shown that ABHD12 is predominantly localized to the endoplasmic reticulum (ER) membrane, and has a luminal orientation of the enzyme active site, that regulates the secretion of lyso-PS lipids from different mammalian cells[90] **(Fig 2.2)**. Further, from *in vitro* biochemical assays, we demonstrate that ABHD12 prefers very-long chain (VLC) variants of lyso-PS as substrates[29,91]. This substrate preference of ABHD12 explains why its deletion results in the highest accumulation of pro-inflammatory VLC lyso-PSs in the mammalian brain, that are largely responsible for neuroinflammation and eventually the neurobehavioral symptoms associated with human PHARC subjects[28]. Finally, by immunohistochemical analysis

coupled with biochemical assays and targeted lipidomics measurements, we have reported that ABHD12 has ubiquitous expression and activity in different anatomical regions of the mammalian brain, and the loss of ABHD12 activity results in dysregulated lyso-PS metabolism in all anatomical regions of the mammalian brain without any exception[32]. These studies from our lab, together with previous literature, provide a nice explanation for the progression of PHARC, and ABHD12's role in the pathogenesis of this neurodegenerative disease.

While significant studies have been done to delineate how the biochemical activity of ABHD12 regulates lyso-PS metabolism and, the association of the ABHD12-lyso-PS signaling axis during PHARC, the absence of any experimentally solved three-dimensional structure has resulted in only a limited understanding of the protein sequence-activity relationship of ABHD12. This can be particularly important in the context of PHARC, as newer ABHD12 mutants are mapped in humans suffering from neurological symptoms via genetic sequencing efforts.

To address this knowledge gap, in our lab, Archit Devarajan performed a thorough bioinformatics survey for the identification of ABHD12 protein sequences across all forms of life. Next, he phylogenetically classified these putative ABHD12 sequences across the evolutionary time scale and found positionally and functionally conserved residues in their protein sequences. Further, using structural modeling and docking studies, we shortlisted residues that might have importance in the biochemical activity of ABHD12.

I performed biochemical assays to show that these residues are indeed of importance for the enzymatic activity of ABHD12. I also found that several missense mutations associated with PHARC, occur in highly conserved residues, and these mutants are catalytically compromised. Finally, from our evolutionary analysis, we find that ABHD12 has an ortholog in flies, CG15111, that also robustly performs lyso-PS lipase activity, and thereby opens new prospects in combination with genetics for modeling pathogenic mutants and thus studying PHARC in fly models.

EXPERIMENTAL PROCEDURES

Materials

Unless otherwise mentioned: all chemicals, buffers, and reagents were procured from Sigma-Aldrich; all mammalian tissue culture media and consumables were procured from HiMedia Laboratories; all LC-MS grade solvents were procured from JT Baker. Wherever applicable, the catalog numbers of materials used in this study are mentioned below. All oligonucleotides used in this study were obtained from Sigma-Aldrich.

Bioinformatics analysis. (Performed with Archit Devarajan)

The bioinformatics analyses were performed as previously reported by our lab for ABHD14B with modifications[92]. Briefly, five iterations of PSI-BLAST searches on the human ABHD12 (hABHD12) (UniProt: Q8N2K0, NCBI: NP_001035937.1) as the reference sequence against the clustered non-redundant (clustered_nr) database was performed to identify distantly-related orthologs of ABHD12[93]. The expect threshold (E-value) was set to 1x 10^{-6} with a maximum return of 1000 hits. The individual members of each cluster (totaling to 2770) were extracted and subject to further analysis. A PSI-BLAST hit was classified as ABHD12 protein sequence if it met all the following criteria: (i) has an N-terminal transmembrane domain, (ii) conserved catalytic triad, (iii) conserved nucleophilic (YIWGHSLGTGV) and acyltransferase (LGYHVVTFDYRG) motifs with up to three mismatches in residues other than the underlined residues (iv) sequence length between 250 and 550 amino acids. DeepTMHMM[94] and CCTOP[95] were used to assess the presence of any transmembrane domains. A previously reported custom script was slightly modified and used to further curate the data based on the presence of the catalytic triad and other key functional residues by carrying out pairwise global alignments using the Needleman-Wunsch algorithm[96]. For plotting the phylogenetic tree, the longest isoform of ABHD12 from each organism was selected and subject to multiple sequence alignment using Clustal Omega[97]. The resulting alignment was fed into MEGA11[98] to plot maximum likelihood trees using the James-Taylor-Thornton (JTT) model and the trees were visualized in iTol[99]. The highly conserved ABHD12 residues were identified using pymsaviz (pypi.org/project/pymsaviz/) and Bio.Align (biopython.org/docs/1.76/api/Bio.Align.html) packages in Python. The functionally conserved residues were identified by manual inspection of filtered protein sequences.

Structural docking studies. (Performed with Archit Devarajan)

All structural docking studies were performed on the AlphaFold[84] generated structure of hABHD12 (UniProt ID: Q8N2K0). To identify a substrate binding pocket that contained the catalytic serine (Ser-246) within hABHD12, a tunnel analysis was performed using the CAVER Web 1.0[100] and MOLE 2.5[101] online servers. Following this, surface electrostatic calculations were performed on the same AlphaFold structure of hABHD12 using the APBS plugin to PyMOL (https://pymolwiki.org/index.php/Apbsplugin) to understand the charge distribution on the protein surface and in the active site. The PARSE force field was used to generate the required PQR files which were subsequently used to calculate the electrostatic surface diagrams. Finally, ligand (C18:0 lyso-PS) docking was performed on the same AlphaFold structure of hABHD12 using Autodock Vina in the PyRx environment using standard reported procedures. Briefly, the structure of hABHD12 and the SDF files of the ligand (C18:0 lyso-PS) was converted into the PDBQT file format using OpenBabel[102]. Thereafter, targeted docking was performed with a (30 x 30 x 30) A^o box roughly centered at the catalytic serine (Ser-246) in the identified ligand binding pocket of hABHD12, and the top nine binding conformations were selected for further investigation.

Overexpression of mouse ABHD12 mutants in HEK293T cells

The *abhd12* gene (encoding ABHD12) was amplified from an in-house generated cDNA library of the mouse brain, and cloned into a *pCMV-Sport6* vector as reported previously[91]. All mutants of mouse ABHD12 (mABHD12) were made in the same plasmid using standard site-directed mutagenesis protocols as per manufacturer's instructions (Promega) (With Archit Devarajan). Wild type (WT) or mutants of mABHD12 were transiently transfected into mammalian HEK293T cells by an established methodology using the polyethylenimine-based PEI MAX® transfection reagent. As a control in these experiments, an empty plasmid (mock control) was used to account for off-targets (if any) from the empty plasmid during these studies. Two days post-transfection, the cells were harvested by scraping, washed with cold sterile Dulbecco's phosphate buffered saline (DPBS) (3 times), and then lysed by sonication. The cellular debris (pellet) was discarded by centrifugation of the lysate at 200g for 5 min at 4 ^oC, and the resulting supernatant was further centrifuged at 100,000g for 45 min at 4 ^oC to obtain the membrane proteomic fraction as reported earlier[91]. The activity and overexpression of mABHD12 variants in membrane proteomic fractions of HEK293T cells were confirmed by gel-based ABPP assays and Western blot analysis, respectively.

Overexpression of CG15111 in insect cells. (Performed with Rohith and Kundan)

The *cg15111* gene (encoding CG15111) was amplified from a laboratory generated cDNA library of the adult fly, and cloned with a C-terminal FLAG tag into the *pRmHa3* vector. The catalytic serine (Ser-241) was mutated to an alanine to yield the S241A CG15111 mutant in the same plasmid using standard site-directed mutagenesis methods as per manufacturer's instructions (Promega). The overexpression of WT or S241A CG15111 was performed in Schneider 2 (S2) insect cells using transfection protocols recently reported by us[103]. The activity and overexpression of CG15111 variants in membrane proteomic fractions of S2 cells were confirmed by gel-based ABPP assays and Western blot analysis, respectively.

Gel-based ABPP assays

All gel-based ABPP assays were done using protocols previously reported by us[91]. Briefly, all protein concentrations were estimated using Bradford's reagent (Sigma-Aldrich, catalog # B6916), and 50 μg of the membrane proteomic fraction (of HEK293T cells or S2 cells) was incubated with 2 μM FP-rhodamine (45 mins, 37 ^{o}C) with constant shaking. Following this, the reaction was quenched using 4x-SDS loading buffer. All gel-based ABPP samples were loaded on a 10% SDS-PAGE gel, and enzymatic activities (of ABHD12 or CG15111 variants) were visualized by in-gel fluorescence on an iBright1500 gel documentation system (Invitrogen).

Western blot analysis.

Following gel-based ABPP assays, the resolved membrane proteomic fractions were transferred to a nitrocellulose membrane (GE Healthcare, catalog # GE10600002) and processed for Western blot analysis using protocols previously reported by us[91]. In the Western blot analysis, Ponceau S staining (Sigma-Aldrich, catalog # A40000279) was used to confirm equal loading of protein samples. The primary antibodies used in our Western blot studies were: anti-ABHD12 (rabbit, Abcam, catalog # ab68949) and anti-FLAG (rabbit, Sigma-Aldrich, catalog # F7425). The secondary antibody used in our Western blot studies was an anti-rabbit conjugated to horseradish peroxidase (HRP) (Thermo Fisher Scientific, catalog # 31460). All Western blots were developed with the Immobilon chemiluminescent HRP substrate (Merck Millipore, catalog # WBKLS0500) and visualized on a G-Box Chemi-XRQ gel documentation system (Syngene).

Lyso-PS lipase assays.

All LC-MS based lyso-PS lipase assays were done by LC-MS analysis using procedures previously reported by us[29,91]. All lyso-PS lipase assays were done with 20 μg of the membrane proteomic fraction (from HEK293T or S2 cells) against 100 μM lyso-PS substrate (C17:1 lyso-PS; Avanti Polar Lipids, catalog # 858141). All assays were analyzed on an Agilent 6545 Quadrupole Time Of Flight (QTOF) LC-MS/MS instrument in the negative ion mode using an electrospray ionization (ESI) source. All LC separations were done using columns and solvent gradients previously reported by us[29,91]. The MS parameters used were as follows: drying and sheath gas temperature = 320 °C; drying and sheath gas flow rate = 10L/min; fragmentor voltage = 150 V; capillary voltage = 4 kV; nebulizer (ion source gas) pressure = 45 Ψ and nozzle voltage = 1 kV. The product release was quantified by measuring the area under the curve for the peak corresponding to C17:1 FFA (produced from C17:1 lyso-PS) and normalizing it to the internal standard. The substrate hydrolysis rate was corrected by subtracting the non-enzymatic rate of hydrolysis, which was obtained by using corresponding heat-denatured (15 min at 95 °C) membrane proteomes.

Credit statement

All bioinformatics analyses (including figures) were primarily done with Archit Devarajan and he is an equal contribution first author in this study. CG15111 was cloned with Rohith C S and insect cell transfections were done with Kundan Kumar, both of whom are co-authors in this study. CG15111 substrate assay was performed with Archit.

Data plotting and analysis

All graphs represented in this study are analyzed and plotted using the GraphPad Prism 10 (version 10.3.0) software for macOS.

RESULTS

Identification of ABHD12 protein sequences (With Archit Devarajan)

ABHD12 is an integral membrane associated lipase from the metabolic SH family, with one predicted N-terminal transmembrane helix, and an invariant catalytic triad[32]. In the absence of any experimentally solved structures of ABHD12, the N-terminal transmembrane helix is predicted to comprise of residues 75 to 92, while the catalytic triad is expected to comprise of Ser-246, Asp-333 and His-372 for human ABHD12 based on a protein sequence analysis (**Fig 2.3**). Further, a previous bioinformatics survey of various ABHD-enzymes suggests that the conserved nucleophilic serine residue essential for catalysis (e.g. Ser-246 for human ABHD12) is part of a canonical nucleophilic GxSxG motif (where x = any amino acid)[104] (**Fig 2.3**). The same survey also finds a putative acyltransferase motif comprising of a HxxxxD motif (x = any amino acid) within the conserved LGYHVVTFDYRG sequence for mammalian ABHD12 sequences[104] (**Figure 2.3**). Hence, based on these bioinformatics studies, we set a stringent threshold, and classified a particular protein sequence as ABHD12 only if it possessed the N-terminal transmembrane domain (helix), conserved catalytic triad, nucleophilic motif and acyltransferase motif. For the acyltransferase motif, the His and Asp of the HxxxxD segment were set as a constant, and up to three mismatches were permitted within the remaining LGYHVVTFDYRG sequence. Finally, we restricted the protein sequence length from 250 to 550 amino acids, to ensure that any promiscuous sequences were filtered out of the analysis.

After setting appropriate selection criteria to obtain a list of possible ABHD12 protein sequences, five independent rounds of iterative PSI-BLAST searches were performed on the clustered non-redundant (clustered_nr) sequences database using human ABHD12 (UniProt: Q8N2K0, NCBI: NP_001035937.1) as the query sequence. This search resulted in the identification of 2770 protein sequences that were then subjected to transmembrane domain prediction using two separate web servers for further filtering. A N-terminal integral transmembrane helix was identified in 2362 of these protein sequences, of which the transmembrane regions in 49 protein sequences were identified by only one of the two web servers. Among these, upon further filtering, only 2223 protein sequences contained the catalytic triad and satisfied the protein length criteria for further selection. After a final round of refinement, a total of 1425 protein sequences that contained both the nucleophilic and

acyltransferase motifs and could be reliably classified as ABHD12 based on passing all our set criteria.

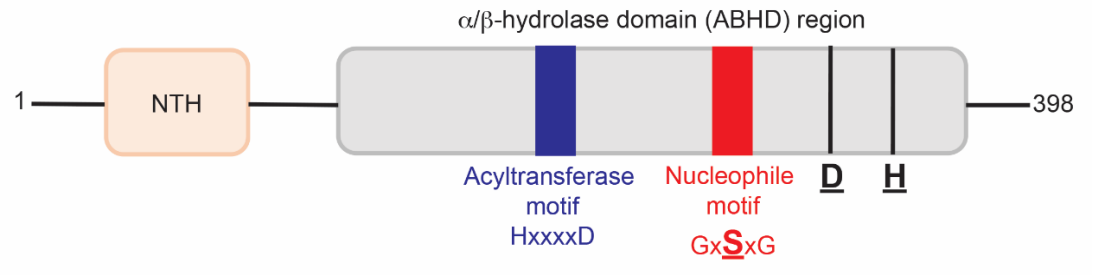

Fig 2.3: Schematic representation of the hABHD12 structure. *hABHD12 is predicted to contain the canonical catalytic triad consisting of Ser-Asp-His, a nucleophilic motif that contains the serine residue as part of a GxSxG sequence, and an acyltransferase motif comprising of an invariant HxxxxD sequence within the ABHD region of the protein. Additionally, hABHD12 also contains an N-terminal transmembrane helix (NTH) that anchors this lipase to the ER membrane.*

Phylogenetic analysis of ABHD12 protein sequences (With Archit Devarajan)

An inspection of the 1425 protein sequences identified as ABHD12 from the bioinformatics analysis showed that several organisms had more than one isoform of ABHD12. Therefore, to retain maximum species-specific information for the ABHD12 protein sequences that satisfy all filtering criteria, the longest isoform from each organism (except human, wherein the query sequence was used) was manually selected. This narrowed down the list of ABHD12 protein sequences to 860 across the same number of unique organisms. Next, to understand the evolutionary time scale of ABHD12, we performed a phylogenetic analysis of these 860 ABHD12 protein sequences (**Fig 2.4A**). This phylogenetic classification showed that two phyla, *Chordata* and *Arthropoda*, almost exclusively contained all the ABHD12 protein sequences. Amongst them, the phylum *Chordata* had the highest prevalence of ABHD12 protein sequences, (727 of 860, 84.5%), with phylum *Arthropoda* containing most of the remaining ABHD12 protein sequences (117 of 860, 13.6%) (**Fig 2.4B**). Within phylum *Chordata*, ABHD12 protein sequences were most prevalent in class *Aves* (birds) (43.1%, 313 of 727 chordates), *Actinopterygii* (bony fish) (25%, 182 of 727 chordates) and *Mammalia* (mammals) (24.8%, 180 of 727 chordates), while a smaller

fraction of ABHD12 protein sequences were also found in classes *Reptilia* (reptiles) (5.9%, 43 of 727 chordates) and *Amphibia* (amphibians) (1.2%, 9 of 727 chordates) (**Fig 2.4C**). From an evolutionary perspective within phylum *Chordata*, the phylogenetic analysis suggests that the ABHD12 protein sequences from reptiles-birds and mammals-amphibians cluster together, while those from fish form a distinct outgroup (**Fig 2.4A**). Notably, amongst phylum *Arthropoda*, class *Insecta* (insects) contains the highest number of ABHD12 protein sequences (81.2%, 95 of 117).

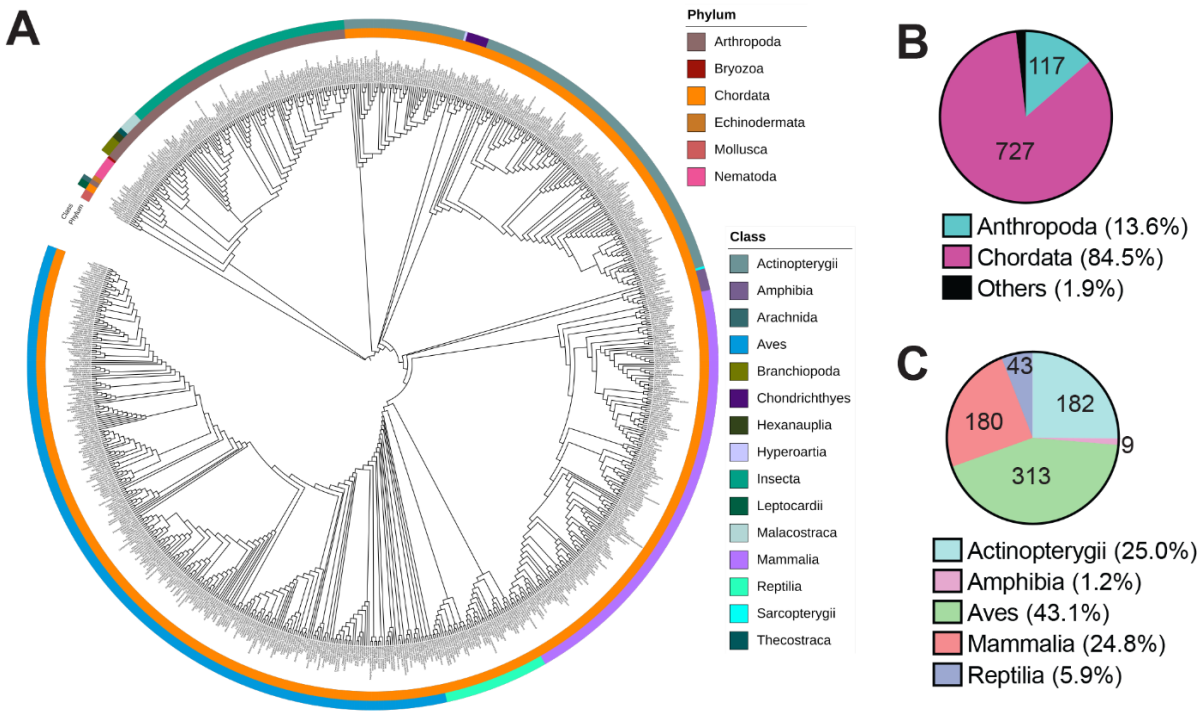

Fig 2.4: Phylogenetic analysis of ABHD12 sequences. *(A) Phylogenetic tree representing the identified ABHD12 sequences from 860 organisms. The outer and inner colored circles represent the Class and Phylum respectively, to which a sequence belongs. (**B, C**) Pie-chart analysis representing the data from the phylogenetic tree from (**B**) different Phyla, and (**C**) various Classes within phylum Chordata. The number on the pie-chart represents number of ABHD12 sequences within that respective category. The pie-chart analysis shows that phylum Chordata contains most of the ABHD12 sequences, distributed in classes Aves, Actinopterygii and Mammalia.*

Sequence conservation within ABHD12 protein sequences (With Archit Devarajan)

To determine the extent of conservation in ABHD12 sequences across various organisms, we performed a multiple sequence alignment analysis on the 860 identified ABHD12 orthologs. From this analysis, we found that 96 residues (out of the 398 residues from human ABHD12) were positionally conserved at a frequency of > 90% across all the 860 identified ABHD12 orthologs, showing that the overall protein sequence conservation across all organisms is ~ 24%. Next, as previously reported by us[92], we formed five distinct groups of functionally conserved amino acid residues **(Table 2)** : e.g. acidic amino acids, basic amino acids, amino acids containing heteroatoms, aromatic amino acids, and hydrophobic amino acids, and assessed the aligned sequences for functionally conserved residues. Based on this analysis, we found that another 69 residues (out of the 398 residues from human ABHD12) were functionally conserved across the identified ABHD12 orthologs, suggesting that the overall conservation in ABHD12 sequences across various organisms was high (~ 42%). Next, a closer inspection of identified ABHD12 sequences within a particular class showed that within a particular class (e.g. *Mammalia*), there was a very-high sequence conservation of ABHD12 (> 80%), and an ABHD12 sequence from that class might serve as a representative example for the entire class. Across different classes within a particular phylum (e.g. *Chordata*), the overall sequence conservation was found to be about 60% for the identified ABHD12 sequences in that phylum. Of note, our sequence conservation analysis shows that several missense mutations in ABHD12 that are associated with the human neurological disorder PHARC (i.e. P87T, T125M, R186P, T202I, T253R, H372Q, L385P)[105–107], occur in residues that are highly conserved across ABHD12 sequences from all organisms, and perhaps, highlight the importance of these residues in the biochemical activity of ABHD12.

Table 2: Groups chosen for pooling amino acids with similar functions

Group 1	Group 2	Group 3	Group 4	Group 5
Glycine (G)	Phenylalanine (F)	Cysteine (C)	Lysine (K)	Glutamine (N)
Alanine (A)	Tryptophan (W)	Serine (S)	Histidine (H)	Glutamate (D)
Valine (V)	Tyrosine (Y)	Threonine (T)	Arginine (R)	Asparagine (Q)
Leucine (L)		Methionine (M)		Aspartate (E)
Isoleucine (I)				
Methionine (M)				

Structural assessment of the ABHD12 protein sequence (With Archit Devarajan)

In the absence of an experimentally solved three-dimensional structure of ABHD12, to establish a structure-sequence relationship, we decided to use the structure of hABHD12 (UniProt ID: Q8N2K0) that was generated by the AlphaFold algorithm[84]. To ensure that this predicted AlphaFold structure was reliable for our analysis, we overlaid this hABHD12 structure with an experimentally solved structure of human ABHD14B (PDB ID: 1imj)[108,109] (**Fig 2.5 A**). From this analysis, we observed that despite being distantly related within the metabolic SH family[88] (sequence identity <15%), the ABHD-folds of both these enzymes overlay well (RMSD ~ 3.5 Å). Furthermore, we also found that the catalytic triad of the active sites (critical for catalysis) for both these enzymes had very similar orientations, poised for optimal catalysis (**Fig 2.5 B**). This congruence in the overall ABHD-fold and the active site orientations, despite the evolutionary distance, provided sufficient confidence that the predicted structure of hABHD12 would be useful for further structural analyses.

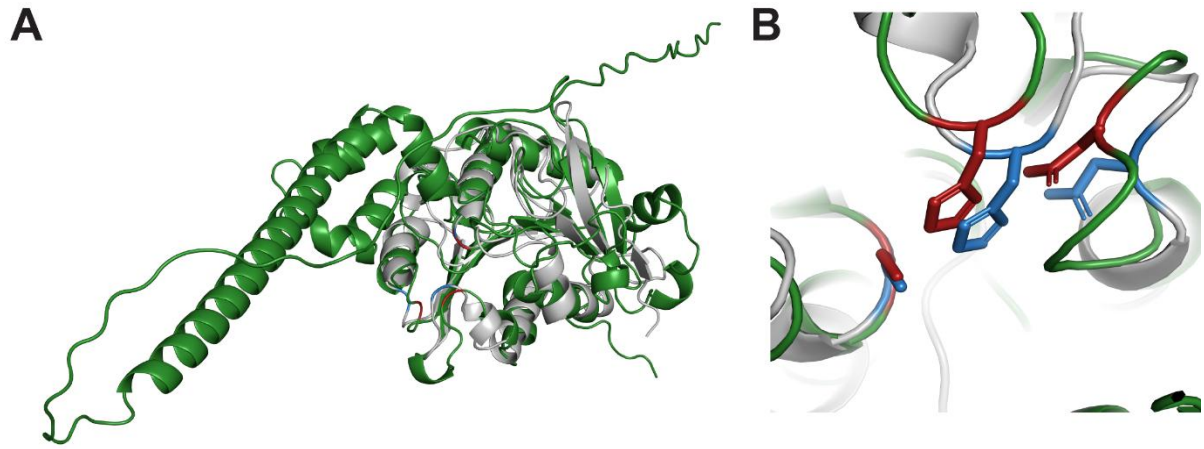

Fig 2.5: Structural alignment of hABHD12 and human ABHD14B. *(A) Overlay of the experimentally solved structure of human ABHD14B (grey) (PDB: 1imj) and the AlphaFold predicted structure of hABHD12 (green) (UniProt ID: Q8N2K0), showing a good overall alignment of both structures, especially the ABHD-portion of the structure. (B) Overlay of the catalytic triad of human ABHD14B (blue) and hABHD12 (red), showing a near perfect orientation of the catalytic triad of the AlphaFold predicted structure of hABHD12.*

Notably, the AlphaFold structure of hABHD12 also displayed an α-helical domain at the N-terminus of the protein sequence that presumably anchors this enzyme to the ER membrane, consistent with previous experimental observations[32,91]. Next, we mapped all the conserved residues (including functionally conserved residues) on the hABHD12 AlphaFold structure

(**Fig 2.6**). From this structural mapping, we found that most conserved residues clustered around the enzyme active site (catalytic triad) and the regions adjoining it, that comprise of a cleft and few flexible loops predicted to recognize and bind the substrate.

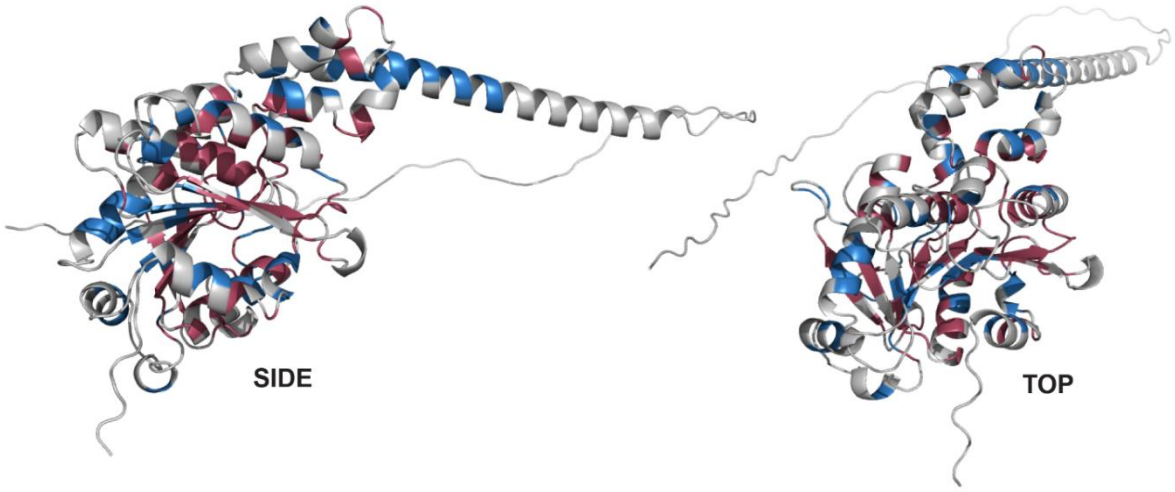

Fig 2.6: Mapping the conserved residues on the hABHD12 AlphaFold structure. *The residues colored in red are fully conserved, while those shown in blue are functionally conserved are shown on the hABHD12 AlphaFold structure (UniProt ID: Q8N2K0) based on the multiple sequence alignment analysis done on all the ABHD12 sequences from 860 different organisms.*

To identify the putative lyso-PS binding pocket of hABHD12 and understand how the substrate accesses the active site, we used two computational tools (CAVER and MOLE 2.5[100,101]) to map possible tunnels in the protein. Both the tools computed multiple tunnels in hABHD12, but only one surface channel/tunnel predicted by both the software included the crucial catalytic serine residue (Ser-246) needed for catalysis (**Fig 2.7 A**). This predicted catalytic pocket of hABHD12 comprises of 24 residues of which 19 are conserved (12 fully conserved + 7 functionally conserved).

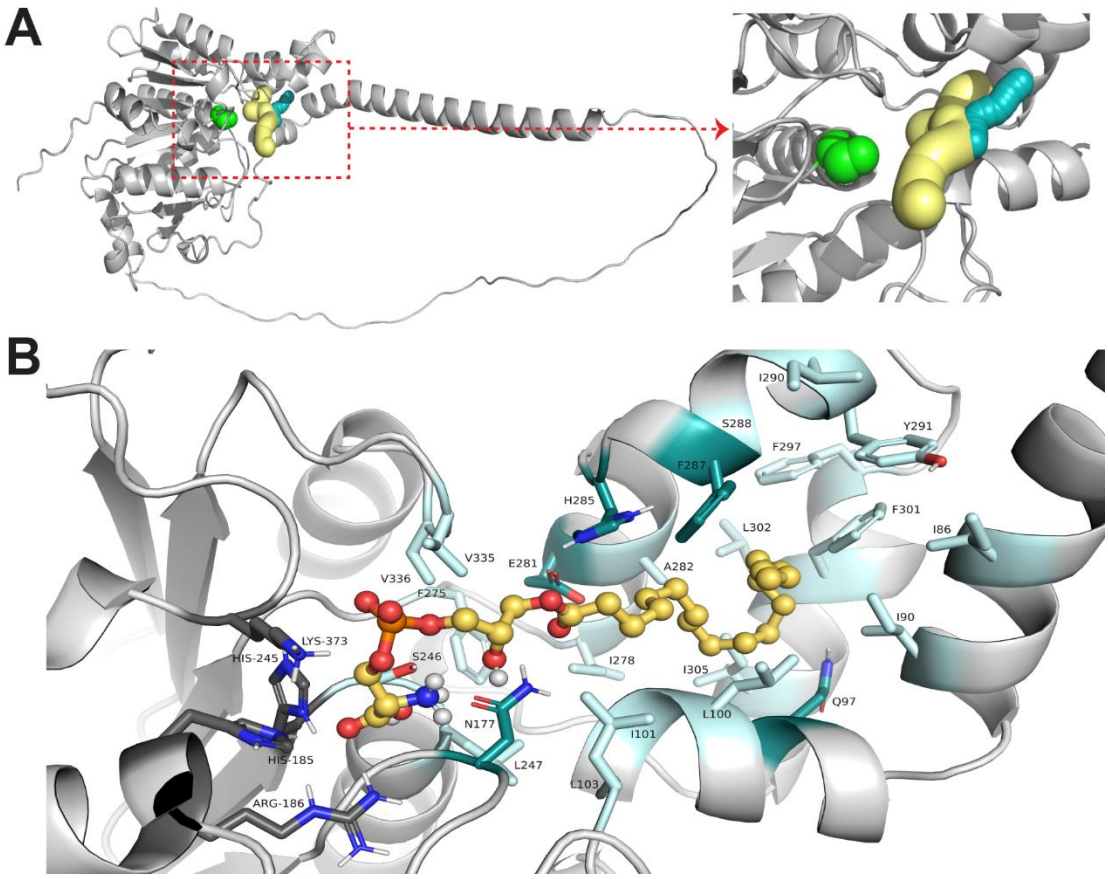

Fig 2.7: The lyso-PS binding pocket in hABHD12. *(**A**) Identification of a lyso-PS binding pocket using two computational tools (CAVER and MOLE 2.5) (left), and a zoomed in version of this lyso-PS binding pocket (right), showing its proximity to the active site serine (Ser-246) residue (green spheres). (**B**) Mapping the putative lyso-PS interacting residues on hABHD12 with C18:0 lyso-PS, which is docked in the lyso-PS binding pocket.*

Further, electrostatic calculations on the hABHD12 structure show a positively charged region in the catalytic pocket, distal to the transmembrane helix (**Fig 2.8**). This region might facilitate the binding and orientation of the negatively charged lyso-PS head group within the active site. Interestingly, Ser-246 is located at the bottom of a deep negatively charged pocket adjacent to this transmembrane helix, and perhaps negative charges push the carbonyl oxygen of the ester of lyso-PS away from the catalytic site, facilitating the nucleophilic attack by Ser-246 (**Fig 2.8**). Finally, molecular docking of C18:0 lyso-PS on hABHD12 indicates that the substrate interacts closely with Asn-177, Glu-281, and His-285 (all fully conserved) and the side chains of some hydrophobic residues (most of which are conserved) in the 9 predicted ligand-binding conformations of C18:0 lyso-PS (**Fig 2.7 B**). In addition to these, our modeling of C18:0 lyso-PS on hABHD12 also suggests that it

makes polar contacts with charged residues located outside the catalytic pocket, namely His-185, Arg-186, His-245, His-372 and Lys-373 (all fully conserved) (**Fig 2.7 B**).

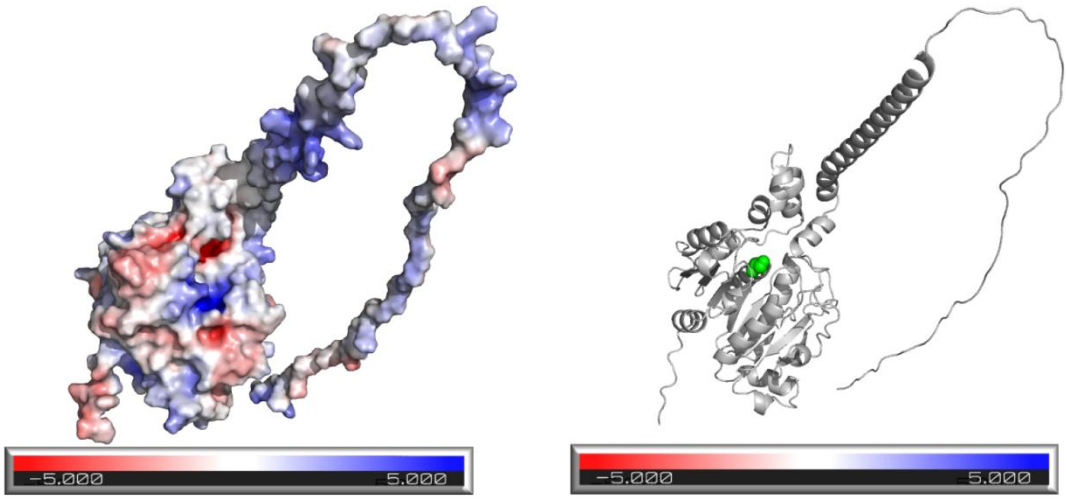

Fig 2.8: Electrostatic map of the predicted hABHD12 cavities. *Left, the predicted electrostatic map of the various cavities on the AlphaFold predicted structure of hABHD12 identified using various software. Right, the same orientation of the structure of hABHD12 showing the position of the catalytic serine residue (green balls), to understand the electrostatic map in the context of the enzyme active site.*

Lastly, as part of this structural analysis, we also mapped the various missense PHARC mutants (P87T, T125M, R186P, T202I, T253R, H372Q, L385P) on the hABHD12 AlphaFold structure (**Fig 2.9**). Quite interestingly, we found that most of these missense mutations are on conserved residues that are part of important structural elements, such as α-helices or β-strands, or near the active site. Based on this structural analysis, we think that these missense PHARC mutations are most probably going to affect local structures, which in turn are likely to affect the stability and overall enzymatic activity of hABHD12.

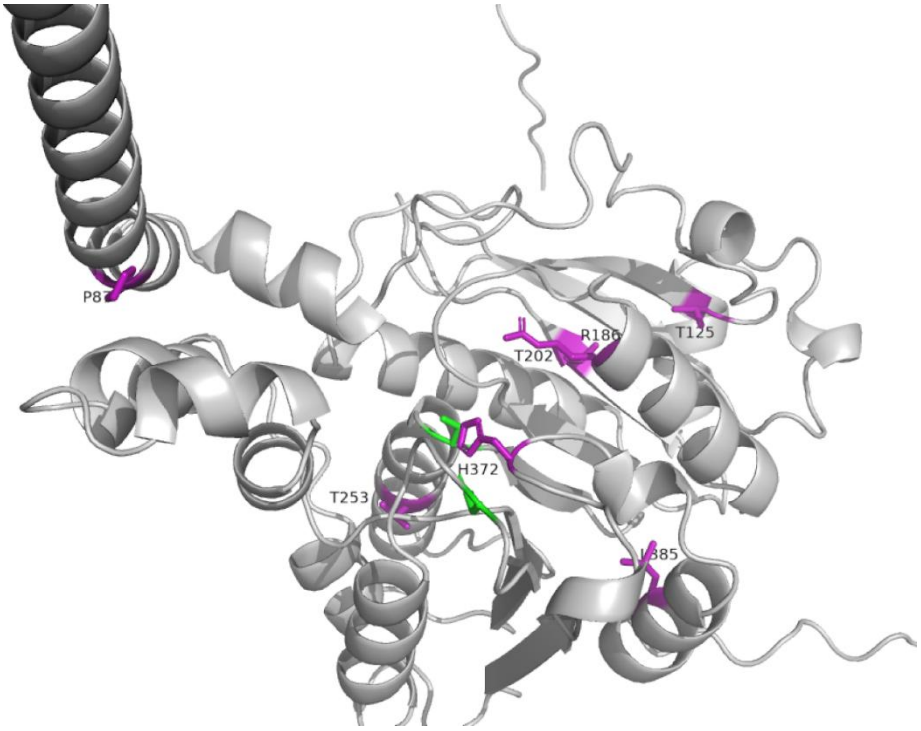

Fig 2.9: Mapping the locations of the identified missense PHARC mutations on the AlphaFold predicted structure of hABHD12 (green) (UniProt ID: Q8N2K0)

Biochemical characterization of mABHD12 variants.

Based on the structural mapping of conserved residues and the modeling of lyso-PS in the active site of hABHD12, we decided to biochemically validate the role of some residues in the enzymatic (lyso-PS lipase) activity. The hABHD12 and mABHD12 homologs are nearly identical in protein sequences (sequence identify 94%), and all residues discussed earlier are completely conserved between these two sequences at the very same position. Hence, since we have previously established the overexpression and activity assays with recombinant mABHD12 from mammalian HEK293T cell membrane proteomes, we decided to perform all biochemical validations using mABHD12[29,91].

From the bioinformatics and structural analysis, we shortlisted 22 conserved residues that were either part of the catalytic triad, proximal to the active site, or interactors of lyso-PS or residues having missense mutations in human PHARC subjects and mutated these to either alanine or the corresponding pathogenic PHARC variants for further biochemical studies (**Table 3**). All mutants were individually assayed using established gel-based ABPP assays and LC-MS based lyso-PS lipase assays to determine the nucleophilicity of the catalytic serine (Ser-246) and its ability to turn over the lyso-PS substrate, respectively.

Table 3: List of conserved residues selected for mutation and biochemical assays.

Category	Mutants Made
Catalytic triad	S246A, D333A, H372A
Proximal to active site	Y205A, W243A, D332A
Lyso-PS interacting residues	Q97A, N177A, H185A, R186A, H245A, N277A, E281A, H285A, F287A, K373A
Possible glycosylation sites	N123A, N277A
PHARC missense mutants	P87T, T125M, R186P, T202I, T253R, H372Q, L385P

First, we assayed the mutants of the residues from the catalytic triad (S246A, D333A and H372A) and those proximal to the active site (Y205A, W243A, and D332A). Gel-based ABPP assays showed that mutations to the residues from the catalytic triad or those proximal to the active site resulted in substantial loss of the nucleophilicity of Ser-246 relative to the WT control (**Fig 2.10 A**). Consistent with the gel-based ABPP assays, we found that except for D333A, mutations to all the aforementioned residues from the catalytic triad or those proximal to the active site resulted in almost complete loss of the lyso-PS lipase activity relative to the WT control (**Fig 2.10 B**). Interestingly, we found that while the D333A mutant resulted in the significant loss of nucleophilicity of Ser-246 based on gel-based ABPP assays (**Fig 2.10 A**), it retained ~ 20% WT mABHD12 lyso-PS lipase activity **Fig 2.10 B**), suggesting that the catalytic dyad of Ser-246 and His-372, were semi-competent in performing the enzymatic activity.

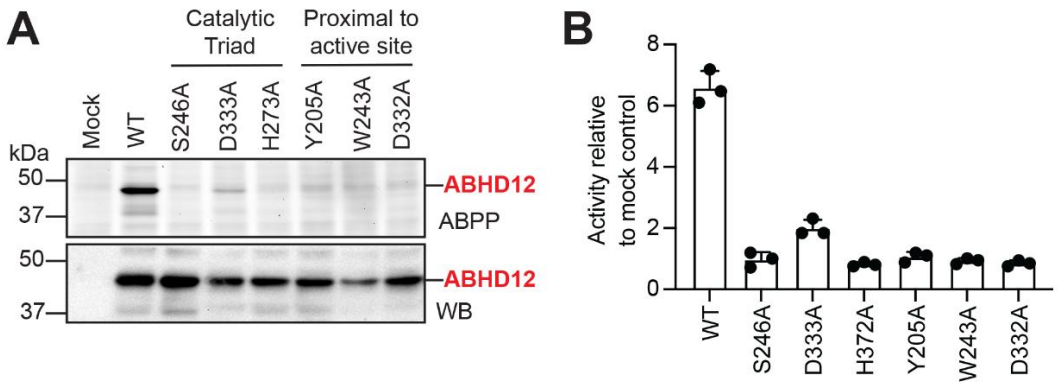

Fig 2.10: Biochemical characterization of mutants of the catalytic triad and residues proximal to the active site of mABHD12. *(**A**) Membrane proteome fractions of HEK293T cells transfected with mock, WT mABHD12, or various mutants of the catalytic triad (S246A, D333A, H372A) or conserved residues proximal to the active site (Y205A, W243A, D332A) were assessed by gel-based ABPP (top panel), and Western blot (WB) analysis using an anti-ABHD12 antibody (bottom panel). The band corresponding to ABHD12 (in red) represents the activity (top panel) and expression (bottom panel) of mABHD12 variants in membrane proteome fractions of HEK293T cells. This experiment was done three times with reproducible results each time. (**B**) The lyso-PS lipase activity shown by membrane proteome fractions of HEK293T cells transfected with mock, WT mABHD12, or various mutants of the catalytic triad (S246A, D333A, H372A) or conserved residues proximal to the active site (Y205A, W243A, D332A). The bar data represents the mean ± standard deviation from three biological replicates per group. In **(B)**, all data points have been normalized to a "mock" control (not shown, average value = 1).*

Next, we assayed all the mutants of the residues predicted to interact with lyso-PS (based on the docking studies) (Q97A, N177A, H185A, R186A, H245A, N277A, E281A, H285A, F287A, K373A), and the possible glycosylation sites (N123A, N277A). We have previously shown that glycosylation is critical for ABHD12 activity[91], and hence, we were interested in mapping the glycosylation site on ABHD12. Gel-based ABPP assays showed that while both mutants (N123A, N277A) showed diminished nucleophilicity of Ser-246, the N123A mutant, but not the N277A mutant, migrated significantly lower on the gel (based on the Western blot analysis) relative to the WT control, consistent with a non-glycosylated variant of mABHD12 (**Fig 2.11 A**). Further, lyso-PS lipase activity assays showed that both mutants (N123A, N277A) had almost complete loss of this enzymatic activity relative to the WT control (**Fig 2.11 B**), suggesting that Asn-123 is likely the site of glycosylation on

ABHD12, while Asn-277 is an important lyso-PS interacting residue on ABHD12. Further, gel-based ABPP assays showed that amongst the various mutants for the lyso-PS interacting residues, Q97A, N177A, H185A, H285A, F287A, and K373A showed almost WT equivalent nucleophilicity of Ser-246 (**Fig 2.11 A**). Quite surprisingly, the E281A mutant showed substantially more activity relative to the WT control in gel-based ABPP assays (**Fig 2.11 A**). Amongst these lyso-PS interacting residue mutants, R186A and H245A (along with N277A) showed no discernable activity relative to the WT control (**Fig 2.11 A**). Interestingly, while several mutants showed that the nucleophilicity of the active site Ser-246 was comparable to the WT control, lyso-PS lipase assays showed that only E281A mutant (~ 90% of WT control), and to a lesser extent, Q97 and F287A (~ 50% of WT control), had this enzymatic activity (**Fig 2.11 B**). Mutations to all other lyso-PS interacting residues resulted in an almost complete loss of lyso-PS lipase activity, suggesting their importance in binding lyso-PS (**Fig 2.11 B**).

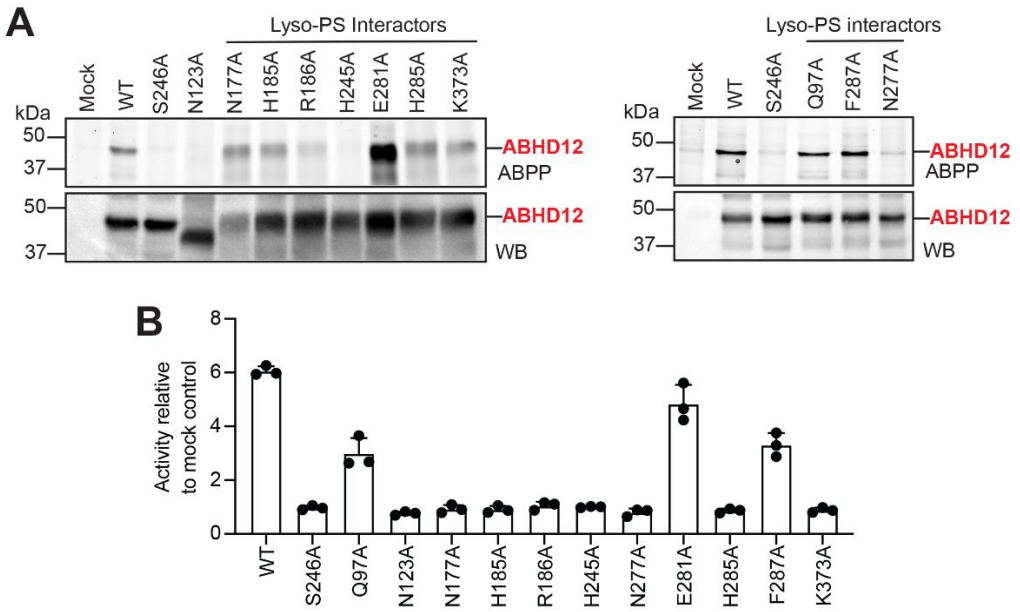

Fig 2.11. Biochemical characterization of mutants of residues predicted to bind lyso-PS or involved in glycosylation of mABHD12. *(**A**) Membrane proteome fractions of HEK293T cells transfected with mock, WT mABHD12, S246A mABHD12, or various mutants of residues predicted to bind/interact with lyso-PS (Q97A, N177A, H185A, R186A, H245A, N277A, E281A, H285A, F287A, K373A) or involved in glycosylation of mABHD12 (N123A, N277A) were assessed by gel-based ABPP (top panel), and Western blot (WB) analysis using an anti-ABHD12 antibody (bottom panel). The band corresponding to ABHD12 (in red)*

*represents the activity (top panel) and expression (bottom panel) of mABHD12 variants in membrane proteome fractions of HEK293T cells. This experiment was done three times with reproducible results each time. (**B**) The lyso-PS lipase activity shown by membrane proteome fractions of HEK293T cells transfected with mock, WT mABHD12, S246A mABHD12, or various mutants of residues predicted to bind/interact with lyso-PS (Q97A, N177A, H185A, R186A, H245A, N277A, E281A, H285A, F287A, K373A) or involved in glycosylation of mABHD12 (N123A, N277A). The bar data represents the mean ± standard deviation from three biological replicates per group. In both (**A**) and (**B**), the S246A mutant was used as an additional no activity controls in the assays. In **(B)**, all data points have been normalized to a "mock" control (not shown, average value = 1).*

Finally, we assayed all the missense mutants reported from human PHARC subjects (P87T, T125M, R186P, T202I, T253R, H372Q, L385P) using both the gel-based ABPP (**Fig 2.12 A**) and lyso-PS lipase activity (**Fig 2.12 B**) assays. Not surprisingly, we found that both the complementary assays showed that all the missense mutants reported from human PHARC subjects (P87T, T125M, R186P, T202I, T253R, H372Q, L385P) showed no discernable activity relative to the WT control. His-372 is part of the catalytic triad (**Fig 2.10**), and Arg-186 is an important residue involved in binding lyso-PS (**Fig 2.11**), and hence, together with our biochemical studies, missense mutations of these residues lacking enzymatic activity is expected. Based on the AlphaFold structure of hABHD12, we find that Pro-87, Thr-202, Thr-253 and Leu-385 are all highly conserved residues that are present on structurally conserved α-helices (**Fig 2.9**).

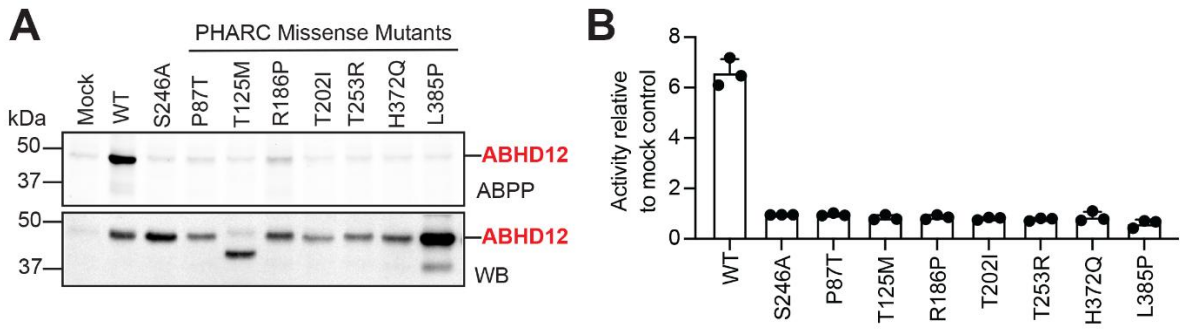

Fig 2.12: Biochemical characterization of missense mutations from human PHARC subjects. *(**A**) Membrane proteome fractions of HEK293T cells transfected with mock, WT mABHD12, S246A mABHD12, or various mutants of missense mutations from human PHARC subjects (P87T, T125M, R186P, T202I, T253R, H372Q, L385P) were assessed by*

*gel-based ABPP (top panel), and Western blot (WB) analysis using an anti-ABHD12 antibody (bottom panel). The band corresponding to ABHD12 (in red) represents the activity (top panel) and expression (bottom panel) of mABHD12 variants in membrane proteome fractions of HEK293T cells. This experiment was done three times with reproducible results each time. (**B**) The lyso-PS lipase activity shown by membrane proteome fractions of HEK293T cells transfected with mock, WT mABHD12, S246A mABHD12, or various mutants of missense mutations from human PHARC subjects (P87T, T125M, R186P, T202I, T253R, H372Q, L385P). The bar data represents the mean ± standard deviation from three biological replicates per group. In both (**A**) and (**B**), the S246A mutant was used as an additional no activity controls in the assays. In **(B)**, all data points have been normalized to a "mock" control (not shown, average value = 1).*

We hypothesize that the missense mutations to these residues (P87T, T202I, T253R, L385P) most likely destabilize the local structure and perhaps, result in the loss of enzymatic activity of ABHD12. Amongst the missense mutations, interestingly, we find by Western blot analysis that T125M migrates significantly lower on the gel (**Fig 2.12 A**), and appears to exist predominantly in the non-glycosylated form of ABHD12. Given its proximity to Asn-123 (the putative glycosylation site on ABHD12), the T125M mutation likely disrupts the glycosylation of ABHD12, and, by doing so, hampers the enzymatic activity.

Lyso-PS lipase activity of CG15111. (With Archit, Kundan, Rohith)

To understand the physiological and functional role that ABHD12 activity plays in the context of PHARC, two animal models, namely mouse (*Mus musculus*)[25] and zebrafish (*Danio rerio*)[107], have been reported. Over the years, *Drosophila melanogaster* (common fruit fly) has also served as an excellent animal model for studying various human neurodegenerative diseases, given the ease of genetically manipulating them[110,111]. A bioinformatics and phylogenetic analysis done previously in our lab identified an uncharacterized lipase CG15111 from the metabolic SH family in *D. melanogaster* as an ortholog of hABHD12 (sequence identity 37%)[112] (**Fig 2.13**).

Fig 2.13: Sequence alignment of hABHD12, mABHD12 and CG15111*. Sequence alignment of hABHD12, mABHD12 and CG15111 showing very high sequence homology between hABHD12 and mABHD12 (~ 94%), and high conservation between the three sequences for the acyltransferase motif (highlighted in blue), nucleophilic motif (highlighted in red), conserved aspartate (highlighted in green) and conserved histidine (highlighted in yellow), that together form the enzyme active site.*

To test if CG15111 possesses any lyso-PS lipase activity similar to that of mammalian ABHD12, we cloned and expressed wild-type (WT) CG15111 in insect (S2) cells using established protocols. Bioinformatics analysis suggested that Ser-241 of CG15111 is the catalytic nucleophile[112], and hence we made the S241A CG15111 mutant, and also expressed this in insect cells, as a negative control for the biochemical assays with CG15111.

By Western blot analysis, we found that relative to the "mock" control, both WT CG15111 and S241A CG15111 showed comparable overexpression in the membrane proteomic lysates of insect cells (**Fig 2.14 A**). Next, using gel-based ABPP assays, we showed that WT CG15111, but not the S241A CG15111 mutant, is active in the membrane proteomic lysates of insect cells (**Fig 2.14 A**). Furthermore, to ascertain if CG15111 can hydrolyze lyso-PS, we assayed all the aforementioned membrane proteomic lysates of insect cells, namely mock, WT CG15111, and S241A CG15111 for lyso-PS lipase activity. From this experiment we found that relative to "mock" control lysates, WT CG15111 had robust lyso-PS lipase activity, while the S241A CG15111 had negligible enzymatic activity for the same reaction (**Fig 2.14 B**). Taken together, these results confirm the bioinformatics prediction that CG15111 is indeed an ortholog of mammalian ABHD12 that possesses robust lyso-PS lipase activity, and Ser-241 of CG15111 is the conserved nucleophilic serine residue critical for catalysis.

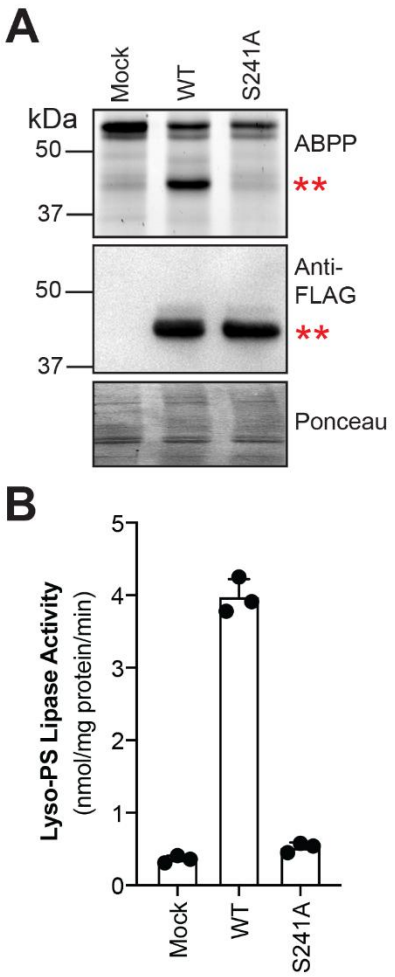

Fig 2.14: Enzymatic activity of CG15111 expressed in S2 cells. *(**A**) Membrane proteomic fractions of S2 cells transfected with mock, WT CG15111, or S241A CG15111 were assessed by gel-based ABPP (top panel), Western blot analysis using an anti-FLAG antibody (middle panel), and Ponceau S staining (bottom panel). The double red asterisk represents the activity (top panel) and expression (middle panel) of CG15111 in membrane proteomic fractions of S2 cells. This experiment was done three times with reproducible results each time. (**B**) The lyso-PS lipase activity shown by membrane proteomic fractions of S2 cells transfected with mock, WT CG15111, or S241A CG15111. The data shows that WT CG15111, but not S241A CG15111, has robust lyso-PS lipase activity. The bar data represents the mean ± standard deviation from three biological replicates per group.*

DISCUSSION

Advances in DNA sequencing technologies have greatly facilitated our understanding of the genetic basis of hereditary human disorders[113]. Of note, to date, genome mapping and sequencing efforts from human subjects suffering from a variety of clinical symptoms have led to the identification of >4500 inherited human diseases (cataloged in the OMIM database), with newer pathogenic mutations still being discovered at a rapid rate. As newer disease-causing mutations continue to be mapped in humans, it is becoming apparent that many of the affected genes code for proteins that are uncharacterized and/or have poorly understood biochemical function[114]. Hence, mechanistically characterizing the biochemical functions of such proteins is going to be critical to achieve a deeper mechanistic understanding of human genetic disorders and for identifying potential strategies for treating them. The neurological disorder PHARC serves as a nice example of this premise in the context of human hereditary diseases[72]. In 2010, genome sequencing efforts led to the identification of PHARC as an autosomal recessive genetic disorder in humans caused by deleterious mutations in the *abhd12* gene[69,70]. Since this discovery, over the past decade, >30 distinct homozygous or compound heterozygous mutations (deletion-insertion, nonsense, frameshift, splice site, and missense type mutations) in the *abhd12* gene have now been identified, all leading to the symptoms associated with PHARC in humans[72]. The *abhd12* gene encodes an integral membrane associated lipase ABHD12 from the metabolic SH family, that physiologically functions as the major lyso-PS lipase in the mammalian central nervous and immune systems (**Fig 2.1, Fig 2.2, Fig 2.3**)[25,91]. While mutations (e.g., deletion-insertion, nonsense, frameshift, and splice site) leading to the truncated full-length ABHD12 protein in the context of PHARC have been easy to reconcile in terms of the enzymatic activity of this lipase, the various missense mutations associated with PHARC in particular, remain difficult to biochemically explain in the absence of any detailed protein sequence-enzyme activity relationship studies for ABHD12.

To overcome this knowledge gap and develop a protein sequence-enzyme activity relationship profile for ABHD12, we first performed a thorough bioinformatics analysis and collated all putative ABHD12 sequences from all sequenced organisms across the evolutionary time scale (**Fig 2.4**). Next, complementarily using multiple sequence alignment analysis and the AlphaFold structure of hABHd12, we generated a map of the structurally conserved residues across all ABHD12 sequences, and found that a significant portion of the overall ABHD12 structure is conserved across all organisms (**Fig 2.6**). Further, using this

information along with molecular docking of C18:0 lyso-PS into ABHD12, we identified a hydrophobic cavity near the active site that is capable of binding lyso-PS, and shortlisted putative lyso-PS interacting residues from this analysis **(Fig 2.7)**. Following up on all the *in-silico* analysis, using gel-based ABPP and LC-MS based lyso-PS lipase activity assays, we biochemically assayed several ABHD12 mutants. These ABHD12 mutants **(Table 3)** comprised of residues that are part of the catalytic triad or proximal to the active site (**Fig 2.10**), or residues that interact with and enable binding of lyso-PS (**Fig 2.11**) or missense mutants that are found in human PHARC subjects (**Fig 2.12**). Together, these studies establish the first exhaustive sequence-enzyme activity relationship for ABHD12, and explain why missense mutations found in human PHARC subjects lack lyso-PS lipase activity. Finally, our evolutionary analysis identified a fly ortholog of hABHD12, CG15111 **(Fig 2.13)**. We recombinantly expressed this fly ortholog of hABHD12 and showed that CG15111 has robust lyso-PS lipase activity (**Fig 2.14**).

Moving forward, firstly, the bioinformatics and the sequence-enzyme activity relationship data generated in this study might prove to be a valuable predictive tool in understanding why emerging missense mutations in ABHD12 associated with human PHARC subjects result in diminished lyso-PS lipase activity. Secondly, we have shown that ABHD12 needs to be glycosylated for optimal activity, and prefers VLC lyso-PSs as substrates. While there is enough biochemical evidence in support of the need for glycosylation and the substrate preference of ABHD12, the AlphaFold predicted structure of hABHD12 and molecular docking studies cannot fully explain both of these. Hence, solving the structure of ABHD12 experimentally might be needed to corroborate these biochemical findings and understand in more detail the substrate preference and the structural effect that glycosylation has on the enzymatic activity of ABHD12. Lastly, our identification of CG15111, the fly ortholog of hABHD12, opens several new research avenues to biochemically explore how dysregulated ABHD12 activity might contribute to PHARC. For example, given the lifespan of flies (relative to mice models), understanding the age-dependent progression and neurobehavioral defects associated with PHARC can be studied in a quicker time scale, particularly in the context of the missense mutations found in human PHARC subjects. Towards this, it would also be interesting to see if genetic tools (such as CRISPR/Cas9) can be used in flies to first model the missense mutations found in human PHARC subjects, and then, if these mutations can also be reversed (or rescued) using the same genetic approaches. Such studies from fly models in the future may hold promise in

personalized gene therapy for treating PHARC and perhaps, even other similar hereditary human diseases.

PUBLICATION

Chakraborty, Arnab, Devarajan, Archit, Kundan Kumar, Rohith C.S., M.S. Madhusudhan, Girish S. Ratnaparkhi, and Siddhesh S. Kamat. " Bioinformatics Analysis Identifies Sequence Determinants of Enzymatic Activity for the PHARC-Associated Lipase ABHD12" ***Biochemistry*** (2025) 10.1021/acs.biochem.4c00865

Chapter 3: Identification of ABHD6 as a lyso-PS lipase in the mammalian liver and kidneys

Chapter summary: Lysophosphatidylserine (lyso-PS) is a potent hormone-like signaling lysophospholipid, which regulates many facets of mammalian biology and dysregulation in its metabolism is associated with several human neurological and autoimmune diseases. Despite the physiological importance and causal relation with human pathophysiology, little is known about the metabolism of lyso-PS in tissues other than the nervous and immune systems. To address this problem, we attempted to identify one (or more) lipase(s) capable of degrading lyso-PS in different mammalian tissues. We found that the membrane proteomic fractions of most mammalian tissues possess lyso-PS lipase activity, yet interestingly, the only bona fide lyso-PS lipase ABHD12 displays this enzymatic activity and has control over lyso-PS metabolism only in the mammalian brain. We subsequently performed a literature survey to identify metabolic serine hydrolases that could be putative lyso-PS lipases. These enzymes were overexpressed in HEK293T cells and were assayed for their lyso-PS lipase activity, but were unable to find any enzymes that could robustly degrade lyso-PS compared to ABHD12. Next, using an *in vitro* inhibitor screen against membrane proteomic fractions of different tissues, we found that another lipase from the metabolic serine hydrolase family, ABHD6, is a putative lyso-PS lipase in the mouse liver and kidney. Finally, using pharmacological tools, we validated the lyso-PS lipase activity of ABHD6 *in vivo*, and functionally designated this enzyme as a major lyso-PS lipase in primary hepatocytes, and the mammalian liver and kidneys. Finally, we confirmed the lyso-PS lipase activity of ABHD6 by overexpressing it in HEK293T cells and validating it against a lyso-PS substrate.

INTRODUCTION

Discussed in detail in Chapter 1, the glycerolysophospholipid lysophosphatidylserine (lyso-PS) is fast emerging as an important signaling lipid, which is central to the functioning of many important biological processes in mammals, including humans[10]. Given its indispensable role in physiology, over the past two decades, the biochemical activities and mechanisms associated with lyso-PS metabolism and signaling have been extensively investigated, mostly in the context of the mammalian central nervous and immune system[10]. This study bias stems from numerous genetic mapping of human subjects (patients) or population-level genome-wide association studies, which causally link the dysregulation in lyso-PS metabolism or signaling to an array of hereditary neurological and autoimmune diseases in humans[10,70,73,74,79,80]. Despite this, it is now apparent from several recent reports that lyso-PS is quite abundant in almost all mammalian tissues, and yet, very little remains

known of its physiological role or metabolism beyond the human nervous and immune systems.

Given its amphiphilic (hydrophilic and lipophilic) chemical nature, lyso-PS acts as a very potent hormone-like signaling molecule. Hence, the physiological concentrations of lyso-PS are tightly regulated by dedicated enzymes in all mammalian tissues. For example, lyso-PS is biosynthesized from phosphatidylserine (PS) precursors by the action of PS-specific phospholipases. In the mammalian central nervous and immune systems, the α/β-hydrolase domain containing protein # 16A (ABHD16A)[26,32] and PS-specific phospholipase A1 (PS-PLA1)[115,116] have been functionally characterized as PS lipases that tightly control concentrations of intracellular and secreted lyso-PS respectively. On the other hand, lyso-PS signaling in mammals is presumably terminated in all tissues either by its hydrolysis to free fatty acid and glycerophosphoserine by the action of lyso-PS lipases (**Fig 3.1**) or via its conversion back to PS by the enzymatic action of lyso-PS specific acyltransferases[10].To date, in mammals (including humans), the α/β-hydrolase domain containing protein # 12 (ABHD12) remains the only functionally characterized lyso-PS lipase and its functions have been extensively investigated in diverse neurological and immunological settings[25,29,31,91]. More recently, the lysophosphatidylcholine-specific acyltransferase 3 (LPCAT3) was shown to have selectivity towards arachidonoyl-coenzyme A (C20:4 Co-A) in the mammalian brain, where it specifically converts long chain lyso-PS species via an acyltransferase activity with C20:4-CoA to C20:4-containing PS lipids in this tissue[117]. Together, these studies show that it is the dynamic interplay between these lyso-PS metabolic enzymes, namely ABHD16A/PS-PLA1, ABHD12, and LPCAT3, that tightly regulates lyso-PS concentrations in the mammalian central nervous and immune systems. While the specifics of mammalian lyso-PS metabolism (both biosynthesis and degradation) have been well worked out in different neurological and immunological paradigms, comparatively, little is known of the enzymes that regulate this metabolism in other peripheral tissues.

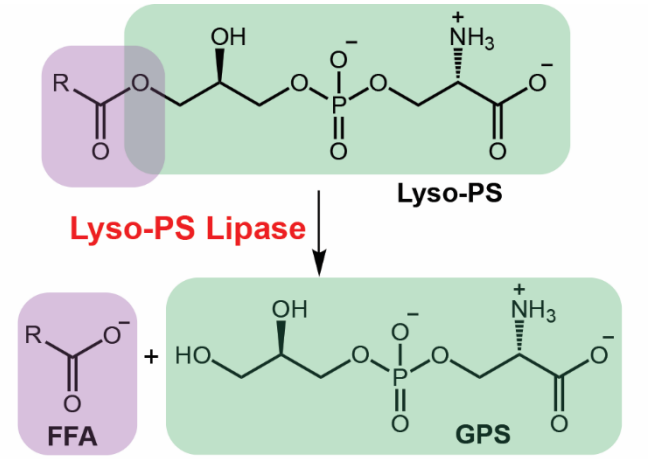

Fig 3.1: *Lyso-PS lipase reaction: The enzymatic reaction for the conversion of lyso-PS to free fatty acid (FFA) and glycerophosphoserine (GPS) by a lyso-PS lipase.*

To bridge this knowledge gap, we decided to determine whether peripheral tissues (tissues other than the brain) in mammals have lyso-PS lipase activity, and if ABHD12 and/or any other lipases regulate tissue lyso-PS levels via this enzymatic activity. Using tissue proteomic fractionation and substrate profiling assays, we found that all mouse tissues except the muscle possess lyso-PS lipase activity enriched in the membrane proteomic fraction, and this activity was largely contributed by one (or more) lipase(s) from the metabolic serine hydrolase (mSH) family of enzymes[86,88]. Further, using ABHD12 knockout mice[25], we found that this lyso-PS lipase can regulate lyso-PS concentrations only in the brain, and no other tissue. Using a focused inhibitor screen, we found that another lipase from the mSH enzyme family, the α/β-hydrolase domain containing protein # 6 (ABHD6) is possibly a lyso-PS lipase in the mouse liver and kidneys. By pharmacologically inhibiting ABHD6, we showed that this lipase controls concentrations of lyso-PS *in vivo* in primary hepatocytes and the liver and kidneys of mice, and thus functionally annotated ABHD6 as a major lyso-PS lipase in these mammalian tissues.

EXPERIMENTAL PROCEDURES

Materials.

Unless otherwise mentioned, all chemicals, buffers, and reagents were procured from Sigma Aldrich; all lipid standards were purchased from Avanti Polar Lipids; all mammalian tissue culture media and consumables were purchased from HiMedia; and all LC-MS grade solvents

were purchased from JT Baker. Wherever applicable, the materials' catalog numbers are mentioned in the respective sections below.

Mice Experiments.

All mouse studies and experiments described in this thesis have received formal approval from the Indian Institute of Science Education and Research, Pune – Institutional Animal Ethics Committee (application nos: IISER_Pune IAEC/2021_01/09; IISER_Pune IAEC/2022_01/05) constituted as per the guidelines and norms provided by the Committee for the Purpose of Control and Supervision of Experiments in Animals, Government of India. All experimental mice were housed in the National Facility for Gene Function in Health and Disease (NFGFHD), IISER Pune, and were studied between 2 – 3 months of age. All mice used in this study were from the C57BL/6J genetic background (RRID: IMSR_JAX:000664), and had *ab libitum* access to food and water. In all experiments, equal number of male and female mice were used. For studies involving ABHD12 knockout mice, age/sex matched littermates were used as controls. Primary hepatocytes were generated using established protocols previously reported by Ullas Kolthur's lab[118,119].

Preparation of Tissue Proteomic Fractions.

Mice were deeply anesthetized with isoflurane, and euthanized by cervical dislocation. Thereafter, the tissues of interest were surgically harvested, washed with cold sterile Dulbecco's phosphate buffered saline (DPBS) (HiMedia, catalog no: TL1006) (three times), weighed, flash-frozen in liquid nitrogen, and stored at -80 °C till further use. The pre-weighed tissues were thawed on ice, resuspended in 500 µL of ice-cold DPBS, and homogenized using a Bullet Blender 24 (Next Advance) using one scoop of 0.5-mm diameter glass beads (Next Advance) for brains, one scoop of 2.3-mm diameter stainless steel beads (Next Advance) for the liver, heart and spleen, and one scoop of 1-mm diameter zirconium oxide beads (Next Advance) for the kidneys and lungs, at a speed setting of 8 for 3 min at 4 °C (two times). To this tissue homogenate, 500 µL of cold sterile DPBS was added and mixed by pipetting. These homogenates were subsequently probe sonicated for 90 seconds (2 seconds on/off pulses at 60% amplitude) using a medium-sized probe, and these lysates were centrifuged at 1000g for 5 minutes at 4 °C to separate the beads and tissue debris from the tissue proteome. The resulting tissue lysate (supernatant, ~800 µL) was separated by pipetting and centrifuged at 100,000g for 45 minutes at 4 °C in an Optima MAX-XP Beckman coulter ultracentrifuge. Following ultracentrifugation, the resulting supernatant

(~500 µL) was separated by pipetting and labeled as the soluble proteomic fraction. The resulting pellet was washed three times with cold sterile DPBS, and resuspended in 400 µL cold sterile DPBS by sonication. The resulting lysate was labeled as the membrane proteomic fraction for a particular tissue. The protein concentrations of the membrane and soluble proteomic fractions were measured using the Pierce BCA Protein Assay Kits (Thermo Fisher Scientific, catalog no: 23225).

Preparation of Cellular Proteomic Fractions.

HEK293T (RRID: CVCL_0063, female) cells were purchased from the ATCC, and cultured and maintained as reported earlier[29]. Primary hepatocytes were generated using established protocols previously reported by Ullas Kolthur's lab[118,119]. All mammalian cells were harvested by scraping, and washed three-times with cold sterile DPBS. The cellular protein lysates were prepared by resuspending the cells in 500 µL DPBS, and probe sonicating them for 30 seconds (2 seconds on/off pulses at 60% amplitude) using a medium-sized probe. These lysates were subsequently centrifuged at 1000g for 5 minutes at 4 °C to separate the unlysed cells and debris from the proteome. The resulting cell lysate (supernatant, ~400 µL) was separated by pipetting and centrifuged at 100,000g for 45 minutes at 4 °C in an Optima MAX-XP Beckman coulter ultracentrifuge. Following ultracentrifugation, the resulting supernatant (~300 µL) was separated by pipetting and labeled as the soluble proteomic fraction. The resulting pellet was washed three times with cold sterile DPBS, and resuspended in 400 µL cold sterile DPBS by sonication. This resulting lysate was labeled as the membrane proteomic fraction for particular mammalian cells. The protein concentrations of the membrane and soluble proteomic fractions were measured using the Pierce BCA Protein Assay Kits (Thermo Fisher Scientific, catalog no: 23225).

Lyso-PS Lipase Substrate Assays.

All lyso-PS lipase substrate assays were done using LC-MS protocols previously reported by us[29,32]. Briefly, 20 µg of the soluble or membrane proteomic fraction obtained from mammalian tissues or cells was incubated with 100 µM lyso-PS substrate (C17:1 lyso-PS; Avanti Polar Lipids, catalog no: 858141) in DPBS to a final volume of 100 µL at 37 °C with constant shaking (Eppendorf, Thermo Mixer C). After letting the reaction proceed to 30 minutes, it was quenched with 300 µL of 2:1 chloroform ($CHCl_3$): methanol (MeOH) spiked with an internal standard (0.5 nmol of C15:0 free fatty acid (FFA); Sigma Aldrich, catalog

no: P6125). The mixture was vortexed vigorously and centrifuged at 2300g to separate the aqueous (top) and organic (bottom) phases. The organic phase was dried under a stream of nitrogen gas and resolubilized in 150 µL of 2:1 $CHCl_3$: MeOH for LC-MS analysis. This organic extract was injected into an Agilent G6125B single quadrupole LC/MSD and analyzed in the negative ion mode using an electrospray ionization (ESI) source. The LC separation was performed using a Gemini 5U C-18 column (Phenomenex) coupled with a Gemini guard column (Phenomenex, 4x3 mm, Phenomenex security cartridge). The solvents used were buffer A: 95:5 = Water: MeOH; and buffer B: 60:35:5 Isopropanol (IPA): MeOH: water. All runs were 15 minutes, starting with 0.3 mL/min 100% buffer A for 1.5 minutes, 0.5 mL/min linear gradient to 100% buffer B over 5 minutes, 0.5 mL/min 100% buffer B for 5.5 minutes, and equilibration with 0.5 mL/min 100% buffer A for 3 minutes. The following MS parameters were used: Drying gas flow = 10 L/min, nebulizer pressure = 45 Ψ, drying gas temperature = 250 °C, capillary voltage = 4 kV. The product release was quantified by measuring the area under the curve for the peak corresponding to C17:1 FFA (produced from C17:1 lyso-PS), and normalizing it to the internal standard (C15:0 FFA). The substrate hydrolysis rate was corrected by subtracting the non-enzymatic rate of hydrolysis, which was obtained by using heat-denatured (15 min at 95 °C) control proteomes.

Inhibitor Screen in Tissue Membrane Proteomic Fractions.

Membrane proteomic fractions (50 µL of 1 mg/mL) from different mouse tissues were incubated with different lipase inhibitors from the focused library **(Table 3)** at a concentration of 10 µM for 45 minutes. Following this, the lysates were subsequently assayed for lyso-PS lipase activity as described earlier. DMSO was used as a vehicle control (high control), whereas FP-rhodamine treatment (10 µM for 45 minutes; in case of liver, kidney, spleen) or heat denatured proteome (in case of heart, lungs) was used as loss of lyso-PS lipase control (low control) in this inhibitor screen.

Lyso-PS Measurements in Cells and Tissues.

Phospholipids, including lyso-PS, were extracted from mammalian cells or tissues using a modified Folch lipid extraction procedure[24] previously reported by us[32,91]. During the extraction, C17:1 lyso-PS (1 nmol per sample) was used as an internal standard. The dried

lipid extract was resuspended in 200 µL 2:1 $CHCl_3$: MeOH, and 10 µL of this was injected into an Agilent Technologies 6470 Triple Quadrupole LC/MS for quantification of lyso-PS using established multiple reaction monitoring (MRM) transition-based analysis previously reported in literature[25,26,32]. The LC parameters and runtime were identical to those described for the lyso-PS lipase substrate hydrolysis assays. All LC-MS analysis was performed in negative ion mode using ESI source the following parameters: drying and sheath gas temperature = 320 °C; drying and sheath gas flow = 10 L/min; nebulizer pressure = 45 Ψ; fragmentor voltage = 160 V; capillary voltage = 3000 V; and nozzle voltage = 1000 V. All lyso-PS species were quantified by normalizing their respective areas under the curve and normalizing it to the area under the curve of the internal standard (C17:1 lyso-PS) and then normalizing to tissue weight or total cellular proteins.

Untargeted Lipid Measurements.

The dried lipid extracts described in the previous section were resolubilized in 200 µL of 2:1 $CHCl_3$: MeOH and 10 µL was injected into an Agilent 6545 Quadrupole Time-Of-Flight (QTOF) LC-MS/MS for semi-quantitative analysis using high-resolution auto MS/MS methods and chromatography techniques. A Gemini 5U C-18 column (Phenomenex) coupled with a Gemini guard column (Phenomenex, 4x3 mm, Phenomenex security cartridge) was used for LC separation. The solvents used for the LC-MS analysis were buffer A: 95:5 water: MeOH, and buffer B: 60:35:5 IPA: MeOH: water. For negative ion mode analysis, 0.1% (v/v) ammonium hydroxide was added in each buffer, while 0.1% (v/v) formic acid + 10 mM ammonium formate were used as additives for analysis in the positive ion mode. All untargeted lipid measurement runs were 60 minutes, starting with 0.3 mL/min 100% buffer A for 5 minutes, 0.5 mL/min linear gradient to 100% buffer B over 40 minutes, 0.5 mL/min 100% buffer B for 10 minutes, and then equilibration with 0.5 mL/min 100% buffer A for 5 minutes. All LC-MS runs were performed using ESI source with the following MS parameters: drying and sheath gas temperature = 320 °C; drying and sheath gas flow rate = 10L/min; fragmentor voltage = 150 V; capillary voltage = 4 kV; nebulizer (ion source gas) pressure = 45 Ψ and nozzle voltage = 1 kV. For analysis of different lipids, particularly lysophospholipids, a curated lipid library was employed in the form of a Personal Compound Database Library (PCDL), and the peaks were validated based on relative retention times and MS/MS fragments obtained. All lipid species were quantified by normalizing areas under the

curve relative to the internal standard added and then normalized either to the tissue weight or total cellular proteins.

Gel-based ABPP Assays.

50 µL of 1mg/mL soluble or membrane proteomic fraction from mammalian cells or tissues were incubated with 2 µM FP-rhodamine for 45 minutes at 37°C with constant shaking (Eppendorf, Thermo Mixer C). The reactions were quenched by adding 20 µL of 4x SDS-PAGE loading buffer followed by boiling for 5 minutes, and 40µL of this sample was loaded on a 12.5% SDS-PAGE gel. Competitive gel-based ABPP experiments were done as reported earlier[29]. All gels were visualized using an iBright1500 gel documentation system (Invitrogen).

Overexpression of different lipases in HEK293T cells.

cDNA for mABHD6, mPLA2G15, hPLA2G15, hLYPLA2, mLYPLA1, hLYPLA1, mPNPLA7 and hPNPLA7 in pCMV-Sport6 vector were purchased from Horizon Discovery and the details are in **Table 4**. The full-length cDNA of mouse ABHD6 (Horizon Discovery Clone No.: 5369937) was cloned into pcDNA3.1 myc-His A(-) vector between EcoRI and BamHI restriction sites. The S148A mutant of mouse ABHD6 mutant was generated from the same plasmid using PFU DNA polymerase (Promega, catalog no.: M7745) and DpnI (New England Biolabs, catalog no.: R0176L) as per manufacturer instructions.

HEK293T cells were cultured in RPMI1640 medium (HiMedia, catalog no.: AL028A-500ML) supplemented with 10% (v/v) Fetal Bovine Serum (FBS) (Invitrogen) and 1x penicillin-streptomycin (MP Biomedicals) at 37 ºC with 5% (v/v) CO_2. The cells were grown to 40% confluence and transiently transfected with the cDNA of WT or S148A ABHD6 using polyethyleneimine "MAX" (MW 40,000) (PEI) (Polysciences Inc.). Mock transfected cells were transiently transfected with an empty vector to be used as a control for subsequent experiments. The HEK293T cells were harvested 48 hours post transfection by scraping, washed with cold sterile DPBS (3X on ice), re-suspended in 1 mL of SPBS, and lysed by sonication. The membrane proteomic fraction was prepared as described in an earlier section. The overexpression of WT or S148A ABHD6 was confirmed by Western blot analysis. The primary and secondary antibodies used in this Western blot analysis were anti-6X His tag

antibody [HIS.H8] (Abcam, catalog no.: ab18184) and goat anti-mouse IgG H&L (HRP) (Abcam, catalog no.: ab6789) respectively.

Credit statement

Theja Sajeevan and Prajwal Punnamraju partially performed a few biochemical assays in this study and have been credited in those respective sections. Arshdeep Kaur cultured primary hepatocytes from mice and provided the plated cells.

RESULTS

Survey of lyso-PS lipase activity in peripheral tissues

While it is now clear that lyso-PS is present ubiquitously in almost all tissues in mammals, most studies pertaining to the metabolism (biosynthesis and degradation) of lyso-PS have surprisingly been restricted to the central nervous and immune systems[10]. Specifically, ABHD12 remains the only bona fide lyso-PS lipase to date [25,29,32,91], and it remains unknown if it can regulate levels of lyso-PSs in different peripheral tissues or if there exist other tissue-resident lipases that can independently regulate the levels of this signaling lysophospholipid in specific tissues. To investigate this, we harvested different mouse tissues (brain, liver, kidney, spleen, heart, lungs, muscle), generated protein lysates, and fractioned these lysates into soluble or membrane proteomic fractions by ultracentrifugation. Next, we profiled these different soluble and membrane proteomic fractions using a well-established liquid-chromatography coupled to mass spectrometry (LC-MS) assay to quantify lyso-PS lipase activity in different mouse tissues (**Fig 3.2 A**). From this profiling study, we found that all tissues except muscle had significant specific lyso-PS lipase activity, that was highly enriched in the membrane proteomic fraction (**Fig 3.2 A**). Interestingly, relative to the brain membrane lyso-PS lipase activity, this enzymatic activity in the liver and lungs was higher, while that in the kidney, spleen, and heart was comparable (**Fig 3.2 A**). This result suggests that one (or more) membrane-associated lipase(s) might be responsible for the lyso-PS lipase activities observed in different mouse tissues.

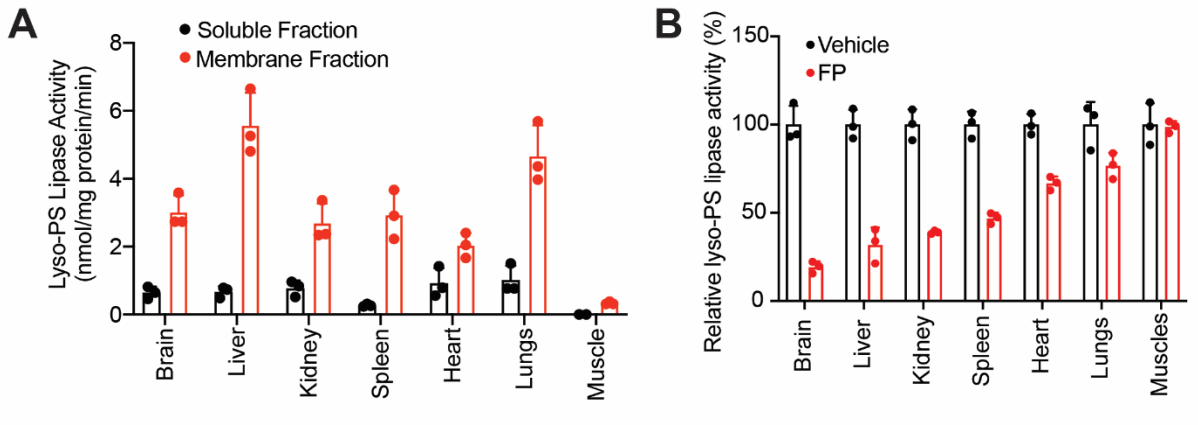

Fig 3.2: Profiling lyso-PS activity in different mammalian tissues. *(**A**) The lyso-PS lipase activity in the soluble and membrane proteomic fractions of different mouse tissues. (**B**) The relative lyso-PS lipase activity in the membrane proteomic fractions of different mouse tissues treated with vehicle (DMSO) or FP-rhodamine (20 μM, 45 min). All assays shown in (**A**) and (**B**) were done using 20 μg of proteome against 100 μM C17:1 lyso-PS for 30 min at 37 ℃. The bar data presented in (**A**) and (**B**) represents mean ± standard deviation from three biological replicates. Both these experiments were performed in part by Theja Sajeevan. Data points in (B) were plotted by normalizing all data points to the DMSO group in each tissue.*

In mammals, the mSH family of enzymes consists of a large number of membrane-associated lipases, a substantial fraction of which still lack any functional assignment [86,88]. Fluorophosphonate (FP) compounds serve as excellent active-site covalent inhibitors and in turn, activity-based probes for the mSHs. **(Fig 3.3)** Hence over the years, they have evolved as versatile chemical tools for fishing out unknown biological activities from this enzyme

family[120–123].

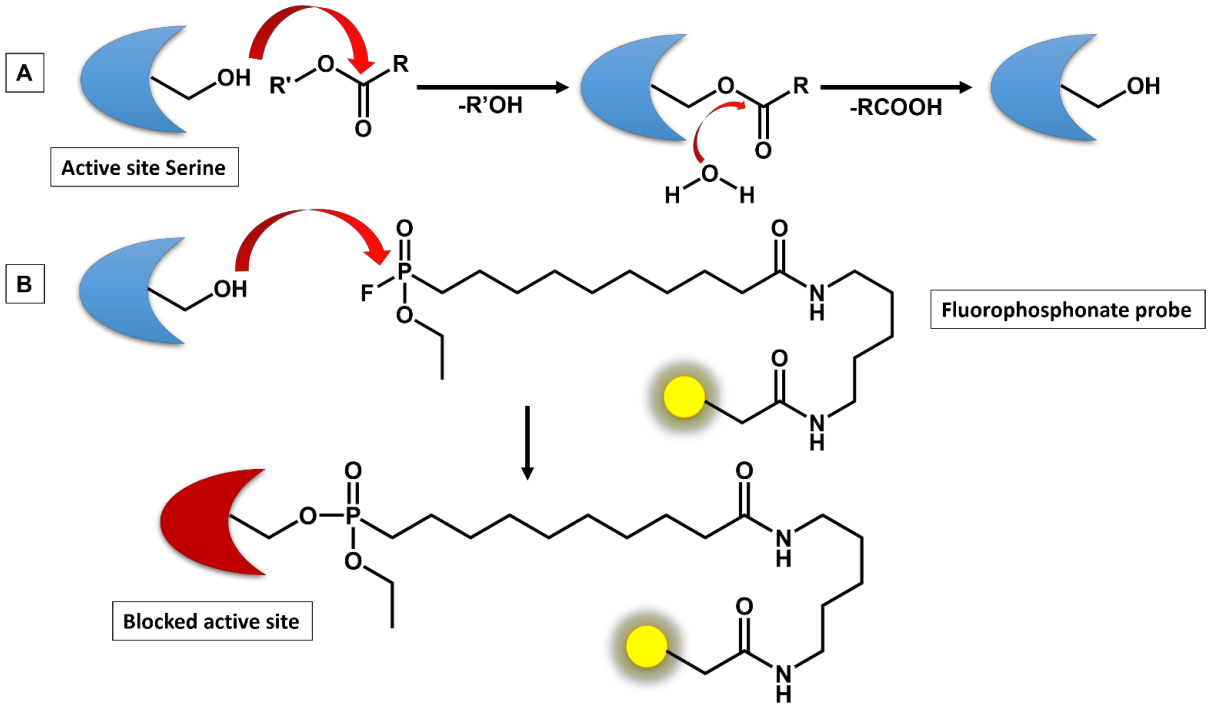

Fig 3.3: Serine Hydrolase catalysis and inhibition schematic *A. Mechanism of Serine Hydrolase catalysis. B. Inhibition of the active site by using a small molecule (Fluorophosphonate attached to a fluorescent molecule, in this case)*

To determine if one or more mSHs are indeed involved in the lyso-PS lipase activity observed in various mouse tissues, we treated the different tissue membrane proteomic fractions with a FP-probe (FP-rhodamine, 20 μM, 45 min), and subsequently assayed these lysates for lyso-PS lipase activity. From this experiment, we found that, except for the lungs and muscles, the lyso-PS lipase activity in most tissues was inhibited by a FP-probe (**Fig 3.2 B**). Specifically, FP-probe treatment showed the highest inhibition in the brain, but there was also >50% inhibition of the lyso-PS lipase activity in the membrane proteomic fraction of the liver and kidney (**Fig 3.2 B**). We also performed the same experiment in the soluble proteomic fractions of different tissues and found that FP-probe treatment did not have any effect (**Fig 3.4 A**). Together, this result shows that there is one (or more) membrane-associated mSH(s) that functions as a lyso-PS lipase in different mammalian tissues.

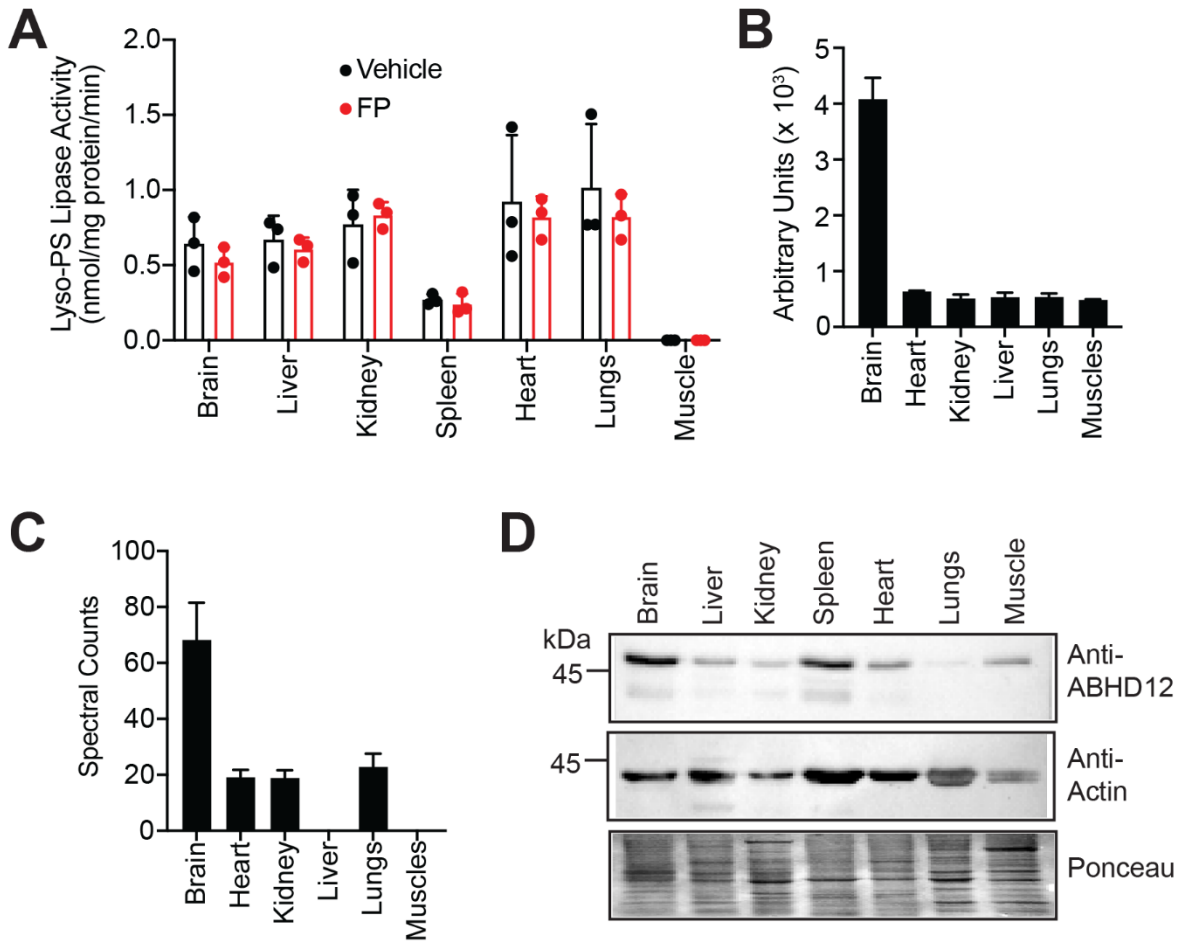

Fig 3.4: ABHD12 controls lyso-PS levels only in the mouse brain. *(**A**) The lyso-PS lipase activity in the soluble proteomic fractions of different mouse tissues treated with vehicle (DMSO) or FP-rhodamine (20 μM, 45 min). All assays were done using 20 μg of proteome against 100 μM C17:1 lyso-PS for 30 min at 37 °C. (**B**) The mRNA expression data exported from the large-scale gene expression database BioGPS, showing the heightened expression of ABHD12 in the mouse brain. (**C**) The activity of ABHD12 in various mouse tissues from a publicly available LC-MS based ABPP dataset (spectral counting-based data), showing the heightened activity of ABHD12 in the membrane proteomic fraction of the mouse brain. (**D**) A representative western blot, showing the tissue distribution of ABHD12, further confirming highest protein levels on ABHD12 in the membrane proteomic fraction of the mouse brain consistent with data from (**B**) and (**C**). 50 μg of each membrane proteome was loaded onto the gel, and both β-Actin and Ponceau staining were used as loading controls for this experiment. This immunoblotting study was done three times with reproducible result each time. (All bar plots presented in this figure represents mean ± standard deviation from two*

*(for **B**) or three (**A** and **C**) biological replicates. The experiment in Fig **A** was performed in part by Theja Sajeevan.*

As mentioned previously, studies have now conclusively shown that majority of the brain lyso-PS lipase activity comes from ABHD12, an integral membrane mSH enzyme. Since ABHD12 is the only functionally characterized lyso-PS lipase, we wanted to see if ABHD12 regulates lyso-PS levels in other tissues. Towards this, we first looked at a publicly available gene expression database (biogps.org)[124,125] (**Fig 3.4 B**), tissue-wide chemical proteomics datasets of mSHs[86] (**Fig 3.4 C**), and performed immunoblotting analysis on membrane proteomic fractions of different mouse tissues described earlier (**Fig 3.4 D**). Based on all of this data, we found that ABHD12 had the highest expression and enzymatic activity in the mammalian brain, and not much in other peripheral tissues. Additionally, we also performed lyso-PS lipase activity assays on the membrane proteomic fractions of different tissues obtained from wild-type or ABHD12 knockout mice, and found that except for the brain, the lyso-PS lipase activities were comparable in all other tissues for both the genotypes (**Fig 3.5 A**). Finally, we measured the lyso-PS levels in different tissues from wild-type and ABHD12 knockout mice and found that except for the brain (where there is a massive accumulation of lyso-PS, particularly very-long chain lyso-PS), ABHD12 deletion did not affect the lyso-PS levels in any other tissue profiled (**Fig 3.5 B**). Taken together, this suggests that at a tissue-level, ABHD12 regulates the levels of lyso-PS only in the mammalian brain, and that there must exist other lipases from the mSH family which are capable of degrading (hydrolyzing) lyso-PS, and in turn, regulating lyso-PS levels in tissues that possess FP-sensitive lyso-PS lipase activity (e.g. liver, kidney).

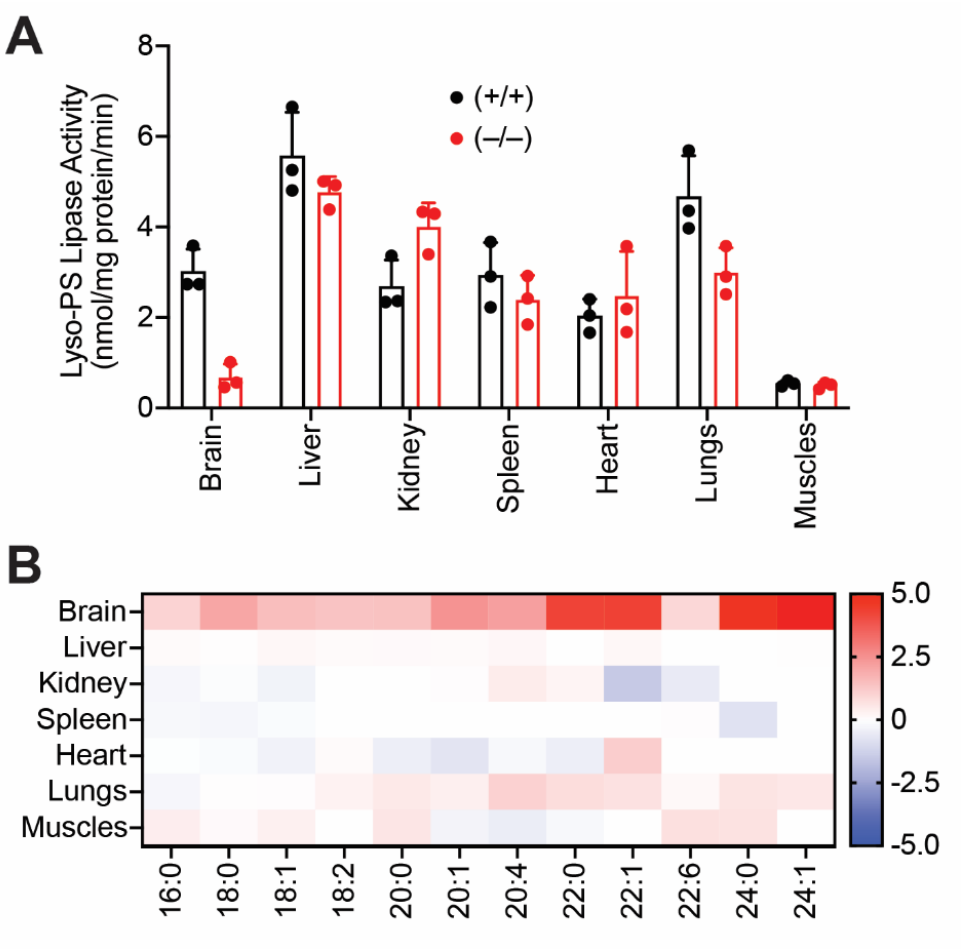

Fig 3.5: ABHD12 controls lyso-PS levels only in the mouse brain. *(**A**) The lyso-PS lipase activity in the membrane proteomic fractions of different mouse tissues obtained from wild type (+/+) or ABHD12 knockout (–/–) mice. All assays were done using 20 μg of proteome against 100 μM C17:1 lyso-PS for 30 min at 37 °C. The bar plots represent mean ± standard deviation from three biological replicates. (**B**) Heat map plot showing relative levels of various detectable lyso-PS species from different mouse tissues following deletion of ABHD12. The relative concentration data for each lyso-PS species was obtained by taking the ratio of the knockout value (from ABHD12 knockout mice) to the wild type value (from wild-type mice), where the respective value was calculated as an average from four biological replicates per genotype. The scale adjoining the heat map plot is $\log_2$[ratio of knockout value to wild type value].*

Literature survey to search for candidate lipases

Over the past decade, biochemical studies have identified a few enzymes from the mSH family that possess a general lysophospholipase activity (**Fig 3.6 A**), with lyso-PS being a potential substrate for these enzymes.

The most characterized amongst these lysophospholipases is the α/β-hydrolase domain protein # 6 (ABHD6). Like ABHD12, ABHD6 was first identified as a lipase capable of hydrolyzing the endocannabinoid 2-AG[89], and since then, has extensively been explored as a regulator of endocannabinoid signaling in the mammalian brain[126–129]. In mammals, ABHD6 is a 35-kDa (~ 335 amino acids) integral membrane enzyme from the mSH family that has ubiquitous expression in all tissues, with the highest expression in the liver and brain (UniProt ID: Q9BV23 for human ABHD6)[88,125,129]. Interestingly, a recent study exploring the role of ABHD6 in regulating metabolic syndrome showed that depleting ABHD6 activity in peripheral tissues (tissues other than the brain) in mice results in hepatic accumulation of several lysophospholipids, including lyso-PS[130]. Further in the same study, biochemical studies showed that along with the 2-AG hydrolase activity, ABHD6 also shows lysophospholipase activity, with lyso-PS also being a substrate for this enzyme[130]. It remains unclear whether the lysophospholipase activity of ABHD6 has any role to play under some physiological context and/or condition in specifically regulating lyso-PS metabolism in these peripheral tissues. Both knockout mice model systems[130] and *in vivo*-active specific inhibitors (**Fig 3.6 B**)[131,132] are described for ABHD6, and these genetic and pharmacological tools can be used in tandem to ascertain the role that mammalian ABHD6 plays in regulating lyso-PS metabolism in peripheral tissues.

The patatin-like phospholipase domain containing protein # 7 (PNPLA7) is another candidate mammalian enzyme that possesses a general lysophospholipase activity[133,134]. In mammals, PNPLA7 is a 150-kDa (~ 1300 amino acids) ER-resident integral membrane enzyme from the mSH family that shows expression and activity only in the metabolic active tissues (primarily liver and kidneys, and to a lesser extent in the lungs) (UniProt ID: Q6ZV29 for human PNPLA7)[88,124,125]. Recent *in vitro* biochemical studies have shown that PNPLA7 has robust lysophospholipase activity against several lysophospholipid substrates, including lyso-PS[133]. Overexpression of PNPLA7 activity in mammalian COS-7 cells results in decreased production of several lysophospholipids, including lyso-PS[133]. However, there are no *in vivo* studies which show if PNPLA7 can regulate lyso-PS metabolism *in vivo* in

mammalian tissues. There are also no specific inhibitors for PNPLA7 to date, while recently, the PNPLA7 knockout mouse model has been reported and characterized[135].

Another candidate lyso-PS lipase is the calcium-independent phospholipase Lysosomal phospholipase A and acyltransferase (PLA2G15/PAG15). In mammals, PLA2G15 is a 46.5-kDa (~ 400 amino acids) lysosomal membrane enzyme from the mSH family that shows expression and activity only in the metabolic active tissues (primarily liver) (UniProt ID: Q8NCC3 for human PNPLA7)[88,124,125]. I*n vitro* biochemical studies have shown that PLA2G15 has a generic phospholipase activity against a broad range of substrates and a robust lysophospholipase activity against lyso-PCs[136,137]. It has also been recently characterized as a lysosomal BMP hydrolase having implications in lysosomal disease[138]. Knockout mice have been reported in literature[137], while no specific inhibitors for this enzyme are commercially available yet.

Finally, the enzymes lysophospholipase 1 (LYPLA1)[139] and lysophospholipase 2 (LYPLA2)[140] are closely related members of the mSH family that also possess a general lysophospholipase activity. Both enzymes within a mammalian species have ~ 65% sequence identity, and are capable of hydrolyzing a variety of lysophospholipids, and hence, are monikered[139–141]. Besides their lysophospholipase activity, LYPLA1 and LYPLA2 also possess thioesterase or esterase activity on protein and/or peptide substrates that are post-translationally acylated at cysteine or serine residues. Both these lysophospholipases are cytosolic proteins, which are ubiquitously expressed in all tissues, with LYPLA1 and LYPLA2 having molecular weights of 24-kDa (~ 230 amino acids) (UniProt ID: O75608 for human LYPLA1), and 25-kDa (~ 230 amino acids) (UniProt ID: O95372 for human LYPLA2) respectively. While the roles of LYPLA1 and LYPLA2 in modulating protein palmitoylation are fairly well understood[142,143], little remains known on the ability of these lipases to modulate lysophospholipid metabolism, including lyso-PS metabolism, in physiological contexts. Specific inhibitors (**Fig 3.6 C**)[144] and knockout mice[145] are available for both LYPLA1 and LYPLA2, and these can potentially be used to study the role that these lysophospholipases play in the physiological regulation of lyso-PS metabolism.

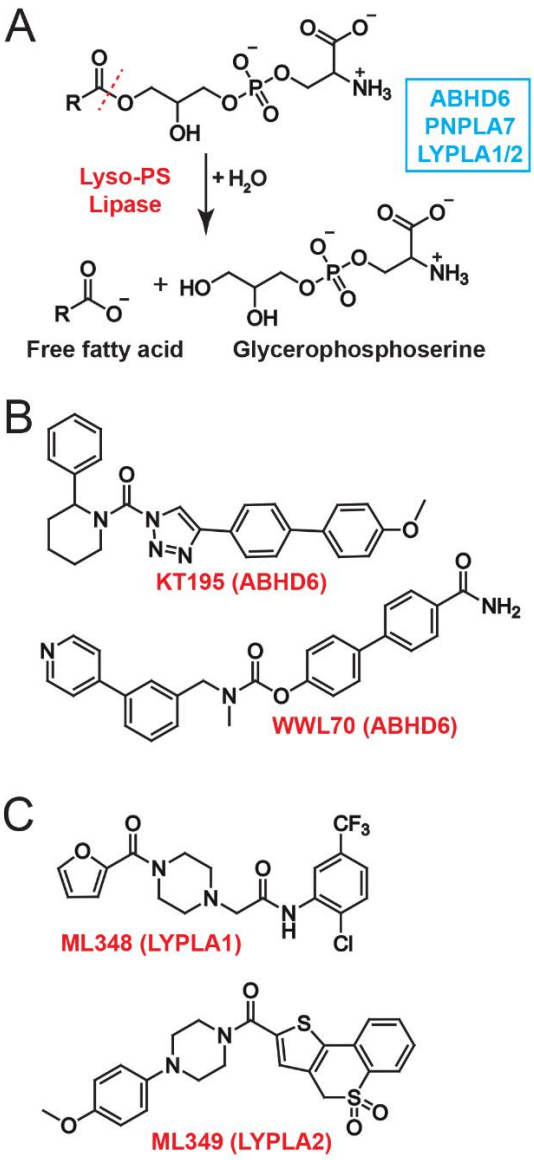

Fig 3.6. Candidate lyso-PS lipases and their inhibitors (**A**) The potential lyso-PS lipase activity of the general lysophospholipases: ABHD6, PNPLA7, LYPLA1, and LYPLA2. (**B**) Structure of the ABHD6-selective inhibitors KT195 and WWL70. (**C**) Structure of the LYPLA1 and LYPLA2-selective inhibitors ML348 and ML349 respectively.

As a first pass, we purchased clones of ABHD6, LYPLA1, LYPLA2, PNPLA7, and PLA2G15 in a pCMV Sport 6 vector for overexpression in mammalian systems under a CMV promoter. **(Table 4)**

Table 4: All commercial clones for candidate lipases used for screening their lyso-PS lipase activity

Gene	Organism	Clone ID	Mammalian organ of expression
ABHD6	Mouse	6466700	Heart, Liver
LYPLA1	Human	3865775	Heart, Kidney
LYPLA2	Human	3845764	Heart, Lungs, Liver, Kidney
PNPLA7	Human	5199366	Liver
PLA2G15	Human	5162981	Liver

These clones were transiently transfected into HEK293T cells and assayed for their Serine Hydrolase pool using gel-based ABPP utilizing FP-Rd as a probe. **(Fig 3.7 A)** ABHD12 and ABHD12 S246A (catalytically dead mutant of ABHD12) were used as controls for further substrate assays, while ABHD16A was used as a transfection control against a "mock" empty vector control. Active PLA2G15, LYPLA1, and LYPLA2 were successfully overexpressed, while ABHD6 and PNPLA7 were not. These overexpressed fractions were then assayed for their lyso-PS lipase activity and compared to a "mock" control and ABHD12, since it is the only bona fide lyso-PS lipase thus far. However, none of the successfully expressed candidate lipases showed any robust lyso-PS lipase activity. In the meantime, during this literature review, we had curated a list of different inhibitors and designed an inhibitor screen to fish out more candidate lipases, which is detailed in the next section.

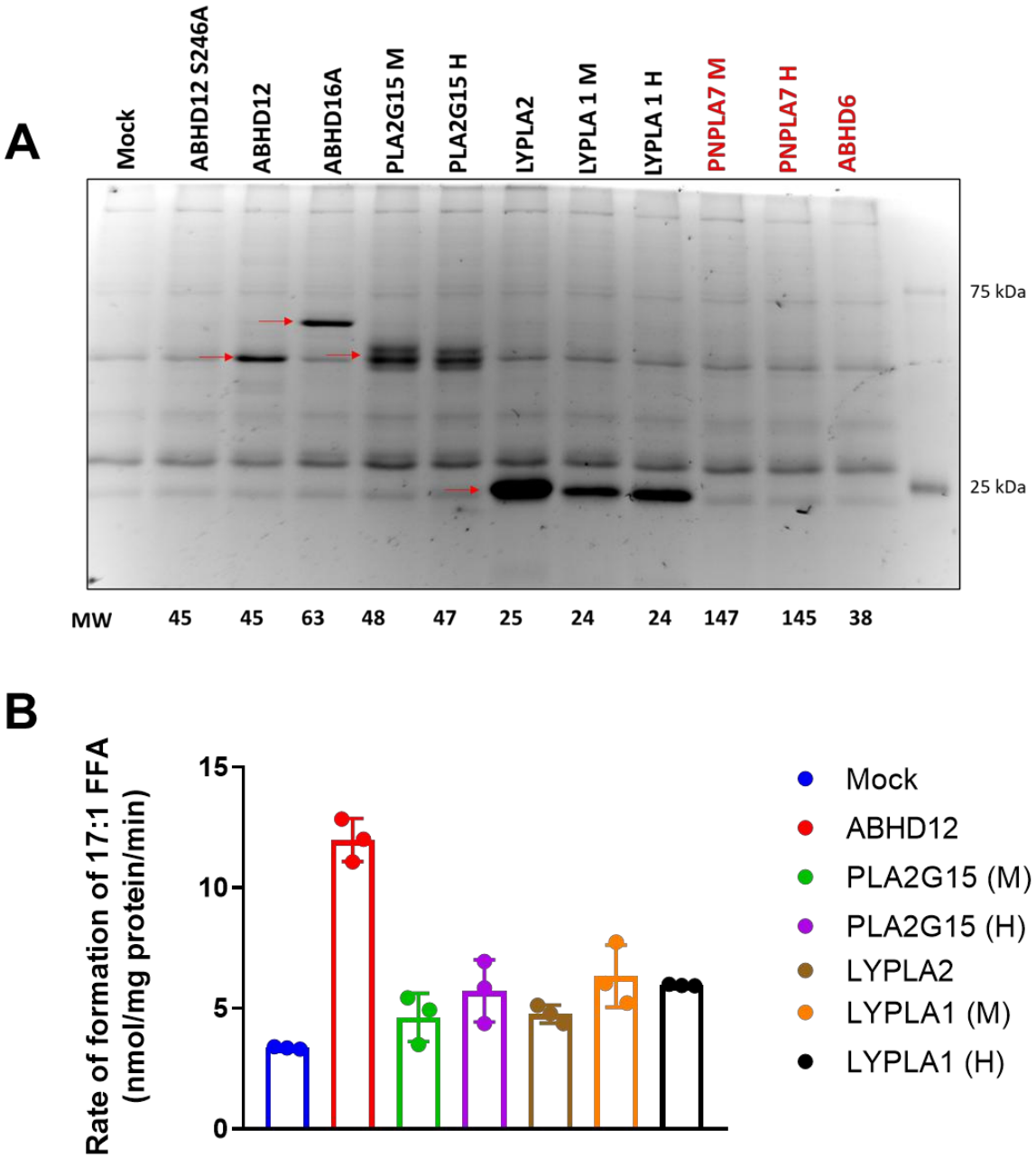

Fig 3.7: Overexpression of candidate lyso-PS lipases curated from a literature survey (A) *A representative ABPP gel showing the overexpression of different candidate lipases in the membrane proteomic fraction in HEK293T (**B**) The lyso-PS lipase activity in the membrane proteomic fractions of HEK cells transfected with different candidate lipases compared to a "mock" control. All assays were done using 20 µg of proteome against 100 µM C17:1 lyso-PS for 30 min at 37 ℃. The bar plots represent mean ± standard deviation from three biological replicates.*

Identification of ABHD6 as a putative lyso-PS lipase using an inhibitor screen

In an effort to identify one (or more) enzyme(s) from different peripheral mouse tissues capable of hydrolyzing lyso-PS, we first collated a focused library of 30 compounds that serve as potent inhibitors (mostly covalent, ranging from very specific to broad spectrum) to lipases from the mSH family[90] (**Table 5**).

Table 5: A list of inhibitors used for the inhibitor screen *with their corresponding targets, including off target enzymes. If one target is more specific among other off targets, it has been highlighted in* ***bold formatting****.*

Sr. No.	Compound Name	Lipase or serine hydrolase target(s) (> 90% inhibtion at 10 µM)
1	ABC5	**ABHD3, ABHD4**, PPT1, ABHD6, DDHD2
2	ABC16	ABHD4
3	ABC45	ABHD4, LIPA, DDHD2, PPT1
4	ABC51	ABHD4, PAFAH2, PLA2G7
5	ABL127	PPME-1
6	ATGLStatin	ATGL
7	BAY59-9435	HSL
8	Bromoenol lactone (BEL)	Ca2+ independent PLA2, PAP-1
9	CAY10499	MAGL, HSL, FAAH
10	CAY10502	cPLA2α
11	Darapladib	PLA2G7
12	GSK264220A	LPL, LIPG
13	JJH254	FAAH, LYPLA1/2
14	JW480	**KIAA1363**, CES1
15	JZL184	MAGL, FAAH
16	KC01	**ABHD16A**, ABHD2, AIG1
17	KC02	ABHD2, ABHD11
18	KT195	**ABHD6**, CES1, CES2, CES3, LYPLA2, PLA2G15
19	Lalistat2	**LAL**, HSL, ATGL, MGLL, PNPLA6, ABHD6, NCEH1

20	ML348	LYPLA1
21	ML349	LYPLA2
22	P11	PAFAH1b2/1b3
23	Palmostatin-M	**LYPLA1/2**, ABHD17A/B/C, AFMID, PLA2G4A, PRCP, PREPL, ABHD12, CPVL, ESD, PAFAH2, PNPLA8, SCPEP1, ABHD16A, AOAH, LIPA
24	PF7845	FAAH
25	Pyrrophenone	PLA2G4A
26	RHC80267	DAGLa/b, PLA2G7
27	Tetrahydrolipstatin (THL)	**ABHD12, ABHD16A**, FASN, DPP9, HSL, ABHD6, DAGLA/B, PLA2G7, PNPLA6, PNPLA7, CES1, CES2, CES3, CTSA, LPL, PLA2G4A, TPP2, PREPL
28	Trans-5c	ABHD16A, CES2, PNPLA4, ABHD2, FAAH
29	WWL229	CES1, CES3
30	XEN445	LIPG

Next, we treated the membrane proteomic fraction of different mouse tissues that showed ABHD12-independent lyso-PS lipase activity (liver, kidney, spleen, heart, and lungs) (**Fig 3.5 A**) with this inhibitor library (10 μM, 45 min), and subsequently assayed them for lyso-PS lipase activity. In this experiment, we considered an inhibitor as a "hit", if it inhibited the membrane proteomic fraction lyso-PS lipase activity of a particular tissue by >80%. Here, corroborating the results from the lyso-PS lipase assays performed using a FP-probe (**Fig 3.2 B**), we found several hits from the inhibitor library in the membrane proteomic fraction of the liver (4 hits), kidney (4 hits), and spleen (2 hits), but not in the heart and lungs (**Fig 3.8 A**). Since the heart and lungs did not show any hits from the inhibitor library (**Fig 3.8 A**) and are not sensitive to FP-probe treatment (**Fig 3.2 B**), it suggests that the lyso-PS lipase activity in these tissues likely comes from a lipase that is not a mSH enzyme.

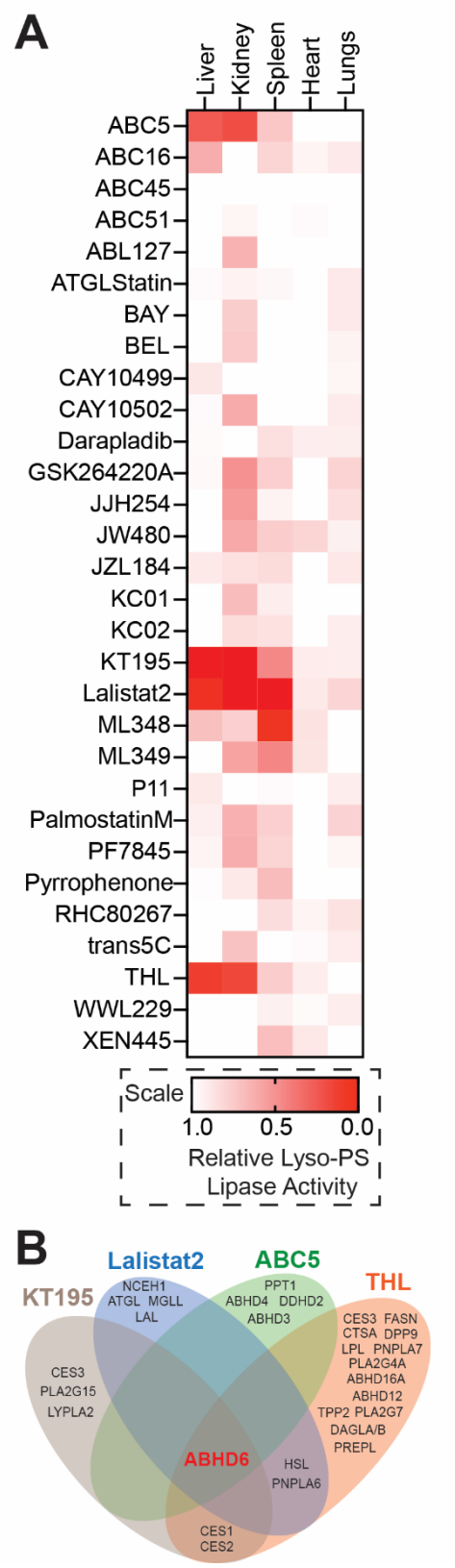

Fig 3.8. A screen identifying tissue-wide lyso-PS lipase inhibitors. *(A) Heat map plot showing relative lyso-PS lipase activity from the membrane proteomic fractions of different mouse tissues treated with 30 different lipase inhibitors. The relative lyso-PS lipase activity*

*was obtained by taking the ratio of inhibitor treated samples to vehicle controls, where the respective value was calculated as an average from three biological replicates per group. (**B**) Venn diagram analysis of the various known biological targets of the "hits" obtained from the inhibitor library, showing that ABHD6 is the only common mSH target.*

Since the liver and kidney showed significant lyso-PS lipase activity that was significantly inhibited by both a FP-probe and compounds from the inhibitor library, we decided to pursue these tissues further. Interestingly, we found that the four hits from the inhibitor library in both these tissues were identical (**Fig 3.8 A**), suggesting that, most likely, the same mSH regulates the lyso-PS lipase activity in the liver and kidneys. All four hits from the inhibitor library were covalent inhibitors of various mSHs: 2 broad spectrum inhibitors (THL[90] and Lalistat2[146,147]), and 2 specific inhibitors (KT195 for ABHD6[131,132]; ABC5 for ABHD4, PPT1[148]), and we decided to assess the overlapping targets between them (**Fig 3.8 B**). Based on publicly available reports and chemoproteomics datasets assessing the targets of these 4 inhibitors, quite surprisingly, we found that the only common mSH target for all these 4 hits was the integral membrane lipase ABHD6 (**Fig 3.8 B**).

Previous studies have shown that recombinant mammalian ABHD6 functions both as a monoacylglycerol lipase[89,149] and a lysophospholipase[130], and we wanted to see if endogenous ABHD6 had any lyso-PS lipase activity. For this, we needed a cell line that was devoid of ABHD12 but had sufficient ABHD6 expression and activity, so we looked at BV-2, HEK293T, Neuro-2A and RAW264.7 cell lines. Amongst these we found HEK293T cells suitable for our assays as it had minimal ABHD12 expression and had active ABHD6 **(Fig 3.9)**.

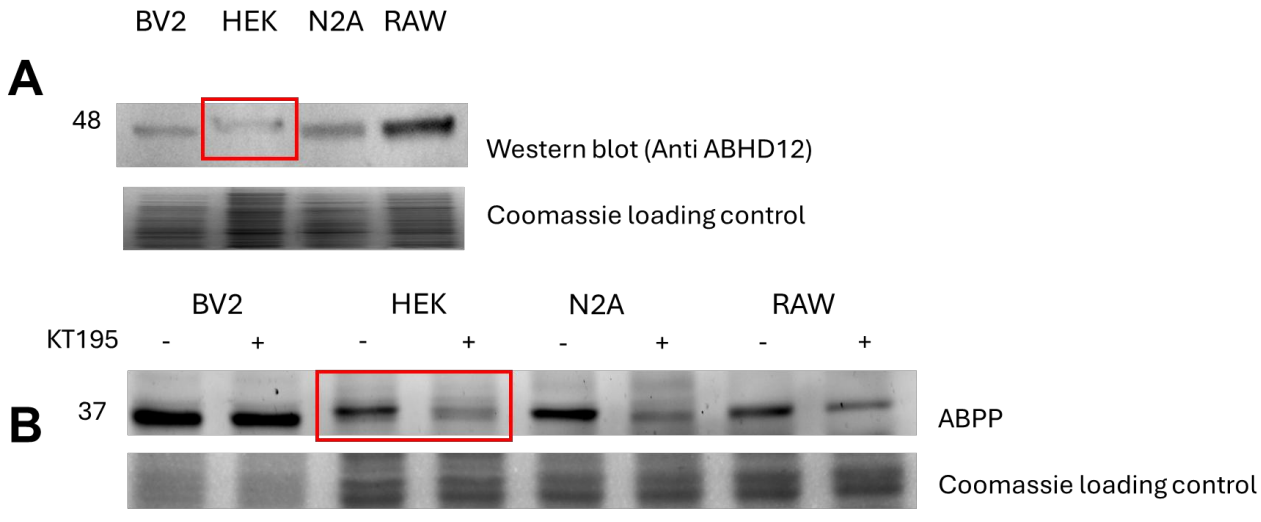

Fig 3.9. Comparison of different cell lines expressing ABHD12 and active ABHD6 *(A) A representative western blot showing the expression of ABHD12 in different cell lines, showing that HEK293T cells are almost devoid of the enzyme* ***(B)*** *A representative ABPP gel showing the inhibition of ABHD6 using KT195 in different cell lines, showing that HEK293 and Neuro 2A cells have active ABHD6. (Abbreviations used: HEK- HEK293T, N2A – Neuro2A, RAW – RAW264.7)*

Treatment of HEK293T cells with the ABHD6-specific inhibitor KT195 (from the inhibitor library) (1 μM, 4 hours) showed the selective loss of ABHD6 by gel-based activity-based protein profiling (ABPP) experiments (**Fig 3.10 A**), and significantly decreased lyso-PS lipase activity (**Fig 3.10 B**) in the membrane proteomic fraction. The loss of lyso-PS lipase activity in HEK293T cells upon KT195 treatment was comparable to the *in vitro* FP-probe treatment (2 μM, 45 min) of the vehicle treated cells, further confirming that all the mSH-associated lyso-PS lipase activity in the membrane proteomic fraction of HEK293T cells was largely coming from ABHD6 (**Fig 3.10 B**).

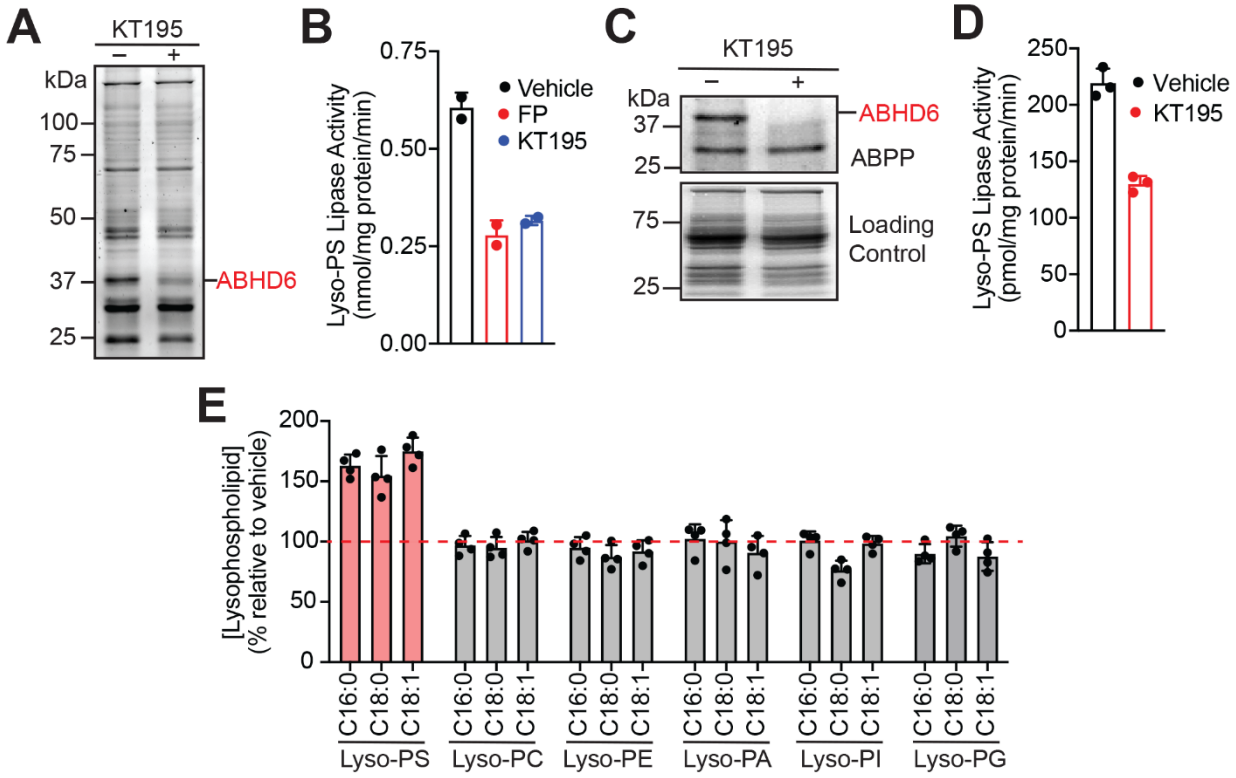

Fig 3.10. Identification of ABHD6 as a putative lyso-PS lipase. *(A) A representative ABPP gel showing the selective loss of ABHD6 activity in the membrane proteomic fraction in*

*HEK293T cells upon KT195 treatment (1 μM, 4 hours). (**B**) The loss of lyso-PS lipase activity in the membrane proteomic fraction in HEK293T cells upon KT195 treatment (1 μM, 4 hours) from the selective inhibition of ABHD6. FP-rhodamine treated membrane proteomic fraction (in vitro treatment, 10 μM, 30 min) was used as a low control in these assay. (**C**) A representative ABPP gel showing the selective loss of ABHD6 activity in the membrane proteomic fraction in primary hepatocytes upon KT195 treatment (1 μM, 4 hours). (**D**) The loss of lyso-PS lipase activity in the membrane proteomic fraction from primary hepatocytes upon KT195 treatment (1 μM, 4 hours) from the selective inhibition of ABHD6. (**E**) Relative levels of different lysophospholipids in primary hepatocytes upon KT195 treatment (1 μM, 4 hours), showing an increase of only lyso-PS, but no other lysophospholipid, from the selective inhibition of ABHD6. The gel-based ABPP experiments shown in (**A**) and (**C**) were performed three times (biological replicates) with reproducible results each time. All assays shown in (**B**) and (**D**) were done using 20 μg of proteome against 100 μM C17:1 lyso-PS for 30 min at 37 ℃. The bar data presented in (**B**), (**D**) and (**E**) represents mean ± standard deviation from two (for **D**) or three (**F** and **G**) biological replicates.*

Having established that endogenous ABHD6 indeed performs lyso-PS lipase activity, next, we wanted to test a more physiologically relevant cell line to assess if ABHD6 can regulate lyso-PS levels. Since ABHD12 has negligible activity in the liver (**Fig 3.4 C**), we chose to study the role of ABHD6 in modulating lyso-PS lipase activity and lyso-PS levels in primary hepatocytes. Treatment of primary hepatocytes with KT195 (1 μM, 4 hours) showed complete inhibition of ABHD6 in the membrane proteomic fraction by gel based ABPP (**Fig 3.10 C**). Concomitant to the inhibition of ABHD6, we found that the lyso-PS lipase activity associated with the membrane proteomic fraction of primary hepatocytes also substantially decreased upon the same KT195 treatment (**Fig 3.10 D**). Since previous studies have shown that ABHD6 functions as a general lysophospholipase[130], besides lyso-PS, we also decided to measure the levels of other lysophospholipids (lyso-PC, lyso-PE, lyso-PA, lyso-PI, and lyso-PG) in primary hepatocytes upon KT195 treatment. Interestingly, here we found that relative to the vehicle control, KT195 treated primary hepatocytes resulted in the accumulation of only lyso-PS (> 1.5-fold), but no other lysophospholipid (**Fig 3.10 E**). Taken together, these studies suggest that ABHD6 functions as putative lyso-PS lipase in primary hepatocytes, and selectively regulates the levels of only this signaling lysophospholipid in these liver cells.

ABHD6 regulates lyso-PS levels in the liver and kidney

A large-scale gene expression database (biogps.org)[124,125] (**Fig 3.11 A**) and ABPP analysis of mSHs[86] (**Fig 3.11 B**) in different mouse tissues have shown that ABHD6 has the highest activity in the membrane proteomic fraction of the brain and liver, and to a lesser extent in the kidneys. Hence, having demonstrated ABHD6's role in the regulation of lyso-PS levels in primary hepatocytes, next, we wanted to see if it performs lyso-PS lipase activity *in vivo* (in the liver and maybe other tissues). Since it has been reported that KT195 is poorly bioavailable in mice models, we chose a structurally related *in vivo* active ABHD6-specific inhibitor, KT185[132], to assess the effect of pharmacological inhibition of ABHD6 on lyso-PS metabolism in different mouse tissues. In the experiment, upon orally dosing mice with KT185 (10 mg/kg body weight, 4 hours), we harvested different tissues and assessed them *ex vivo*.

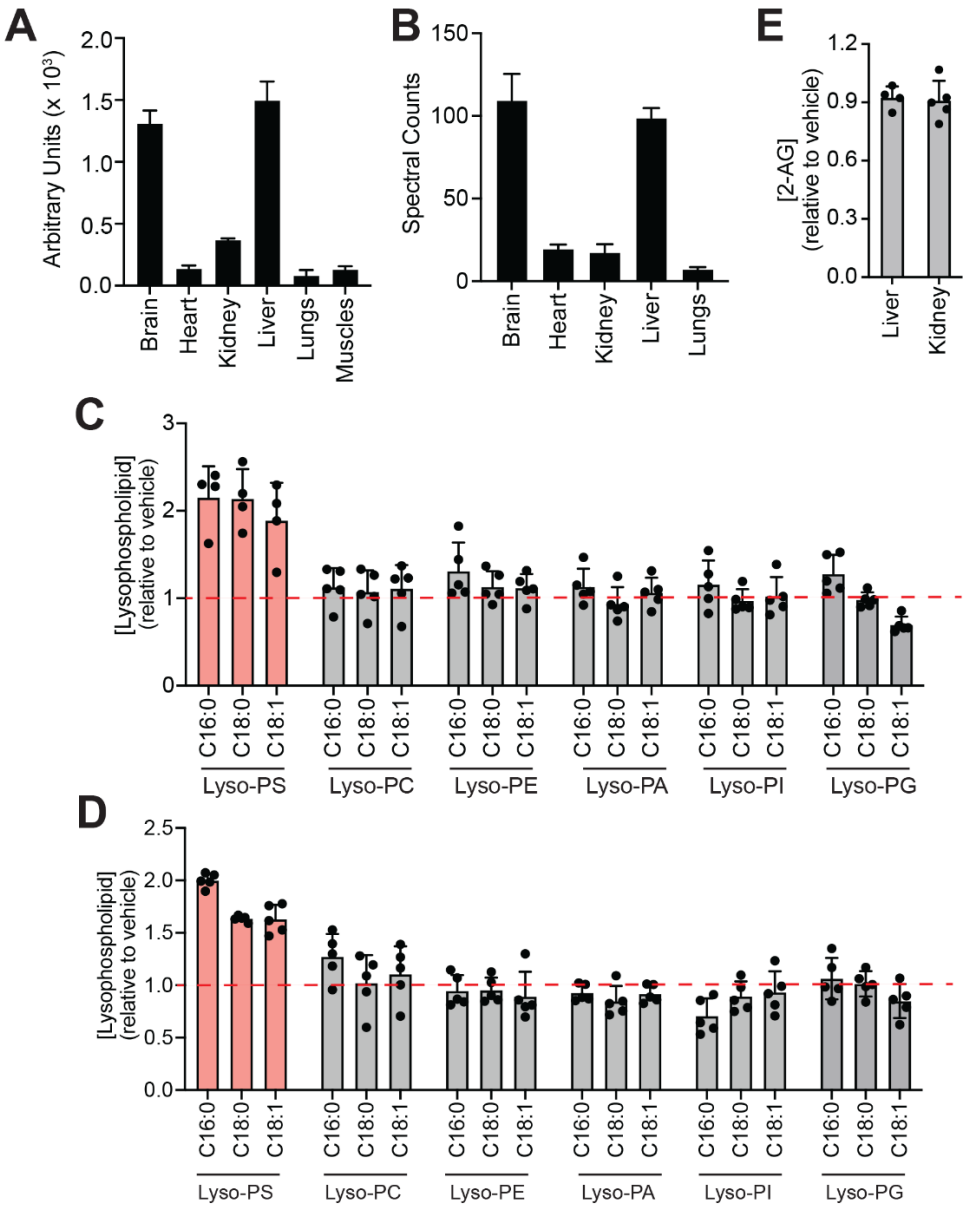

Fig 3.11. ABHD6 is a major lyso-PS lipase in the liver and kidney. ***(A)*** *The mRNA expression data exported from the large-scale gene expression database BioGPS, showing the heightened expression of ABHD6 in the mouse brain and liver, and to a lesser extent in the kidney. (**B**) The activity of ABHD6 in various mouse tissues from a publicly available LC-MS based ABPP dataset (spectral counting-based data) (3), showing the heightened activity of ABHD12 in the membrane proteomic fraction of the mouse brain and liver. (**C, D, E**) Relative levels of different lysophospholipids in the liver (**C**), and kidney (**D**) and 2-AG (**E**), upon KT185 treatment (10 mg/kg body weight, 4 hours), showing an increase of only lyso-PS, but no other lysophospholipid, from the selective inhibition of ABHD6. All bar plots*

*presented in this figure represents mean ± standard deviation from two (for **A, B**) or four or more (**C, D** and **E**) biological replicates*

To determine the efficacy of KT185 *in vivo*, we checked for the inhibition of ABHD6 in the membrane proteomic fractions of different mouse tissues using gel-based ABPP (**Fig 3.12 A**). Consistent with available expression and enzyme activity data, we were able to reliably detect ABHD6 activity in the membrane proteomic fractions of the brain, liver and kidney, and found that KT185 treatment (10 mg/kg body weight, 4 hours) in mice resulted in the complete inhibition of ABHD6 in these tissues (**Fig 3.12 A**). However, we were unable to detect any ABHD6 activity in the membrane proteomic fractions of spleen, heart, or lungs in the same gel-based ABPP experiments (**Fig 3.12 A, Fig 3.13A - full gels**). Concomitant to the inhibition of ABHD6 in the liver and kidney, next, we found that the lyso-PS lipase activity in the membrane proteomic fractions of these tissues was also substantially reduced (~ 50% and 40% in the liver and kidneys, respectively) upon KT185 treatment in mice (**Fig 3.12 B**). Like the gel-based ABPP assays, we found no changes in the lyso-PS lipase activity in the spleen, heart or lungs upon KT185 treatment in mice (**Fig 3.12 B**). Interestingly, we found that despite the complete inhibition of ABHD6 by KT185 treatment, there was no change in the lyso-PS lipase activity in the brain membrane proteomic fraction, further confirming that ABHD12 is the major lyso-PS lipase in the mammalian brain, and perhaps ABHD6 has another biochemical function in the central nervous system[129](**Fig 3.12 B**).

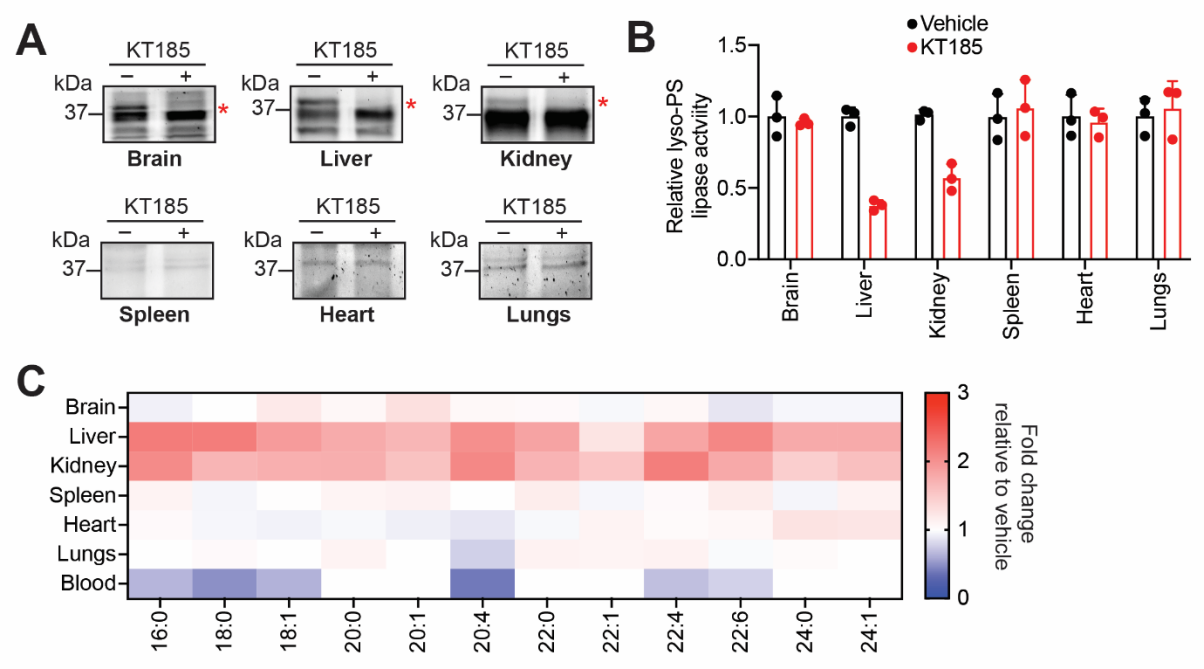

Fig 3.12. ABHD6 functions as a lyso-PS lipase in the liver and kidney. *(**A**) Representative ABPP gels (zoomed) showing the selective loss of ABHD6 activity in the membrane proteomic fraction of the brain, liver and kidney upon KT185 treatment (10 mg/kg body weight, 4 hours). These gel-based ABPP experiments were performed three times (biological replicates) with reproducible results each time. (**B**) The relative lyso-PS lipase activity in the membrane proteomic fractions of different mouse tissues treated with vehicle or KT185 (10 mg/kg body weight, 4 hours) following ABHD6 inhibition. All assays were done using 20 μg of proteome against 100 μM C17:1 lyso-PS for 30 min at 37 °C. The bar data represents mean ± standard deviation from three biological replicates. (**C**) Heat map plot showing relative levels of various detectable lyso-PS species from different mouse tissues following inhibition of ABHD6 by KT185 treatment (10 mg/kg body weight, 4 hours). The relative concentration data for each lyso-PS species was obtained by taking the ratio of the KT185 treated value (from ABHD6 inhibition) to the vehicle treated value, where the respective value was calculated as an average from at least four biological replicates per genotype. The scale adjoining the heat map plot is [ratio of KT185 treated value to vehicle treated value].*

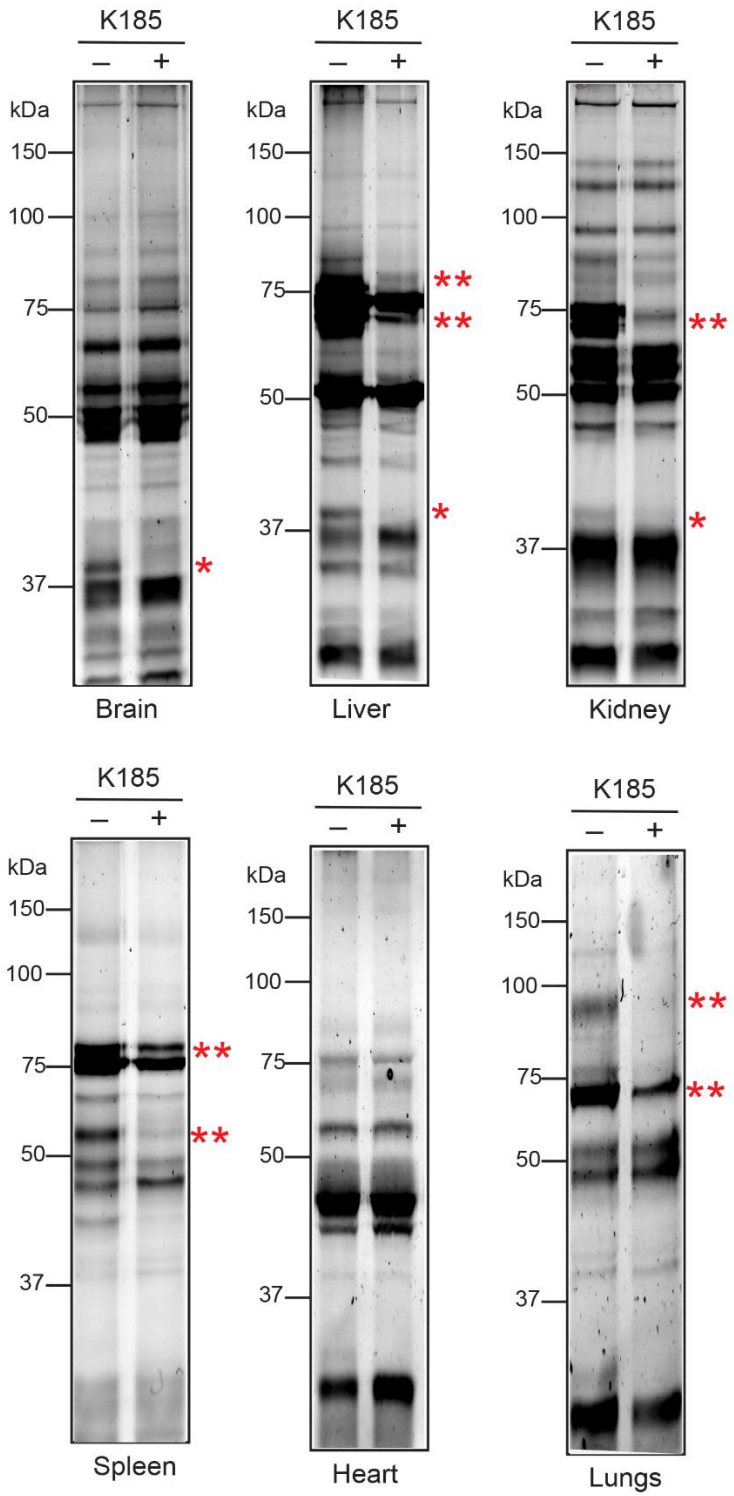

Fig 3.13. Complete ABPP gels from Fig 3.12 A*, showing the loss of ABHD6 activity (band corresponding to the single red asterisk) in the brain, liver and kidney upon treatment with KT185 (orally, 10 mg/kg body weight, 4 hours). No ABHD6 activity (37 kDa) was detected in the spleen, heart and lungs. The off-targets of KT185 (bands corresponding to two red asterisks) seen in the liver, kidney, spleen and lungs are likely enzymes from the CES-family (CES2 and CES3).*

Next, we measured the lyso-PS concentrations in different tissues following KT185 treatment in mice. Here, consistent with complete ABHD6 inhibition and the loss of lyso-PS lipase activity in the liver and kidney, relative to the vehicle control, we found that both these tissues showed a significant accumulation (~ 2 to 3-fold) of different lyso-PS species (**Fig 3.12 C**). Corroborating the gel-based ABPP assays and the lyso-PS lipase activity profiles, we found that all other tissues (brain, spleen, heart and lungs) showed little to no changes in tissue concentrations of lyso-PS (**Fig 3.12 C**). Further, in the liver and kidneys, we also measured the concentrations of several other lysophospholipids, and found that these showed negligible changes upon KT185 treatment in mice (**Fig 3.11 C, Fig 3.11 D**).

Quite surprisingly, we found that KT185 treatment in mice resulted in significantly decreased levels of lyso-PS circulating in the blood (**Fig 3.12 C**), suggesting that ABHD6 activity perhaps has a role to play in the secretion of lyso-PS lipids from the liver and kidneys. Taken together, our gel-based ABPP assays, lyso-PS lipase activity profiles, and lyso-PS measurements in different tissues following KT185 treatment in mice strongly suggest that *in vivo* ABHD6 functions as a major lyso-PS lipase in the liver and kidneys.

ABHD6 performs lyso-PS lipase activity *in vitro*.

To directly test if ABHD6 has the ability to perform lyso-PS lipase activity, we overexpressed wild-type (WT) ABHD6 in HEK293T cells using an established transient transfection protocol. As a control in this experiment, we mutated the invariant catalytically important active-site serine residue (Ser-148) to an alanine, to generate the S148A variant of ABHD6, and also overexpressed this variant in HEK293T cells. By Western blot analysis, we found that relative to the mock control, both WT and S148A variants of ABHD6 overexpressed almost equally in membrane proteomic fractions of HEK293T cells (**Fig 3.14 A**). However, gel-based ABPP analysis showed that relative to the mock control, WT ABHD6, but not the S148A mutant, was highly active (**Fig 3.14 A**). In the same experiment, as additional pharmacological controls, we also treated membrane proteomic fractions of HEK293T cells overexpressing WT ABHD6 with both KT195 or KT185 (1 μM, 45 mins, at 37 ^{o}C), and found by gel-based ABPP analysis that the treatment with both ABHD6-specific inhibitors resulted in almost complete loss of WT ABHD6 activity (**Fig 3.14 A**).

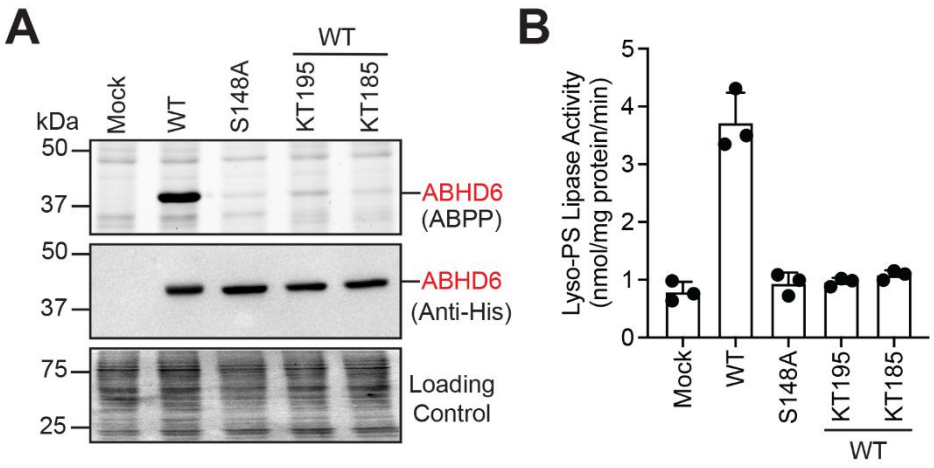

Fig 3.14. ABHD6 possesses lyso-PS lipase activity in vitro. *(**A**) The membrane proteomic fractions of HEK293T cells transfected with mock, WT ABHD6, or S148A ABHD6 were assessed by gel-based ABPP (top panel), Western blot analysis using an anti-His antibody (middle panel) and Ponceau S staining as loading control (bottom panel). The band corresponding to the activity (top panel) or expression (middle panel) of ABHD6 is shown in red here. In addition, membrane proteomic fractions of HEK293T cells transfected with WT ABHD6, that were treated with ABHD6 selective inhibitors, KT195 or KT185 (1 μM, 45 mins, at 37 °C), show complete loss of ABHD6 activity in this experiment. This gel-based ABPP experiment was repeated three times with reproducible results each time. (**B**) Lyso-PS lipase activity of the membrane proteomic fractions of HEK293T cells transfected with mock, WT ABHD6, or S148A ABHD6. In addition, membrane proteomic fractions of HEK293T cells transfected with WT ABHD6, that were treated with ABHD6 selective inhibitors, KT195 or KT185 (1 μM, 45 mins, at 37 °C), were also tested for lyso-PS lipase activity in this experiment. The bar data represent the mean ± standard deviation from three biological replicates per group.*

To ensure that KT195 and KT185 were selective inhibitors of ABHD6, and had no cross-reactivity with the lyso-PS lipase ABHD12, we performed a dose response experiment of both inhibitors against WT ABHD6 and WT ABHD12 using gel-based ABPP as a readout (**Fig 3.15**). From this experiment, we found that both KT195 and KT185 showed potent inhibition of WT ABHD6 (IC_{50} < 10 nM), with no discernable inhibition of WT ABHD12 even at a concentration of 10 μM (**Fig 3.15**).

Finally, we performed a lyso-PS lipase assay on membrane proteomic fractions of HEK293T cells overexpressing WT or S148A variants of ABHD6. Here, we found that relative to the mock control, WT ABHD6, but not the S148A variant, had robust lyso-PS lipase activity (**Fig 3.14 B**). In the same experiment, when the membrane proteomic fractions of HEK293T cells overexpressing WT ABHD6 were treated with KT195 or KT185 (1 μM, 45 mins, at 37 ^{o}C), the selective inhibition of ABHD6 resulted in almost complete loss of the lyso-PS lipase activity (**Fig 3.14 B**). Overall, our *in vitro* biochemical assays show that ABHD6 can robustly hydrolyze lyso-PS, and KT195/KT185 are selective ABHD6 inhibitors, and thus strongly support the cellular and *in vivo* pharmacological studies which show that ABHD6 functions as a lyso-PS lipase in the liver and kidneys.

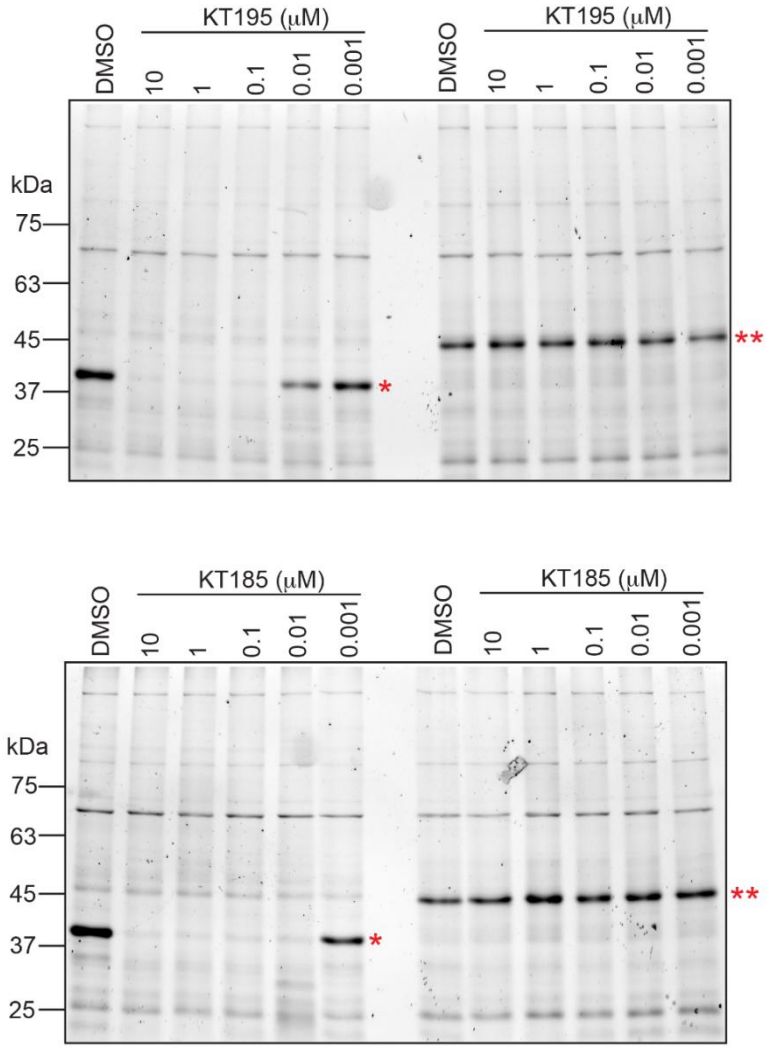

Fig 3.15. KT195 and KT185 are ABHD6 selective inhibitors. *Consistent with published literature (4,5), we find that both KT195 and KT185 selectively and potently inhibit WT*

ABHD6 (IC_{50} < 10 nM) (single red asterisk), but not WT ABHD12 (IC_{50} > 10 μM) (double red asterisk) by gel-based ABPP analysis. All gel-based ABPP assays were done in membrane proteomic fractions of HEK293T cells overexpressing WT ABHD6 or WT ABHD12. This gel-based ABPP experiment was repeated three times with reproducible results each time.

DISCUSSION

Signaling lipids (e.g.: lysophospholipids) are indispensable systemic small-molecule mediators of essential biological processes in mammals, and dysregulation in their metabolism and/or signaling has clearly established links to an array of human diseases [6,7,54]. Over the past two decades, lyso-PS has emerged as yet another biomedically important signaling lysophospholipid, and most of the knowledge pertaining to its metabolism and signaling is restricted to the central nervous and immune systems, given its involvement in several human neurological and autoimmune disorders[10]. Specifically, in the central nervous system, lyso-PS controls the activation of microglial cells, and in turn neuroinflammation, particularly in the cerebellum. On the other hand, in the immune system, this signaling lysophospholipid regulates histamine release from mast cell degranulation, pro-inflammatory responses from macrophages, and the maturation of T cells, to list a few processes. While it is now evident that lyso-PS is ubiquitously present, little remains known on how it is enzymatically produced and metabolized, or what are its physiological functions in other (peripheral) mammalian tissues.

To address this problem in part, we decided to investigate the degradation of this signaling lipid via a lyso-PS lipase activity assay in different mammalian tissues (**Fig 3.1**). We found that other than the muscles, all other mammalian tissues possess significant lyso-PS lipase activity that is enriched in the membrane proteomic fraction (**Fig 3.2 A**). Further profiling suggested that one (or more) mSH enzyme(s) was largely responsible for this activity in the brain, liver, kidney and spleen (**Fig 3.2 B**). Using a combination of biochemical assays and tissue lyso-PS measurements coupled with protein expression data, we showed that the only annotated lyso-PS lipase ABHD12 controls lyso-PS levels only in the brain (and central nervous system[25,32]), and no other peripheral tissue (**Fig 3.4, Fig 3.5**). To identify lyso-PS lipases in different peripheral tissues, we first performed a thorough literature survey of uncharacterized or poorly characterized mSH lipases and found five such

candidate lipases **(Fig 3.6)**. Upon overexpression and characterization of lyso-PS lipase activity using gel-based ABPP and substrate hydrolysis assays, we found that none of these lipases had sufficient lyso-PS lipase activity **(Fig 3.7)**.

Hence, to identify other lipases in peripheral tissues capable of hydrolyzing lyso-PS, we screened the membrane proteomic lysates of different tissues against a focused library of inhibitors of lipases belonging to the mSH family (**Fig 3.8 A**). From this screen, we found that the integral membrane mSH enzyme ABHD6 was a potential lyso-PS lipase in the liver and kidneys (**Fig 3.8 B**). Following this, we validated the ability of ABHD6 to regulate lyso-PS levels in mammalian cells, particularly in primary hepatocytes, where we found that via its lysophospholipase activity, ABHD6 selectively controls levels of only lyso-PS and no other lysophospholipid (**Fig 3.10**). Next, using a selective inhibitor in mice, we showed that the loss of ABHD6 activity results in significantly decreased lyso-PS lipase activity, and a concomitant increase in lyso-PS levels, but no other lysophospholipid, only in the liver and kidney (**Fig 3.11, Fig 3.12**). Finally, we showed using *in vitro* biochemical assays that WT ABHD6, but not the catalytically inactive S148A ABHD6, is active and possesses robust lyso-PS lipase activity (**Fig 3.14**). Taken together, we provide strong evidence in support of ABHD6's ability to function selectively as a lyso-PS lipase in the liver and kidney.

Moving ahead, our studies open several new research opportunities. For instance, in the central nervous system, ABHD6 is designated as a key lipase involved in the metabolism of the endocannabinoid 2-arachidonoylglycerol (2-AG)[89,128,129]. However, it has shown that the long-term loss of ABHD6 (via knock-down) does not alter 2-AG levels in peripheral tissues (e.g. liver, kidney), but results in substantially altered global lipid profiles in the liver, especially under conditions of a high-fat diet[130,150]. Further, ABHD6 is tentatively annotated as a promiscuous lysophospholipase, and shown to function as a general regulator of glycerophospholipid metabolism in the liver in mice models recapitulating high-fat diet induced obesity[130]. Our studies partly corroborate these findings, and show that ABHD6 functions as a lyso-PS-specific lysophospholipase in the liver and kidney in mice, and selectively controls levels of lyso-PS lipids, but not other lysophospholipids, in these tissues under normal physiological conditions (not in high-fat diet paradigms) (**Fig 3.11, Fig 3.12**). Given its recent links to systemic (glucose) metabolism[10], it will be interesting to see how dysregulated lyso-PS signaling in the liver might contribute towards metabolic conditions such as hepatic steatosis or systemic insulin resistance (modulated by ABHD6 activity), and crosstalk with other lipid pathways involved in such human diseases.

Our profiling studies from different mammalian tissues also show that despite having abundant lyso-PS levels, the muscles do not possess any measurable lyso-PS lipase activity (**Fig 3.2**). This result suggests that in muscles, lyso-PS may likely be metabolized via an acyltransferase-type activity. The identification of such a lysophospholipid acyltransferase will shed new insights into lyso-PS metabolism in tissues, where lyso-PS lipases are unable to regulate its physiological concentrations. Recent studies have annotated the lysophospholipid acyltransferase LPCAT3 as an enzyme capable of metabolizing lyso-PS, and shown a functional crosstalk between LPCAT3 and ABHD12 in the mammalian brain[117]. Of note, publicly available gene expression databases show that LPCAT3 has abundant expression in the kidney, liver, brain and skeletal muscles[124,125]. Further, recent studies in mice show an important role for this enzyme in regulating hepatic lipid secretion [151–154]. Hence, it will be interesting to see if LPCAT3 or some other lyso-PS specific acyltransferase can metabolize lyso-PS and regulate its physiological concentrations in the muscles. Additionally, given its expression profiles, and similar to studies done with ABHD12 in the brain[117], it will be important to understand the functional interplay, if any, between LPCAT3 and ABHD6 in regulating lyso-PS metabolism and signaling in the liver and kidney.

Finally, our studies show that the lyso-PS lipase activity from the heart and lungs is not sensitive to a FP-probe (**Fig 3.2**) or selected inhibitors from the screen (**Fig 3.8A**). This suggests that the putative lipase(s) is most likely not a member of the mSH family, and thus opens new directions towards finding the identity of this enzyme(s). We also find from the inhibitor screen, that the lyso-PS lipase activity from the membrane proteomic lysate of the spleen is almost completely inhibited by ML348 (**Fig 3.8A**), a potent yet selective inhibitor of lysophospholipase 1 (LYPLA1) enzyme[142,144]. Since LYPLA1 has ubiquitous expression in all tissues and is poorly characterized in terms of its lysophospholipase activity[139], it will also be worthwhile determining if this lipase indeed functions as a lyso-PS in the spleen, and if so, how it crosstalks with the immune system. Taken together, given the biomedical importance of lyso-PSs, and their direct association to human diseases, our studies illuminate new avenues of research in understanding the metabolism and signaling pathways regulated by this emerging lysophospholipid beyond the mammalian central nervous and immune systems.

SIGNIFICANCE

Lyso-PS is a hormone-like signaling lysophospholipid that controls many facets of mammalian biology. Given its association with numerous neurological and autoimmune disorders in humans, most studies pertaining to the metabolism of lyso-PS and its signaling pathways remain restricted to the mammalian central nervous and immune systems, despite the ubiquitous presence of lyso-PS in all mammalian tissues. In a pursuit to understand the enzymatic degradation of lyso-PS, we profiled the lyso-PS lipase activity associated with different mammalian tissues. We showed that besides muscles, all other tissues possess significant lyso-PS lipase activity, largely coming from membrane-associated mSH enzymes. We showed conclusively that via its enzymatic activity, the only functionally characterized lyso-PS lipase ABHD12 controls lyso-PS levels only in the mammalian brain, and no other tissue. Using a focused inhibitor screen in conjunction with follow up pharmacological studies in primary hepatocytes and mice, we identify ABHD6 as a major lyso-PS lipase in the liver and kidney, where it selectively regulates concentrations of lyso-PS, and no other lysophospholipid[155]. Our findings thus show how lyso-PS is metabolized in peripheral tissues, and open new avenues for studying this emerging signaling lysophospholipid in the context of systemic metabolism and metabolic diseases in humans.

PUBLICATION

Chakraborty, Arnab, Prajwal Punnamraju, Theja Sajeevan, Arshdeep Kaur, Ullas Kolthur-Seetharam, and Siddhesh S. Kamat. "Identification of ABHD6 as a lysophosphatidylserine lipase in the mammalian liver and kidneys." ***Journal of Biological Chemistry*** 301, no. 2 (2025): 108157.

Chapter 4: Development of MS platforms to enable untargeted and targeted detection of different lipids

Chapter summary:

Lipids are challenging macromolecules to study because they function as an ensemble rather than individual units, and there is a lack of advanced techniques available to study them, unlike other molecules. They vary in their composition at the cellular level (cell type variations) and the subcellular level (organelle variations) in both space and time parameters[156]. Studying their roles in diseases is challenging as lipidome compositions are a factor of nutrition, genetics, hormones, and many other confounding variables. While lipids are a diverse class with total species in the order of 10^4, their coverage in a typical LC-MS/MS experiment is around 2-5%, in contrast to 80-90% for other metabolites[157].Another challenge in studying them is the startling species variance ranging from the millimolar scale (e.g., phospholipids) to the femtomolar scale (e.g., prostaglandin) in the same sample[158]. In an effort to identify lipids in a variety of biological samples, we first used a modified folch method to extract lipids[24]. Subsequently, we developed methods to perform untargeted and targeted lipid analysis on quadrupole-time of fight (Q-TOF) and triple quadrupole (Q-Q-Q) mass spectrometers, respectively[159–161]. Our methods enabled relative and absolute quantification of lipid species such as fatty acyls, glycerophospholipids, glycerolipids, and saccharolipids in extracts from organisms ranging from mycobacteria, bacteria, zebrafish to human plasma. I have covered details of different methods used and how changes in lipid levels were useful for assigning novel functions to different proteins or looking at the effects of particular treatments.

INTRODUCTION

Lipids are recognized as physiological mediators of signal transduction along with their classical roles in maintaining membrane integrity and storage of energy. They are integral components of the cell membrane and subcellular organelle membranes, the compositions of which influence the function of specific cell types[162]. Lipids also act as energy storage molecules in the form of lipid droplets (LDs). LDs also mediate stress responses in cells and act as crucial organelles in immune physiology[163]. Lipid levels are tightly regulated through a complex network of metabolic enzymes fitted with feedback systems. A few lipids are

synthesized by enzymes with relatively short half-lives to act as secondary messengers in the cellular signaling cascades at the subcellular level. Hence, it is crucial to study lipids in a lot of biological contexts and to do so, the first step is to identify different lipids in a complex mixture.

The fundamental challenge in understanding lipid structures is the lack of repeating subunits (like in proteins or nucleic acids) to easily 'predict' them. Instead, lipids are synthesized by a complex assembly involving more than 100 total proteins. Modern lipidomics has improved our understanding of lipid species in a cell via shotgun or chromatography-based mass spectrometry. Shotgun-lipidomics has advantages like easier and quicker analysis and high performance, but it is limited to the detection of moderately abundant lipids. Improved sample derivatization techniques (which increases ionization efficiency) using multidimensional MS (MDMS) and methods of detection like neutral loss scanning (NLS) and precursor ion scanning (PIS) have made it the preferred tool in many investigations[159,161]. This is further facilitated by state-of-the-art high-resolution high mass accuracy mass spectrometry (HRAM-MS), which adds to the increasing repertoire of shotgun-lipidomics. LC-MS/MS is the preferred technique to analyze lipids having low abundance as it uses elution time differences of species and higher concentration during peak elution to accurately characterize molecules. This technique also deals with the aspect of mass overlaps caused by isobars in shotgun-lipidomics, making it the most used method. Added to this, bioinformatics approaches to peak alignment and ion analysis have accelerated the applications of lipidomics in identifying and quantifying lipids with high precision.

The advent of lipidomics, with the goal of characterizing, identifying, and quantifying lipid species, has helped us study their roles in diseases and use them as markers to detect pathologies and track their progression. In the 1960s, thin-layer chromatography (TLC) was used to separate lipids based on their classes and was successfully used to isolate metabolites of Arachidonic Acid from biological samples[164]. TLC-separated analytes were measured by gas chromatography-mass spectrometry (GC-MS), which involved plugging the chromatographic separation outlet into the ionization chamber of the mass spectrometer to study volatile compounds. This was followed by the decade of fast atom bombardment-mass spectrometry (FAB-MS), invented by chemist Michael Barber in 1980, which could be used to directly analyze non-volatile molecules for the first time[165].

In 1988, John B. Fenn and Koichi Tanaka developed methods of electrospray ionization (ESI) and soft laser desorption, respectively, for which they were also awarded the Nobel Prize in Chemistry in 2002[166]. Although designed for the soft ionization of peptides, it was soon found that the same principle applied to zwitterionic phospholipids and had a 1000-fold rise in sensitivity compared to FAB. This led to the foundation of 'shotgun' lipidomics involving the direct fusion of analytes to quickly detect a wide range of lipids, the latest technique being HRAM-MS, which gives unmatched resolving power and mass accuracies of >100000 and <2ppm respectively[161].

Lipidomics generates large datasets involving the identification of tens of thousands of molecular species in a sample. Frequently updated databases like LIPID MAPS and Metlin have been created to allow researchers to propose/validate structures from their MS data[16,17,167–169].

We have used reverse-phase LC-MS/MS with an ESI source complemented with databases like LIPID MAPS and Metlin, as well as online feature search tools like XcmsOnline, for the methods discussed in this chapter.

EXPERIMENTAL PROCEDURES

Lipid extraction protocol

Tissue homogenates or cell lysates were prepared in 1mL PBS and made up to a 4 mL mixture of 2:1:1choloroform (CHCl3): methanol (MeOH): PBS[24]. For semi-quantitative analysis of lipids, 1 nmol of C17:0-20:4-PC (Avanti Polar Lipids, Catalog # LM1002) and 1 nmol of pentadecanoic acid (C15:0 FFA) (Sigma Aldrich, Catalog # P6125) were added as internal standards for positive and negative mode analytes respectively. This homogenate mixture was vigorously vortexed and centrifuged at 3000g for 10 minutes to separate the mixture into an organic phase (bottom) and an aqueous phase (top) separated by a protein disk. The organic phase was removed by pipetting and stored on ice (at ~ 0 – 4°C). To enhance the extraction of phospholipids from the aqueous layer, 100 µL of formic acid (MS grade, Honeywell, Catalog # 94318) was added, and this mixture was vigorously mixed. 2mL of chloroform was added, and this mixture was vortexed and centrifuged at the conditions described previously. The organic layer was pooled with the one from the first extraction step and dried under a stream of nitrogen gas **(Fig 4.1)**.

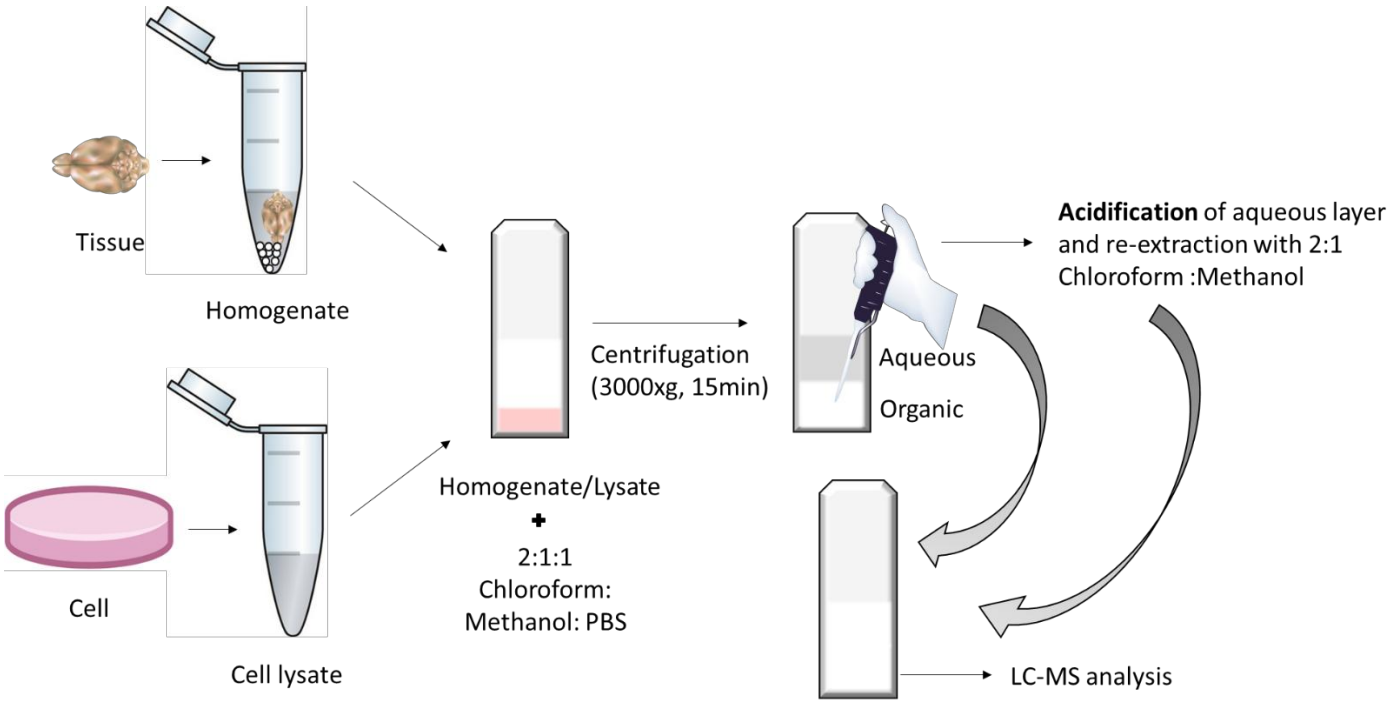

Fig 4.1: A schematic of lipid extraction using a modified Folch method

Standard untargeted LC and MS methods

The dried lipid extracts were re-solubilized in 200 µL of 2:1 CHCl3: MeOH, and 10 µL was injected into an Agilent 6545 LC-QTOF (quadrupole-time-of-flight) LC-MS/MS for semi-quantitative analysis using high-resolution auto MS-MS methods and chromatography techniques. LC separation employed a Gemini 5U C-18 column (Phenomenex) coupled with a Gemini guard column (Phenomenex, 4x3 mm, Phenomenex security cartridge). The buffers for negative ion mode runs consisted of 95:5 H2O: MeOH + 0.1% ammonium hydroxide (buffer A) and 60:35:5 Isopropanol (iPrOH): MeOH: H2O + 0.1% ammonium hydroxide (buffer B). For positive ion mode runs, 0.1% ammonium hydroxide in each buffer was replaced with 0.1% Formic acid + 10mM ammonium formate. Methods spanned 60 minutes, starting with 0.3 mL/min 100% buffer A for 5 minutes, 0.5 mL/min linear gradient to 100% buffer B over 40 minutes, 0.5 mL/min 100% buffer B for 10 minutes, and equilibration with 0.5 mL/min 100% buffer A for 5 minutes. Depending on the complexity of the sample and the number of lipids to be quantified, these LC methods were scaled down to 15 and 30-minute variants **(Fig 4.2)**.

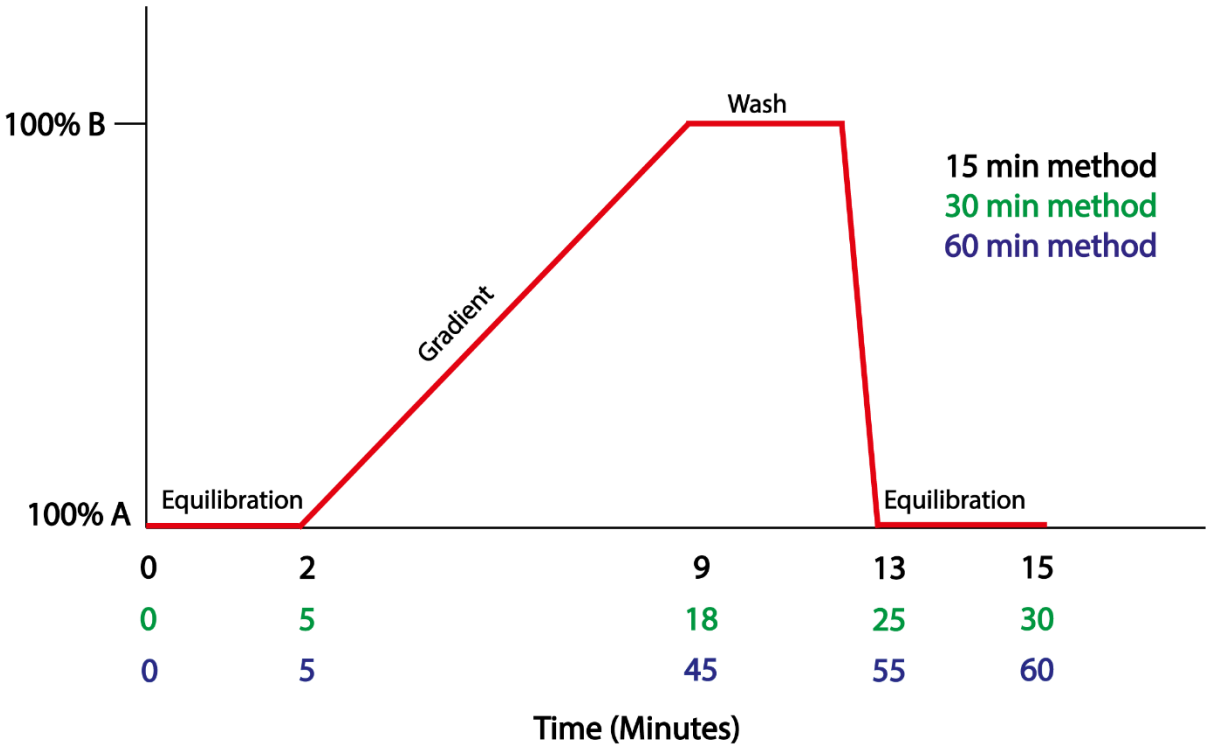

Fig 4.2: LC gradients used for 15, 30, and 60-minute methods for LC/MS.

ESI-MS analysis settings included the parameters detailed in **Table 6**. To summarize, settings included drying gas and sheath gas temperatures at 320 °C, a flow rate of 10L/min for both drying gas and sheath gas, a fragmentor voltage of 150V, capillary voltage of 4000V, nebulizer (ion source gas) pressure set at 45 psi, and nozzle voltage of 1000V.

Table 6: Method parameters for ESI-MS analysis

Parameter	Value
Injection volume	10 µL
Column oven temperature	40 °C
Acquisition type	Auto MS/MS
MS mass range	100-1500 Da
MS/MS mass range	100-1500 Da
Gas temperature	320 °C
Drying gas flow	10 l/min
Nebulizer pressure	45 psi
Sheath gas temperature	320 °C

Sheath gas flow	10 l/min
Capillary voltage	4000V
Nozzle voltage	1000V
Fragmentor voltage	150V
Skimmer voltage	65V
Collision energy	0, 15V, 30V

Finally, for lipid identification from peaks acquired by the LC-MS methods discussed, a lipid library in the form of a Personal Compound Database Library (PCDL) was employed, and peak validation relied on relative retention times and fragments acquired. Quantification of all lipid species involved the normalization of areas under the curve to the corresponding internal standard area and further normalization to the total cell count/tissue weight depending on sample type. Subsequently, log2 fold changes were plotted for each lipid in comparison to the appropriate control within the group whenever needed.

RESULTS AND DISCUSSION

Example case study for an untargeted lipidomics workflow: Identification of extremely long chain PIP variants in *Mycobacterium Smegmatis*

In a double knockout model designed to delineate the function of two enzymes – MSMEG 5284 and MSMEG 5285 in *Mycobacterium Smegmatis*, Vaishnavi Tripathi (at Sheetal Gandotra's lab, IGIB Delhi) saw that there was a severe decrease in a group of lipid species by thin layer chromatography (TLC) **(Fig 4.3)**. We collaborated on this project in order to

identify these lipid species that were diminished in the double knockouts.

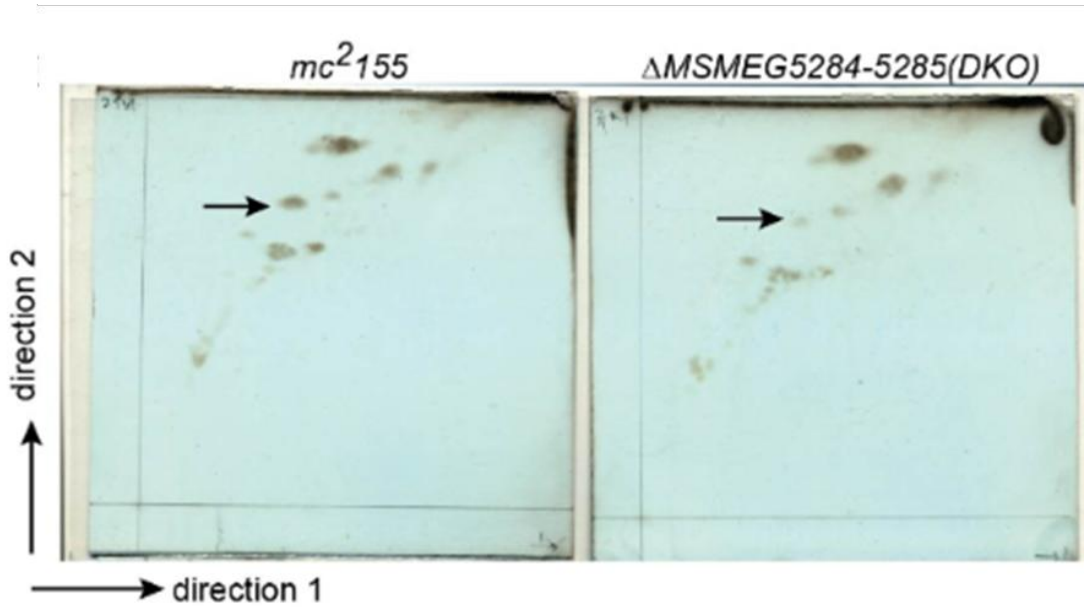

Fig 4.3: TLC image showing that the double knockout of MSMEG5284 and MSMEG5285 results in the reduction of a group of lipids

To this avail, they extracted and sent us the differentially enriched TLC lipid spots. We ran these samples using a 60-minute auto-MS/MS method in the positive and negative ionization modes (detailed in the methods section) to enable untargeted analysis of the lipid species. Since the chromatograms were completely similar in the positive ion mode results, we proceeded with datasets generated from the negative ion mode runs. Further, we annotated the peaks detected by the MS to masses of lipid species that have been previously characterized in mycobacteria[170]. However, we couldn't find any changes in levels of these lipid species, so we proceeded to utilize XCMSOnline, a tool that provides advanced metabolomic data processing to identify features that are differentially enriched between samples[169]. Here, when comparing the WT and DKO datasets, we saw a group of features (ion masses) enriched in the WT sample, highlighted in the red box **(Fig 4.4 A)**. Out of these masses, the feature with the highest fold change was 1109.7, being 5.7 times higher in the WT sample compared to the DKO **(Fig 4.4 B)**. In order to annotate possible lipid species to this feature and others, we used LIPID MAPS and METLIN databases to search for lipids that could produce a negative ion with a mass of 1109.7. Unfortunately, none of the enriched masses matched with any lipid in these databases with the stringency cutoff of <5ppm. Next, we utilized the LIPID MAPS COMP_DB[167], which is a database containing all theoretically possible lipids, irrespective of whether they have been studied or detected before. Here, we found multiple masses matching PIP species with a ~4 ppm error, 1109.7 matching with 48:2

PIP, for instance **(Fig 4.4 C)**. Other masses enriched in **Fig 4.4 A** included 1137.73, 1139.73, and 1111.71, which were matched with PIP 50:2, PIP 50:1, and PIP 48:1, respectively, with a <5 ppm error. Hence, we made a generic PIP structure with these extremely long chain lengths **(Fig 4.4 D)** and based on the fixed and variable regions by virtue of the head groups and fatty acid tails respectively, we came up with a formula to calculate all such theoretically possible species **(Fig 4.4 E)**.

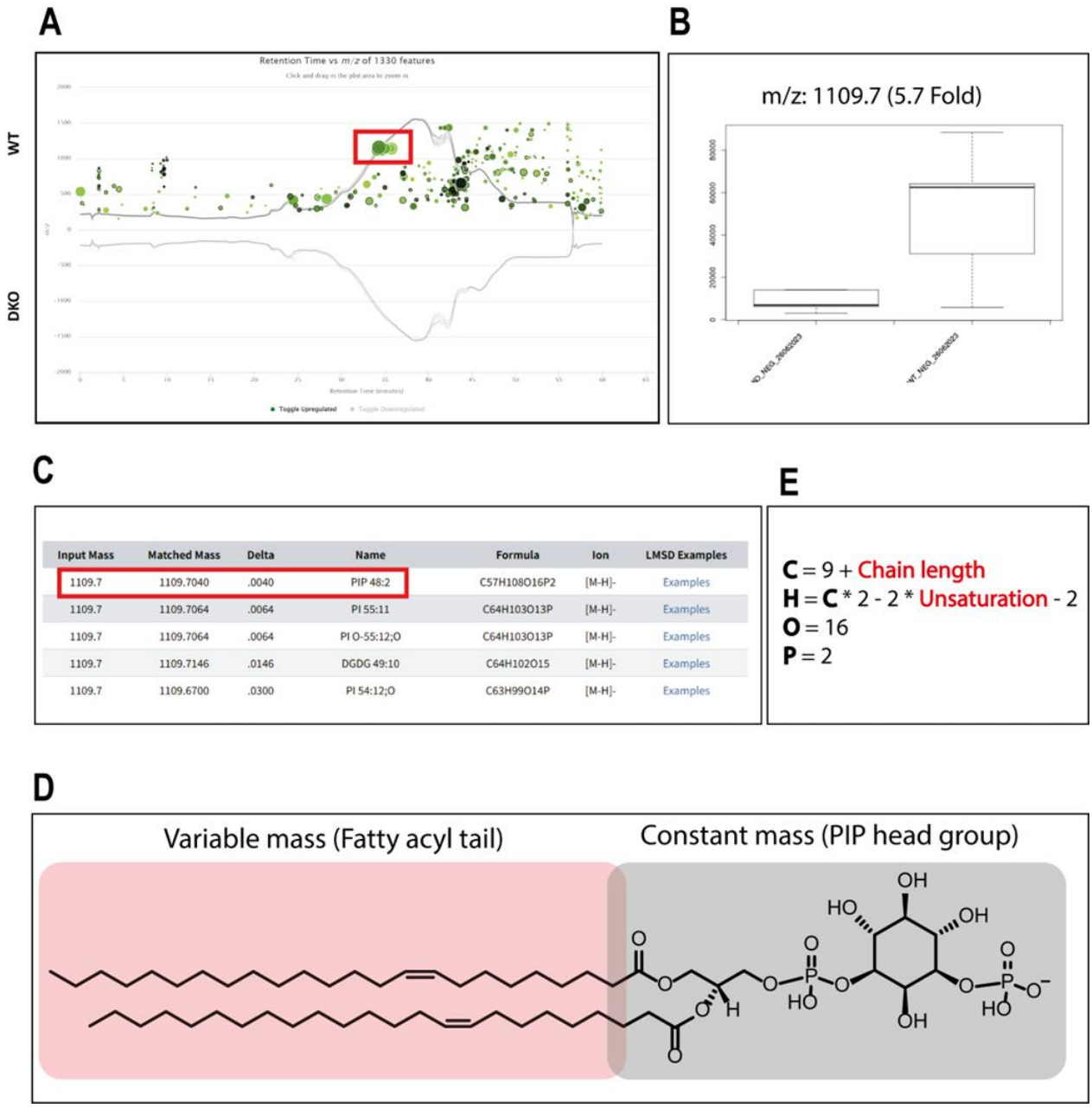

Fig 4.4: Analysis pipeline for untargeted analysis of lipids that do not match with available databases

Plugging in values for chain length (ranging from 46-52) and degree of unsaturation (0-4) into the formula in **Fig 4.4 E**, we generated an exhaustive list of possible PIPs in the mass range (~1000-1150Da) where differentially enriched masses were seen (Table 7).

Table 7: List of possible extremely long chain PIP species in the 1000-1150Da mass range

Chain	Unsaturation	C	H	O	P	Formula	ID
46	0	55	108	16	2	C55H108O16P2	PIP 46:0
46	1	55	106	16	2	C55H106O16P2	PIP 46:1
46	2	55	104	16	2	C55H104O16P2	PIP 46:2
46	3	55	102	16	2	C55H102O16P2	PIP 46:3
46	4	55	100	16	2	C55H100O16P2	PIP 46:4
47	0	56	110	16	2	C56H110O16P2	PIP 47:0
47	1	56	108	16	2	C56H108O16P2	PIP 47:1
47	2	56	106	16	2	C56H106O16P2	PIP 47:2
47	3	56	104	16	2	C56H104O16P2	PIP 47:3
47	4	56	102	16	2	C56H102O16P2	PIP 47:4
48	0	57	112	16	2	C57H112O16P2	PIP 48:0
48	1	57	110	16	2	C57H110O16P2	PIP 48:1
48	2	57	108	16	2	C57H108O16P2	PIP 48:2
48	3	57	106	16	2	C57H106O16P2	PIP 48:3
48	4	57	104	16	2	C57H104O16P2	PIP 48:4
49	0	58	114	16	2	C58H114O16P2	PIP 49:0
49	1	58	112	16	2	C58H112O16P2	PIP 49:1
49	2	58	110	16	2	C58H110O16P2	PIP 49:2
49	3	58	108	16	2	C58H108O16P2	PIP 49:3
49	4	58	106	16	2	C58H106O16P2	PIP 49:4
50	0	59	116	16	2	C59H116O16P2	PIP 50:0
50	1	59	114	16	2	C59H114O16P2	PIP 50:1
50	2	59	112	16	2	C59H112O16P2	PIP 50:2

50	3	59	110	16	2	C59H110O16P2	PIP 50:3
50	4	59	108	16	2	C59H108O16P2	PIP 50:4
51	0	60	118	16	2	C60H118O16P2	PIP 51:0
51	1	60	116	16	2	C60H116O16P2	PIP 51:1
51	2	60	114	16	2	C60H114O16P2	PIP 51:2
51	3	60	112	16	2	C60H112O16P2	PIP 51:3
51	4	60	110	16	2	C60H110O16P2	PIP 51:4
52	0	61	120	16	2	C61H120O16P2	PIP 52:0
52	1	61	118	16	2	C61H118O16P2	PIP 52:1
52	2	61	116	16	2	C61H116O16P2	PIP 52:2
52	3	61	114	16	2	C61H114O16P2	PIP 52:3
52	4	61	112	16	2	C61H112O16P2	PIP 52:4

We added this in the form of a PCDL database, as described in the methods section, and attempted to relatively quantify peak areas in the WT and DKO samples **(Fig 4.5)**. We saw a stark difference in the levels of ~20 different species of PIPs in the TLC spot extracts, where almost negligible levels were seen in the DKO sample compared to robustly detected peaks in the WT sample.

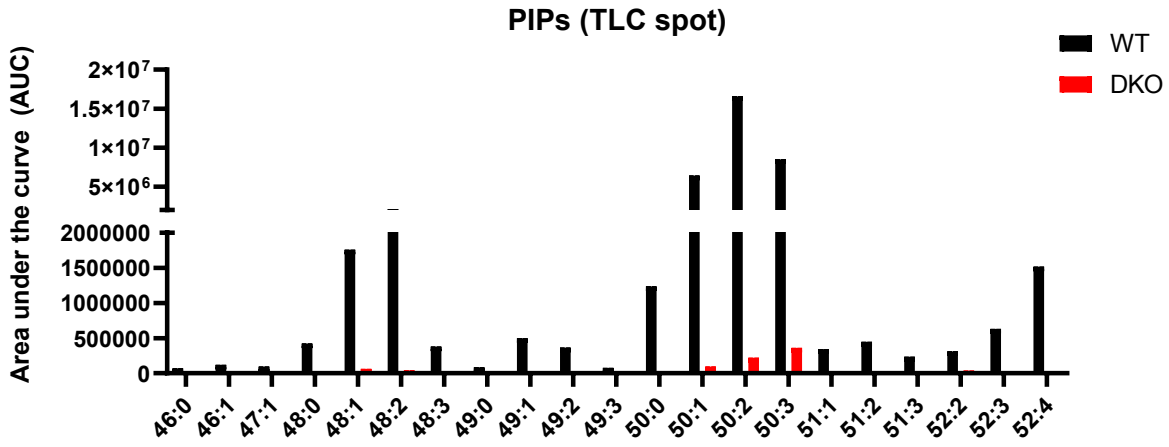

Fig 4.5: Areas under the curve (AUCs) of PIPs in the differentially enriched TLC spot

Finally, to validate whether these extremely long-chain PIPs were the major differentially expressed species, we performed untargeted lipidomics on total lipid extracts

from WT and DKO *Mycobacterium Smegmatis*. Here, we first observed that multiple PIP species in the database **(Table 7)** were indeed negligibly abundant in the DKO samples **(Fig 4.6 A)**. We also analyzed other lipids and found that PI levels were also variable between these samples, while other major lipid classes were unchanged. There was an increase in the levels of PIs in DKO samples, with their lipid tail chain lengths ranging from 46-50, which is similar to the reduced PIPs **(Fig 4.6 B)**.

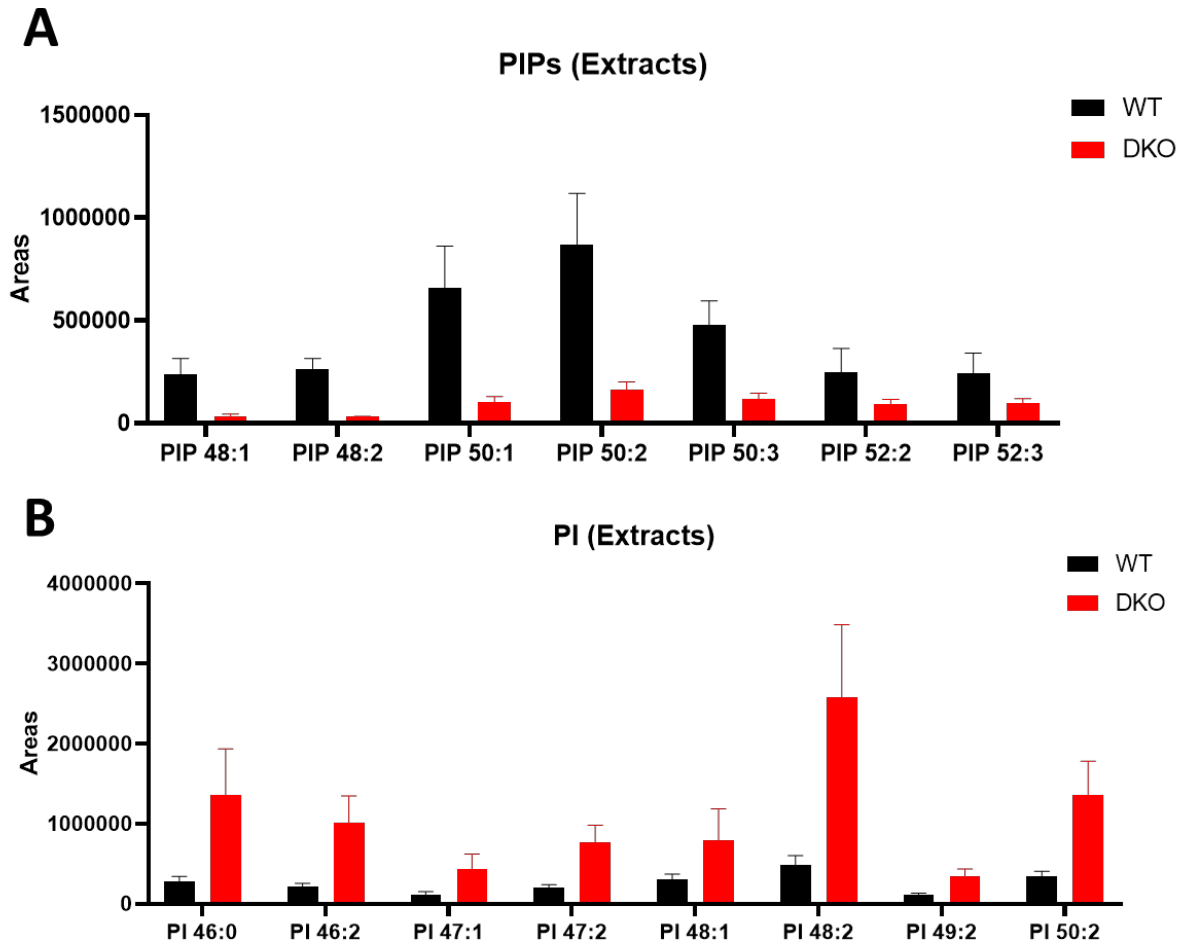

Fig 4.6: Relative abundance of extremely long-chain PIPs (A) and PIs (B) in total lipid extracts of Mycobacterium Smegmatis *The bar data represents the mean ± standard deviation from four biological replicates per group.*

Taken together, our lipidomics data and further biochemical studies performed by Vaishnavi suggest that the enzymes MSMEG 5284 and MSMEG 5285 are active serine hydrolases in Mycobacterium Smegmatis that potentially play a role in the conversion of extremely long-chain PI species into PIP species. (Manuscript under preparation)

Detection of zinc chelating metallophores (Kupyaphores) and their degradation products in Mycobacterium Tuberculosis to assign functions to uncharacterized enzymes (With Rashmi Bhosale, Rajesh Gokhale - NII, Delhi)

Kupyaphores are Mycobacterium tuberculosis (Mtb) metallophores that specifically chelate zinc to support bacterial survival and pathogenesis[171]. They are essential for infection, characterized by their increased levels in early infectious stages followed by their rapid decline, despite increasing bacterial loads, indicating tightly regulated mechanisms of production, consumption, and degradation[171]. Hence, Rashmi aimed to identify enzymes capable of degrading kupyaphores by converting them into other products. We modified our method for two applications relevant to the project – First, we developed a 15 min untargeted lipidomics method with parameters discussed in **Fig 4.2** and **Table 3** for in-vitro substrate hydrolysis assays with different chemically synthesized kupyaphore intermediates and purified candidate enzymes. Secondly, we used a standard 60 minute positive ionization mode untargeted method for detecting these kupyaphore intermediates in biofilms formed by *Mycobacterium Tuberculosis* strains lacking these enzymes. Using a combination of these experiments, we first identified the enzyme Isonitrile Hydratase (Inh), also known as Rv0052, as an enzyme capable of degrading kupyaphores into monoformamide and diformamide species **(Fig 4.7 A)**. Subsequently, we identified N-substituted formamide deformylase (Nfd), also known as Rv0552, as an enzyme that converts diformamide kupyaphores into diamine kupyaphores **(Fig 4.7 B)**. Finally, the enzyme amine oxidase (AO), also known as Rv3170, was found to convert diamine kupyaphores into diketone kupyaphores and we saw that a reaction mixture with all three enzymes (Inh, Nfd, Ao) could convert kupyaphores into mono and di-formamides, diamines and diketones, suggesting that the pathways feed into each other **(Fig 4.7 C)**.

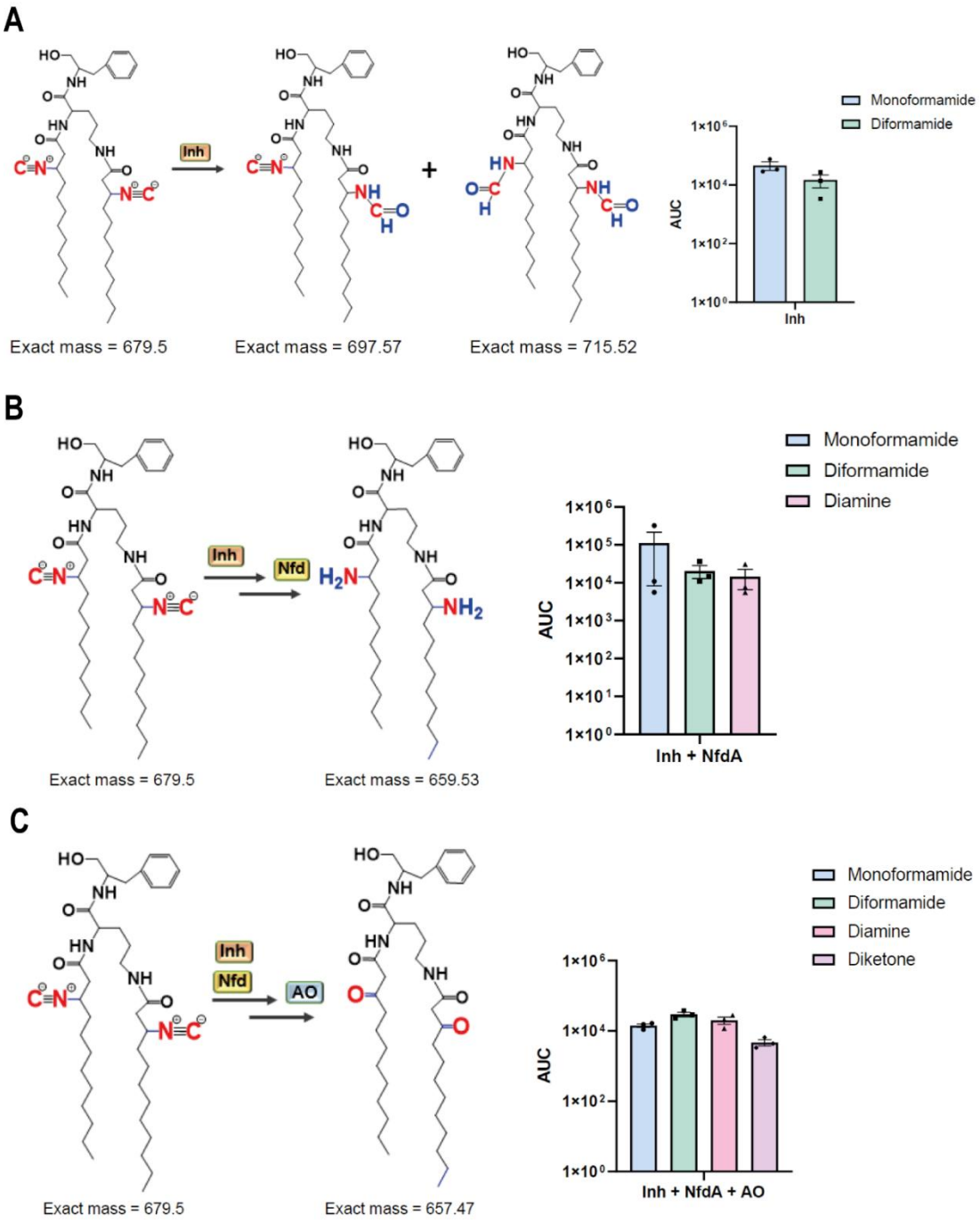

Fig 4.7: Enzymes responsible for kupyaphore degradation. ***(A)*** *Isonitrile Hydratase (Inh) converts kupyaphores into monoformamides and diformamides.* ***(B)*** *Subsequent to (A), N-substituted formamide deformylase (Nfd) catalyzes the production of diamine kupyaphores.* ***(C)*** *After (B), amine oxidase (AO) produces diketone kupyaphores as the final degradation products. The bar data represents the mean ± standard deviation from three biological replicates per group.*

We could also detect different chain lengths of kupyaphores along with all the degradation products in biofilms from cultures expressing these three enzymes **(Fig 4.8 A,**

Table 8). Finally, in a murine lung infection model of Mtb, we could again detect and quantify these degradation products, suggesting that the degradation pathway is active *in-vivo* too **(Fig 4.8 B)**.

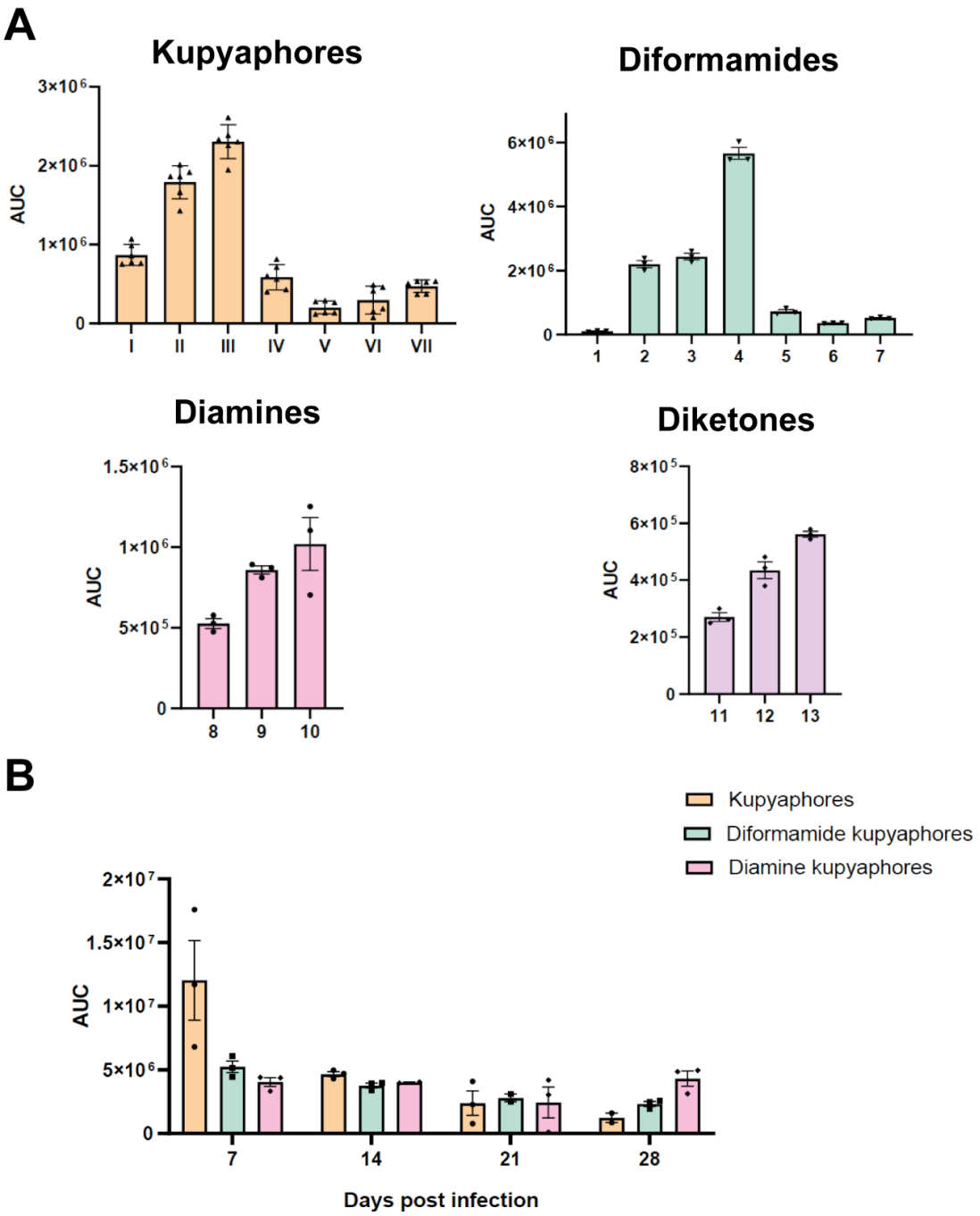

Fig 4.8: Relative intensity plots of kupyaphores, diformamides, diamines and diketone kupyaphores (A) *with different chain lengths* ***(Table 8)*** *as detected on LC-MS from WT Mtb extract, cultured in chelated Sauton's media.* ***(B)*** *averaged in a mouse lung infection model of Mtb. The bar data represents the mean ± standard deviation from three biological replicates per group.*

Table 8: List of all detected kupyaphores and degradation products in WT Mtb biofilm cultures

Category	Chain length	ID
Kupyaphores	**25**	**I**
	27	**II**
	28	**III**
	30	**IV**
	35	**V**
	36	**VI**
	37	**VII**
Diformamides	**27**	**1**
	31	**2**
	33	**3**
	34	**4**
	35	**5**
	36	**6**
	37	**7**
Diamines	**30**	**8**
	37	**9**
	40	**10**
Diketones	**32**	**11**
	35	**12**
	36	**13**

The manuscript containing multiple figures from our contributions is currently under review at ***ACS Chemical Biology***

"Bhosale, Rashmi, **Arnab Chakraborty**, Tsung-Yun Wong, Dattatraya P. Masal, Rahul Choudhury, Sonali S. Srivastava, D. Srinivasa Redd4, Courtney C. Aldrich, Siddhesh S. Kamat, Debasisa Mohanty, Rajesh S. Gokhale " Enzymatic pathway for kupyaphore degradation in Mycobacterium tuberculosis: mechanism of metal homeostasis and turnover"

Summary of other published collaborative studies

Following a similar untargeted lipidomics workflow with minor modifications, our methods and analyses have helped identify lipidome changes across different interventions, and our contributions to different studies are summarized briefly in the following subsections.

Relative quantification of lipidome changes upon inhibition of de novo lipogenesis to identify a therapeutic vulnerability in therapy-resistant colorectal cancer (with Nazia Chaudhary - ACTREC, Mumbai)

The development of therapy resistance is a major clinical challenge in patients with colorectal cancer (CRC), which challenges patient survival by leading to a relapse. This therapy resistance and relapse in CRC is known to be associated with the amplification of de novo lipogenesis (DNL) and accompanied by the formation of lipid droplets (LD)[172]. Nazia first identified lipin1 and DGAT2 as a target proteins for this study since they were highly abundant in CRC patients who were non-responders to chemotherapy. To understand their role in DNL and therapy resistance, she developed drug-tolerant persister (DTP) cell models by treating colon cancer cell lines with different therapies, including single-drug DTPs and combination therapy DTPs[172].

We performed untargeted lipidomics on these different cell pellets and specifically found an increase in DAG and TAG levels in cells with combination therapy DTPs compared to single-drug DTPs. Alongside western blotting and immunofluorescence analyses to show that lipin1 and DGAT2 were also significantly upregulated in combination therapy DTPs, the data suggests that these CRC persisters rewire free fatty acids into DAGs and TAGs through the action of the enzymes LPIN1 and DGAT2, respectively.

Our findings are part of Fig 2 in the following publication:

"Jog, Eeshrita, Ashwin Kumar Jainarayanan, Alessandro La Ferlita, **Arnab Chakraborty**, Afiya Dalwai, Showket Yahya, Anusha Shivashankar et al. "Inhibiting de novo lipogenesis identifies a therapeutic vulnerability in therapy-resistant colorectal cancer." ***Redox Biology*** (2024): 103458."

Assigning a lipid homeostasis function to Wag31, a mycobacterium membrane tether protein, by identifying differentially upregulated lipids (with Yogita Kapoor, Vinay Nandicoori - CCMB, Hyderabad)

Wag31 is a cytoskeletal protein in mycobacteria that maintains cell shape and has significant roles in cell elongation and growth. In an effort to further characterize its specific roles, Yogita made conditional mutants of Wag31 and saw changes in cell morphology and a significant presence of intracellular lipid inclusions (ILIs, a term used to differentiate similar bodies from lipid droplets, which are host-acquired) in the cytosol, among other phenotypes[173]. Our lipidomics analysis of these Wag31 depleted mycobacteria showed a significant accumulation of very long-chain containing (>C36) phosphatidylethanolamines (~5-32 fold) and unsaturated diacylglycerols (~3-5 fold)[173]. Besides these changes, we also saw increased levels of different chain lengths (C18-C24) of free fatty acids (~1.7-4 fold) and reduced levels of cardiolipins C70:0 and C70:1 (~3 fold) as compared to controls. In another comparison, Wag31 overexpression resulted in a 2-fold increase in the level of different species of alpha-mycolic acids ranging from C74 to C78.

Using contributions from our lipidomics analysis and multiple other experiments studying the membrane tethering aspects of Wag31, the protein was characterized as a crucial regulator of lipid homeostasis. Our findings are part of Fig 2 in the following publication:

“Kapoor, Yogita, Himani Khurana, **Arnab Chakraborty**, Debatri Dutta, Anshu Priya, Archana Singh, Siddhesh Kamat, Neeraj Dhar, Thomas Pucadyil, and Vinay Nandicoori. "Wag31, a membrane tether, is crucial for lipid homeostasis in mycobacteria." ***eLife*** (2025): 2025-1.”

PUBLICATIONS

Besides the studies described in detail primarily involving work done by me involving the development of newer methods, Siddhesh, Neelay and I have also contributed to other studies using previous methods in the lab by performing relative and absolute quantification of diacylglycerols, triacylglycerols and free fatty acids[118,119,174]. These publications are listed below:

- Shambhavi, Sakshi, Sudipta Mondal, **Arnab Chakraborty**, Nikita Shukla, Bapin Kumar Panda, Santhosh Kumar, Priyadarshan Kinatukara, Biswajit Pal, **Siddhesh S. Kamat**, and Rajan Sankaranarayanan. "Emergence of Dip2-mediated Specific DAG-based PKC Signalling Axis in Eukaryotes." ***eLife*** (2024): 2024-12.
- Talwadekar, Manasi, Subhash Khatri, Chinthapalli Balaji, **Arnab Chakraborty**, Nandini-Pal Basak, **Siddhesh S. Kamat**, and Ullas Kolthur-Seetharam. "Metabolic transitions regulate global protein fatty acylation." ***Journal of Biological Chemistry*** 300, no. 1 (2024).
- Sen, Devashish, Babukrishna Maniyadath, Shreyam Chowdhury, Arshdeep Kaur, Subhash Khatri, **Arnab Chakraborty**, **Neelay Mehendale** et al. "Metabolic regulation of CTCF expression and chromatin association dictates starvation response in mice and flies." ***Iscience*** 26, no. 7 (2023).

References

1. Eyster, K. M. The membrane and lipids as integral participants in signal transduction: lipid signal transduction for the non-lipid biochemist. *Adv Physiol Educ* **31**, 5–16 (2007).
2. Fernandis, A. Z. & Wenk, M. R. Membrane lipids as signaling molecules. *Current Opinion in Lipidology* **18**, 121–128 (2007).
3. Sunshine, H. & Iruela-Arispe, M. L. Membrane lipids and cell signaling. *Current Opinion in Lipidology* **28**, 408 (2017).
4. Ricciotti, E. & FitzGerald, G. A. Prostaglandins and Inflammation. *Arteriosclerosis, Thrombosis, and Vascular Biology* **31**, 986–1000 (2011).
5. Cristino, L., Bisogno, T. & Di Marzo, V. Cannabinoids and the expanded endocannabinoid system in neurological disorders. *Nat Rev Neurol* **16**, 9–29 (2020).
6. Kano, K., Aoki, J. & Hla, T. Lysophospholipid Mediators in Health and Disease. *Annual Review of Pathology: Mechanisms of Disease* **17**, 459–483 (2022).
7. Yanagida, K. & Valentine, W. J. Druggable Lysophospholipid Signaling Pathways. in *Druggable Lipid Signaling Pathways* (ed. Kihara, Y.) 137–176 (Springer International Publishing, Cham, 2020). doi:10.1007/978-3-030-50621-6_7.
8. Gonzalez-Cabrera, P. J., Brown, S., Studer, S. M. & Rosen, H. S1P signaling: new therapies and opportunities. *F1000Prime Rep* **6**, (2014).
9. Contos, J. J., Ishii, I. & Chun, J. Lysophosphatidic acid receptors. *Mol Pharmacol* **58**, 1188–1196 (2000).
10. Chakraborty, A. & Kamat, S. S. Lysophosphatidylserine: A Signaling Lipid with Implications in Human Diseases. *Chem Rev* **124**, 5470–5504 (2024).
11. Shanbhag, K., Mhetre, A., Khandelwal, N. & Kamat, S. S. The Lysophosphatidylserines—An Emerging Class of Signalling Lysophospholipids. *J Membrane Biol* **253**, 381–397 (2020).
12. Omi, J., Kano, K. & Aoki, J. Current Knowledge on the Biology of Lysophosphatidylserine as an Emerging Bioactive Lipid. *Cell Biochem Biophys* (2021) doi:10.1007/s12013-021-00988-9.
13. Silver, M. J., Turner, D. L., Holburn, R. R. & Tocantins, L. M. Anticoagulant Activity of Phosphatidvlserine Free of Lysophosphatidylserine. *Proceedings of the Society for Experimental Biology and Medicine* **100**, 692–695 (1959).

14. Mushett, C. W., Goldsmith, D. P. J. & Kelley, K. L. STUDIES ON LIPIDE ANTICOAGULANTS: I. ASSAYS IN VITRO. *Journal of Biological Chemistry* **211**, 163–168 (1954).
15. Goldsmith, D. P. J. & Mushett, C. W. STUDIES ON LIPIDE ANTICOAGULANTS: II. ISOLATION PROCEDURES. *Journal of Biological Chemistry* **211**, 169–181 (1954).
16. Sud, M. *et al.* LMSD: LIPID MAPS structure database. *Nucleic Acids Res.* **35**, D527-532 (2007).
17. Fahy, E., Cotter, D., Sud, M. & Subramaniam, S. Lipid classification, structures and tools. *Biochim Biophys Acta* **1811**, 637–647 (2011).
18. Mallik, S., Prasad, R., Bhattacharya, A. & Sen, P. Synthesis of Phosphatidylserine and Its Stereoisomers: Their Role in Activation of Blood Coagulation. *ACS Med Chem Lett* **9**, 434–439 (2018).
19. Okudaira, M. *et al.* Separation and quantification of 2-acyl-1-lysophospholipids and 1-acyl-2-lysophospholipids in biological samples by LC-MS/MS. *J Lipid Res* **55**, 2178–2192 (2014).
20. Plueckthun, A. & Dennis, E. A. Acyl and phosphoryl migration in lysophospholipids: importance in phospholipid synthesis and phospholipase specificity. *Biochemistry* **21**, 1743–1750 (1982).
21. Brügger, B. Lipidomics: Analysis of the Lipid Composition of Cells and Subcellular Organelles by Electrospray Ionization Mass Spectrometry. *Annual Review of Biochemistry* **83**, 79–98 (2014).
22. Zamboni, N., Saghatelian, A. & Patti, G. J. Defining the Metabolome: Size, Flux, and Regulation. *Molecular Cell* **58**, 699–706 (2015).
23. Dennis, E. A. Lipidomics In Disease And Drug Discovery. *The FASEB Journal* **30**, 114.3-114.3 (2016).
24. Folch, J., Lees, M. & Stanley, G. H. S. A SIMPLE METHOD FOR THE ISOLATION AND PURIFICATION OF TOTAL LIPIDES FROM ANIMAL TISSUES. *Journal of Biological Chemistry* **226**, 497–509 (1957).
25. Blankman, J. L., Long, J. Z., Trauger, S. A., Siuzdak, G. & Cravatt, B. F. ABHD12 controls brain lysophosphatidylserine pathways that are deregulated in a murine model of the neurodegenerative disease PHARC. *PNAS* **110**, 1500–1505 (2013).
26. Kamat, S. S. *et al.* Immunomodulatory lysophosphatidylserines are regulated by ABHD16A and ABHD12 interplay. *Nat Chem Biol* **11**, 164–171 (2015).

27. Li, H. *et al.* Development and validation of a simple and rapid HILIC-MS/MS method for the quantification of low-abundant lysoglycerophospholipids in human plasma. *Anal Bioanal Chem* **415**, 411–425 (2023).
28. Singh, S. & Kamat, S. S. The loss of enzymatic activity of the PHARC-associated lipase ABHD12 results in increased phagocytosis that causes neuroinflammation. *European Journal of Neuroscience* **54**, 7442–7457 (2021).
29. Khandelwal, N. *et al.* Fatty acid chain length drives lysophosphatidylserine-dependent immunological outputs. *Cell Chemical Biology* **28**, 1169-1179.e6 (2021).
30. Minamihata, T., Takano, K., Nakamura, Y., Seto, R. & Moriyama, M. Increase in Cellular Lysophosphatidylserine Content Exacerbates Inflammatory Responses in LPS-Activated Microglia. *Neurochem Res* **47**, 2602–2616 (2022).
31. Ogasawara, D. *et al.* Selective blockade of the lyso-PS lipase ABHD12 stimulates immune responses in vivo. *Nature Chemical Biology* **14**, 1099–1108 (2018).
32. Singh, S., Joshi, A. & Kamat, S. S. Mapping the Neuroanatomy of ABHD16A, ABHD12, and Lysophosphatidylserines Provides New Insights into the Pathophysiology of the Human Neurological Disorder PHARC. *Biochemistry* **59**, 2299–2311 (2020).
33. Sonoda, H. *et al.* Changes in Lysophospholipid Components in Ulcerative Colitis and Colitis-associated Cancer. *Anticancer Research* **42**, 2461–2468 (2022).
34. Kitamura, C. *et al.* The component changes of lysophospholipid mediators in colorectal cancer. *Tumour Biol* **41**, 1010428319848616 (2019).
35. Otake-Kasamoto, Y. *et al.* Lysophosphatidylserines derived from microbiota in Crohn's disease elicit pathological Th1 response. *Journal of Experimental Medicine* **219**, e20211291 (2022).
36. Kurano, M. *et al.* Modulations of bioactive lipids and their receptors in postmortem Alzheimer's disease brains. *Front. Aging Neurosci.* **14**, (2022).
37. Yaginuma, S., Omi, J., Uwamizu, A. & Aoki, J. Emerging roles of lysophosphatidylserine as an immune modulator. *Immunological Reviews* **317**, 20–29 (2023).
38. Torres, R. M. & Cyster, J. Lipid mediators in the regulation of innate and adaptive immunity. *Immunological Reviews* **317**, 4–7 (2023).
39. Krystel-Whittemore, M., Dileepan, K. N. & Wood, J. G. Mast Cell: A Multi-Functional Master Cell. *Front. Immunol.* **6**, (2016).

40. Chakravarty, N., Goth, A. & Sen, P. Potentiation of Dextran-Induced Histamine Release from Rat Mast Cells by Phosphatidyl Serine. *Acta Physiologica Scandinavica* **88**, 469–480 (1973).

41. Kolster, L. *et al.* Effect of lysophosphatidylserine on immunological histamine release. *Biochimica et Biophysica Acta (BBA) - Molecular Cell Research* **927**, 196–202 (1987).

42. TAMORI-NATORI, Y., HORIGOME, K., INOUE, K. & NOJIMA, S. Metabolism of Lysophosphatidylserine, a Potentiator of Histamine Release in Rat Mast Cells. *The Journal of Biochemistry* **100**, 581–590 (1986).

43. Wynn, T. A., Chawla, A. & Pollard, J. W. Macrophage biology in development, homeostasis and disease. *Nature* **496**, 445–455 (2013).

44. Martin, C. J., Peters, K. N. & Behar, S. M. Macrophages clean up: efferocytosis and microbial control. *Current Opinion in Microbiology* **17**, 17–23 (2014).

45. Korns, D. R., Frasch, S. C., Fernandez-Boyanapalli, R., Henson, P. M. & Bratton, D. L. Modulation of Macrophage Efferocytosis in Inflammation. *Front. Immunol.* **2**, (2011).

46. Frasch, S. C. & Bratton, D. L. Emerging roles for lysophosphatidylserine in resolution of inflammation. *Progress in Lipid Research* **51**, 199–207 (2012).

47. Mayadas, T. N., Cullere, X. & Lowell, C. A. The Multifaceted Functions of Neutrophils. *Annual Review of Pathology: Mechanisms of Disease* **9**, 181–218 (2014).

48. Frasch, S. C. *et al.* NADPH Oxidase-dependent Generation of Lysophosphatidylserine Enhances Clearance of Activated and Dying Neutrophils via G2A*. *Journal of Biological Chemistry* **283**, 33736–33749 (2008).

49. Frasch, S. C. *et al.* Signaling via Macrophage G2A Enhances Efferocytosis of Dying Neutrophils by Augmentation of Rac Activity*. *Journal of Biological Chemistry* **286**, 12108–12122 (2011).

50. Caselli, E. *et al.* Inhibition of DNA synthesis in peripheral blood mononuclear cells treated with phosphatidylserines containing unsaturated acyl chains. *Immunopharmacology* **23**, 205–213 (1992).

51. Caselli, E., Bellini, F., Diego, P., Baricordi, O. R. & Bruni, A. Role of protein kinase C in the phosphatidylserine-induced inhibition of DNA synthesis in blood mononuclear cells. *Immunopharmacology* **24**, 191–201 (1992).

52. Bellini, F. & Bruni, A. Role of a serum phospholipase A1 in the phosphatidylserine-induced T cell inhibition. *FEBS Letters* **316**, 1–4 (1993).

53. Barnes, M. J. *et al.* The lysophosphatidylserine receptor GPR174 constrains regulatory T cell development and function. *Journal of Experimental Medicine* **212**, 1011–1020 (2015).
54. Tan, S. T., Ramesh, T., Toh, X. R. & Nguyen, L. N. Emerging roles of lysophospholipids in health and disease. *Progress in Lipid Research* **80**, 101068 (2020).
55. Lee, S. Y. *et al.* Lysophosphatidylserine stimulates chemotactic migration in U87 human glioma cells. *Biochem Biophys Res Commun* **374**, 147–151 (2008).
56. Park, K. S. *et al.* Lysophosphatidylserine Stimulates L2071 Mouse Fibroblast Chemotactic Migration via a Process Involving Pertussis Toxin-Sensitive Trimeric G-Proteins. *Molecular Pharmacology* **69**, 1066–1073 (2006).
57. Park, K. S., Lee, H. Y., Kim, M.-K., Shin, E. H. & Bae, Y.-S. Lysophosphatidylserine stimulates leukemic cells but not normal leukocytes. *Biochemical and Biophysical Research Communications* **333**, 353–358 (2005).
58. Iida, Y. *et al.* Lysophosphatidylserine stimulates chemotactic migration of colorectal cancer cells through GPR34 and PI3K/Akt pathway. *Anticancer Res* **34**, 5465–5472 (2014).
59. Zuo, B. *et al.* G-protein coupled receptor 34 activates Erk and phosphatidylinositol 3-kinase/Akt pathways and functions as alternative pathway to mediate p185Bcr–Abl-induced transformation and leukemogenesis. *Leukemia & Lymphoma* **56**, 2170–2181 (2015).
60. Yu, W. *et al.* Upregulation of GPR34 expression affects the progression and prognosis of human gastric adenocarcinoma by PI3K/PDK1/AKT pathway. *Histol Histopathol* **28**, 1629–1638 (2013).
61. Rosenbaum, D. M., Rasmussen, S. G. F. & Kobilka, B. K. The structure and function of G-protein-coupled receptors. *Nature* **459**, 356–363 (2009).
62. Ansell, S. M. *et al.* t(X;14)(p11;q32) in MALT lymphoma involving *GPR34* reveals a role for GPR34 in tumor cell growth. *Blood* **120**, 3949–3957 (2012).
63. Moody, S. *et al.* Novel GPR34 and CCR6 mutation and distinct genetic profiles in MALT lymphomas of different sites. *Haematologica* **103**, 1329–1336 (2018).
64. Tan, Y., Wang, H. & Zhang, C. MicroRNA-381 targets G protein-Coupled receptor 34 (GPR34) to regulate the growth, migration and invasion of human cervical cancer cells. *Environmental Toxicology and Pharmacology* **81**, 103514 (2021).
65. Chang, H. W., Inoue, K., Bruni, A., Boarato, E. & Toffano, G. Stereoselective effects of lysophosphatidylserine in rodents. *Br J Pharmacol* **93**, 647–653 (1988).

66. Klip, A., McGraw, T. E. & James, D. E. Thirty sweet years of GLUT4. *Journal of Biological Chemistry* **294**, 11369–11381 (2019).
67. Bryant, N. J., Govers, R. & James, D. E. Regulated transport of the glucose transporter GLUT4. *Nat Rev Mol Cell Biol* **3**, 267–277 (2002).
68. Yea, K. *et al.* Lysophosphatidylserine regulates blood glucose by enhancing glucose transport in myotubes and adipocytes. *Biochemical and Biophysical Research Communications* **378**, 783–788 (2009).
69. Fiskerstrand, T. *et al.* A novel Refsum-like disorder that maps to chromosome 20. *Neurology* **72**, 20–27 (2009).
70. Fiskerstrand, T. *et al.* Mutations in ABHD12 Cause the Neurodegenerative Disease PHARC: An Inborn Error of Endocannabinoid Metabolism. *Am J Hum Genet* **87**, 410–417 (2010).
71. Amberger, J. S., Bocchini, C. A., Schiettecatte, F., Scott, A. F. & Hamosh, A. OMIM.org: Online Mendelian Inheritance in Man (OMIM®), an online catalog of human genes and genetic disorders. *Nucleic Acids Research* **43**, D789–D798 (2015).
72. Harutyunyan, L., Callaerts, P. & Vermeer, S. PHARC syndrome: an overview. *Orphanet Journal of Rare Diseases* **19**, 416 (2024).
73. Lemire, G. *et al.* ABHD16A deficiency causes a complicated form of hereditary spastic paraplegia associated with intellectual disability and cerebral anomalies. *The American Journal of Human Genetics* **108**, 2017–2023 (2021).
74. Yahia, A. *et al.* Pathogenic Variants in ABHD16A Cause a Novel Psychomotor Developmental Disorder With Spastic Paraplegia. *Frontiers in Neurology* **12**, 1455 (2021).
75. Miyake, N. *et al.* A homozygous variant causes a complex hereditary spastic paraplegia with developmental delay, absent speech, and characteristic face. *Clinical Genetics* **101**, 359–363 (2022).
76. Lin, L.-L. *et al.* GPR34 Knockdown Relieves Cognitive Deficits and Suppresses Neuroinflammation in Alzheimer's Disease via the ERK/NF-κB Signal. *Neuroscience* **528**, 129–139 (2023).
77. Yan, C.-Y. *et al.* Candidate gene associations reveal sex-specific Graves' disease risk alleles among Chinese Han populations. *Mol Genet Genomic Med* **8**, e1249 (2020).
78. Szymański, K. *et al.* rs3827440, a nonsynonymous single nucleotide polymorphism within GPR174 gene in X chromosome, is associated with Graves' disease in Polish Caucasian population. *Tissue Antigens* **83**, 41–44 (2014).

79. Zhang, Q.-Y. *et al.* Genetic Study in a Large Cohort Supported Different Pathogenesis of Graves' Disease and Hashimoto's Hypothyroidism. *J Clin Endocrinol Metab* **105**, dgaa170 (2020).
80. Napier, C., Mitchell, A. L., Gan, E., Wilson, I. & Pearce, S. H. S. Role of the X-Linked Gene GPR174 in Autoimmune Addison's Disease. *The Journal of Clinical Endocrinology & Metabolism* **100**, E187–E190 (2015).
81. Wang, X. *et al.* GPR34-mediated sensing of lysophosphatidylserine released by apoptotic neutrophils activates type 3 innate lymphoid cells to mediate tissue repair. *Immunity* **54**, 1123-1136.e8 (2021).
82. Wei, W. *et al.* Gpr174 Knockout Alleviates DSS-Induced Colitis via Regulating the Immune Function of Dendritic Cells. *Front. Immunol.* **13**, (2022).
83. Gurusamy, M. *et al.* G-protein-coupled receptor P2Y10 facilitates chemokine-induced CD4 T cell migration through autocrine/paracrine mediators. *Nat Commun* **12**, 6798 (2021).
84. Jumper, J. *et al.* Highly accurate protein structure prediction with AlphaFold. *Nature* **596**, 583–589 (2021).
85. Bachovchin, D. A. & Cravatt, B. F. The pharmacological landscape and therapeutic potential of serine hydrolases. *Nature Reviews Drug Discovery* **11**, 52–68 (2012).
86. Bachovchin, D. A. *et al.* Superfamily-wide portrait of serine hydrolase inhibition achieved by library-versus-library screening. *PNAS* **107**, 20941–20946 (2010).
87. Daneshi, A. *et al.* Genetic insights into PHARC syndrome: identification of a novel frameshift mutation in ABHD12. *BMC Medical Genomics* **16**, 235 (2023).
88. Long, J. Z. & Cravatt, B. F. The Metabolic Serine Hydrolases and Their Functions in Mammalian Physiology and Disease. *Chem. Rev.* **111**, 6022–6063 (2011).
89. Blankman, J. L., Simon, G. M. & Cravatt, B. F. A comprehensive profile of brain enzymes that hydrolyze the endocannabinoid 2-arachidonoylglycerol. *Chem Biol* **14**, 1347–1356 (2007).
90. Kelkar, D. S. *et al.* A chemical-genetic screen identifies ABHD12 as an oxidized-phosphatidylserine lipase. *Nat Chem Biol* **15**, 169–178 (2019).
91. Joshi, A. *et al.* Biochemical characterization of the PHARC-associated serine hydrolase ABHD12 reveals its preference for very-long-chain lipids. *J. Biol. Chem.* **293**, 16953–16963 (2018).
92. Vaidya, K. *et al.* Identification of sequence determinants for the ABHD14 enzymes. *Proteins* **93**, 255–266 (2025).

93. Altschul, S. F. *et al.* Gapped BLAST and PSI-BLAST: a new generation of protein database search programs. *Nucleic Acids Research* **25**, 3389–3402 (1997).
94. Möller, S., Croning, M. D. & Apweiler, R. Evaluation of methods for the prediction of membrane spanning regions. *Bioinformatics* **17**, 646–653 (2001).
95. Dobson, L., Reményi, I. & Tusnády, G. E. CCTOP: a Consensus Constrained TOPology prediction web server. *Nucleic Acids Research* **43**, W408–W412 (2015).
96. Needleman, S. B. & Wunsch, C. D. A general method applicable to the search for similarities in the amino acid sequence of two proteins. *J Mol Biol* **48**, 443–453 (1970).
97. Sievers, F. *et al.* Fast, scalable generation of high-quality protein multiple sequence alignments using Clustal Omega. *Mol Syst Biol* **7**, 539 (2011).
98. Tamura, K., Stecher, G. & Kumar, S. MEGA11: Molecular Evolutionary Genetics Analysis Version 11. *Mol Biol Evol* **38**, 3022–3027 (2021).
99. Letunic, I. & Bork, P. Interactive Tree Of Life (iTOL): an online tool for phylogenetic tree display and annotation. *Bioinformatics* **23**, 127–128 (2007).
100. Stourac, J. *et al.* Caver Web 1.0: identification of tunnels and channels in proteins and analysis of ligand transport. *Nucleic Acids Res* **47**, W414–W422 (2019).
101. Pravda, L. *et al.* MOLEonline: a web-based tool for analyzing channels, tunnels and pores (2018 update). *Nucleic Acids Res* **46**, W368–W373 (2018).
102. Nm, O. *et al.* Open Babel: An open chemical toolbox. *Journal of cheminformatics* **3**, (2011).
103. Kumar, K., Pazare, M., Ratnaparkhi, G. S. & Kamat, S. S. CG17192 is a Phospholipase That Regulates Signaling Lipids in the Drosophila Gut upon Infection. *Biochemistry* **63**, 3000–3010 (2024).
104. Lord, C. C., Thomas, G. & Brown, J. M. Mammalian alpha beta hydrolase domain (ABHD) proteins: Lipid metabolizing enzymes at the interface of cell signaling and energy metabolism. *Biochim Biophys Acta* **1831**, 792–802 (2013).
105. Nishiguchi, K. M. *et al.* Exome sequencing extends the phenotypic spectrum for ABHD12 mutations: from syndromic to nonsyndromic retinal degeneration. *Ophthalmology* **121**, 1620–1627 (2014).
106. Igelman, A. D. *et al.* Expanding the clinical phenotype in patients with disease causing variants associated with atypical Usher syndrome. *Ophthalmic Genet* **42**, 664–673 (2021).
107. Tingaud-Sequeira, A. *et al.* Functional validation of ABHD12 mutations in the neurodegenerative disease PHARC. *Neurobiol Dis* **98**, 36–51 (2017).

108. Rajendran, A., Vaidya, K., Mendoza, J., Bridwell-Rabb, J. & Kamat, S. S. Functional annotation of ABHD14B, an orphan serine hydrolase enzyme. *Biochemistry* **59**, 183–196 (2019).

109. Padmanabhan, B., Kuzuhara, T., Adachi, N. & Horikoshi, M. The Crystal Structure of CCG1/TAFII250-interacting Factor B (CIB)*. *Journal of Biological Chemistry* **279**, 9615–9624 (2004).

110. Muqit, M. M. K. & Feany, M. B. Modelling neurodegenerative diseases in Drosophila: a fruitful approach? *Nat Rev Neurosci* **3**, 237–243 (2002).

111. McGurk, L., Berson, A. & Bonini, N. M. Drosophila as an In Vivo Model for Human Neurodegenerative Disease. *Genetics* **201**, 377–402 (2015).

112. Kumar, K., Mhetre, A., Ratnaparkhi, G. S. & Kamat, S. S. A Superfamily-wide Activity Atlas of Serine Hydrolases in Drosophila melanogaster. *Biochemistry* **60**, 1312–1324 (2021).

113. Rabbani, B., Mahdieh, N., Hosomichi, K., Nakaoka, H. & Inoue, I. Next-generation sequencing: impact of exome sequencing in characterizing Mendelian disorders. *J Hum Genet* **57**, 621–632 (2012).

114. Galperin, M. Y. & Koonin, E. V. 'Conserved hypothetical' proteins: prioritization of targets for experimental study. *Nucleic Acids Res* **32**, 5452–5463 (2004).

115. Aoki, J., Nagai, Y., Hosono, H., Inoue, K. & Arai, H. Structure and function of phosphatidylserine-specific phospholipase A1. *Biochim Biophys Acta* **1582**, 26–32 (2002).

116. Hosono, H. *et al.* Phosphatidylserine-specific phospholipase A1 stimulates histamine release from rat peritoneal mast cells through production of 2-acyl-1-lysophosphatidylserine. *J Biol Chem* **276**, 29664–29670 (2001).

117. Ichu, T.-A. *et al.* ABHD12 and LPCAT3 interplay regulates a lyso-phosphatidylserine-C20:4 phosphatidylserine lipid network implicated in neurological disease. *Biochemistry* **59**, 1793–1799 (2020).

118. Sen, D. *et al.* Metabolic regulation of CTCF expression and chromatin association dictates starvation response in mice and flies. *iScience* **26**, (2023).

119. Talwadekar, M. *et al.* Metabolic transitions regulate global protein fatty acylation. *Journal of Biological Chemistry* **300**, (2024).

120. Kidd, D., Liu, Y. & Cravatt, B. F. Profiling Serine Hydrolase Activities in Complex Proteomes. *Biochemistry* **40**, 4005–4015 (2001).

121. Liu, Y., Patricelli, M. P. & Cravatt, B. F. Activity-based protein profiling: the serine hydrolases. *Proc Natl Acad Sci U S A* **96**, 14694–14699 (1999).

122. Simon, G. M. & Cravatt, B. F. Activity-based proteomics of enzyme superfamilies: serine hydrolases as a case study. *J Biol Chem* **285**, 11051–11055 (2010).
123. Niphakis, M. J. & Cravatt, B. F. Enzyme inhibitor discovery by activity-based protein profiling. *Annu Rev Biochem* **83**, 341–377 (2014).
124. Wu, C. *et al.* BioGPS: an extensible and customizable portal for querying and organizing gene annotation resources. *Genome Biol* **10**, R130 (2009).
125. Wu, C., Jin, X., Tsueng, G., Afrasiabi, C. & Su, A. I. BioGPS: building your own mash-up of gene annotations and expression profiles. *Nucleic Acids Res* **44**, D313-316 (2016).
126. Deng, L., Viray, K., Singh, S., Cravatt, B. & Stella, N. ABHD6 Controls Amphetamine-Stimulated Hyperlocomotion: Involvement of CB1 Receptors. *Cannabis and Cannabinoid Research* **7**, 188–198 (2022).
127. Manterola, A. *et al.* Deregulation of the endocannabinoid system and therapeutic potential of ABHD6 blockade in the cuprizone model of demyelination. *Biochemical Pharmacology* **157**, 189–201 (2018).
128. Marrs, W. R. *et al.* The serine hydrolase ABHD6 controls the accumulation and efficacy of 2-AG at cannabinoid receptors. *Nat Neurosci* **13**, 951–957 (2010).
129. Cao, J. K., Kaplan, J. & Stella, N. ABHD6: Its Place in Endocannabinoid Signaling and Beyond. *Trends in Pharmacological Sciences* **40**, 267–277 (2019).
130. Thomas, G. *et al.* The Serine Hydrolase ABHD6 Is a Critical Regulator of the Metabolic Syndrome. *Cell Reports* **5**, 508–520 (2013).
131. Hsu, K.-L. *et al.* DAGLβ Inhibition Perturbs a Lipid Network Involved in Macrophage Inflammatory Responses. *Nat Chem Biol* **8**, 999–1007 (2012).
132. Hsu, K.-L. *et al.* Discovery and Optimization of Piperidyl-1,2,3-Triazole Ureas as Potent, Selective, and in Vivo-Active Inhibitors of α/β-Hydrolase Domain Containing 6 (ABHD6). *J. Med. Chem.* **56**, 8270–8279 (2013).
133. Heier, C. *et al.* The phospholipase PNPLA7 functions as a lysophosphatidylcholine hydrolase and interacts with lipid droplets through its catalytic domain. *J Biol Chem* **292**, 19087–19098 (2017).
134. Harada, S. *et al.* The Lysophospholipase PNPLA7 Controls Hepatic Choline and Methionine Metabolism. *Biomolecules* **13**, 471 (2023).
135. Hirabayashi, T. *et al.* Hepatic phosphatidylcholine catabolism driven by PNPLA7 and PNPLA8 supplies endogenous choline to replenish the methionine cycle with methyl groups. *Cell Reports* **42**, 111940 (2023).

136. Abe, A., Hinkovska-Galcheva, V., Bouchev, P., Bouley, R. & Shayman, J. A. The role of lysosomal phospholipase A2 in the catabolism of bis(monoacylglycerol)phosphate and association with phospholipidosis. *Journal of Lipid Research* **65**, 100574 (2024).

137. Taniyama, Y. *et al.* Loss of lysophospholipase 3 increases atherosclerosis in apolipoprotein E-deficient mice. *Biochemical and Biophysical Research Communications* **330**, 104–110 (2005).

138. Nyame, K. *et al.* PLA2G15 is a Lysosomal BMP Hydrolase with Ester Position Specificity and its Targeting Ameliorates Lysosomal Disease. 2024.06.07.597919 Preprint at https://doi.org/10.1101/2024.06.07.597919 (2024).

139. Wang, A., Deems, R. A. & Dennis, E. A. Cloning, Expression, and Catalytic Mechanism of Murine Lysophospholipase I*. *Journal of Biological Chemistry* **272**, 12723–12729 (1997).

140. Toyoda, T., Sugimoto, H. & Yamashita, S. Sequence, expression in Escherichia coli, and characterization of lysophospholipase II. *Biochim Biophys Acta* **1437**, 182–193 (1999).

141. Manna, J. D. *et al.* Identification of the Major Prostaglandin Glycerol Ester Hydrolase in Human Cancer Cells *. *Journal of Biological Chemistry* **289**, 33741–33753 (2014).

142. Won, S. J. *et al.* Molecular Mechanism for Isoform-Selective Inhibition of Acyl Protein Thioesterases 1 and 2 (APT1 and APT2). *ACS Chem. Biol.* **11**, 3374–3382 (2016).

143. Won, S. J., Cheung See Kit, M. & Martin, B. R. Protein depalmitoylases. *Critical Reviews in Biochemistry and Molecular Biology* **53**, 83–98 (2018).

144. Adibekian, A. *et al.* Confirming Target Engagement for Reversible Inhibitors in Vivo by Kinetically Tuned Activity-Based Probes. *J. Am. Chem. Soc.* **134**, 10345–10348 (2012).

145. Won, S. J. & Martin, B. R. Temporal Profiling Establishes a Dynamic S-Palmitoylation Cycle. *ACS Chem. Biol.* **13**, 1560–1568 (2018).

146. Schlager, S. *et al.* Lysosomal lipid hydrolysis provides substrates for lipid mediator synthesis in murine macrophages. *Oncotarget* **8**, 40037–40051 (2017).

147. Bradić, I. *et al.* Off-target effects of the lysosomal acid lipase inhibitors Lalistat-1 and Lalistat-2 on neutral lipid hydrolases. *Mol Metab* **61**, 101510 (2022).

148. Cognetta, A. B. *et al.* Selective N-Hydroxyhydantoin Carbamate Inhibitors of Mammalian Serine Hydrolases. *Chem Biol* **22**, 928–937 (2015).

149. Navia-Paldanius, D., Savinainen, J. R. & Laitinen, J. T. Biochemical and pharmacological characterization of human α/β-hydrolase domain containing 6 (ABHD6) and 12 (ABHD12). *J Lipid Res* **53**, 2413–2424 (2012).

150. Grabner, G. F. *et al.* Metabolic disease and ABHD6 alter the circulating bis(monoacylglycerol)phosphate profile in mice and humans. *J Lipid Res* **60**, 1020–1031 (2019).
151. Rong, X. *et al.* Lpcat3-dependent production of arachidonoyl phospholipids is a key determinant of triglyceride secretion. *eLife* **4**, e06557 (2015).
152. Hashidate-Yoshida, T. *et al.* Fatty acid remodeling by LPCAT3 enriches arachidonate in phospholipid membranes and regulates triglyceride transport. *Elife* **4**, e06328 (2015).
153. Lagrost, L. & Masson, D. The expanding role of lyso-phosphatidylcholine acyltransferase-3 (LPCAT3), a phospholipid remodeling enzyme, in health and disease. *Curr Opin Lipidol* **33**, 193–198 (2022).
154. Shao, G. *et al.* Research progress in the role and mechanism of LPCAT3 in metabolic related diseases and cancer. *J Cancer* **13**, 2430–2439 (2022).
155. Chakraborty, A. *et al.* Identification of ABHD6 as a lysophosphatidylserine lipase in the mammalian liver and kidneys. *Journal of Biological Chemistry* **301**, 108157 (2025).
156. van Meer, G., Voelker, D. R. & Feigenson, G. W. Membrane lipids: where they are and how they behave. *Nature Reviews Molecular Cell Biology* **9**, 112–124 (2008).
157. Lu, W. *et al.* Metabolite Measurement: Pitfalls to Avoid and Practices to Follow. *Annu. Rev. Biochem.* **86**, 277–304 (2017).
158. Zarini, S., Barkley, R. M., Gijón, M. A. & Murphy, R. C. Overview of Lipid Mass Spectrometry and Lipidomics. in *High-Throughput Metabolomics: Methods and Protocols* (ed. D'Alessandro, A.) 81–105 (Springer, New York, NY, 2019). doi:10.1007/978-1-4939-9236-2_6.
159. Han, X. *Lipidomics: Comprehensive Mass Spectrometry of Lipids*. (John Wiley & Sons, Inc, Hoboken, NJ, USA, 2016). doi:10.1002/9781119085263.
160. Buré, C., Ayciriex, S., Testet, E. & Schmitter, J.-M. A single run LC-MS/MS method for phospholipidomics. *Anal Bioanal Chem* **405**, 203–213 (2013).
161. Gross, R. W. The evolution of lipidomics through space and time. *Biochim Biophys Acta Mol Cell Biol Lipids* **1862**, 731–739 (2017).
162. Klose, C., Surma, M. A. & Simons, K. Organellar lipidomics--background and perspectives. *Curr. Opin. Cell Biol.* **25**, 406–413 (2013).
163. Jarc, E. & Petan, T. A twist of FATe: Lipid droplets and inflammatory lipid mediators. *Biochimie* **169**, 69–87 (2020).

164. Zhao, Y.-Y., Cheng, X. & Lin, R.-C. Chapter One - Lipidomics Applications for Discovering Biomarkers of Diseases in Clinical Chemistry. in *International Review of Cell and Molecular Biology* (ed. Jeon, K. W.) vol. 313 1–26 (Academic Press, 2014).

165. Barber, M., Bordoli, R. S., Sedgwick, R. D. & Tyler, A. N. Fast atom bombardment of solids (F.A.B.): a new ion source for mass spectrometry. *J. Chem. Soc., Chem. Commun.* 325–327 (1981) doi:10.1039/C39810000325.

166. Fenn, J. B., Mann, M., Meng, C. K., Wong, S. F. & Whitehouse, C. M. Electrospray ionization for mass spectrometry of large biomolecules. *Science* **246**, 64–71 (1989).

167. Conroy, M. J. *et al.* LIPID MAPS: update to databases and tools for the lipidomics community. *Nucleic Acids Research* **52**, D1677–D1682 (2024).

168. Tautenhahn, R. *et al.* An accelerated workflow for untargeted metabolomics using the METLIN database. *Nat. Biotechnol.* **30**, 826–828 (2012).

169. Gowda, H. *et al.* Interactive XCMS Online: Simplifying Advanced Metabolomic Data Processing and Subsequent Statistical Analyses. *Anal. Chem.* **86**, 6931–6939 (2014).

170. Layre, E. *et al.* A comparative lipidomics platform for chemotaxonomic analysis of Mycobacterium tuberculosis. *Chem Biol* **18**, 1537–1549 (2011).

171. Mehdiratta, K. *et al.* Kupyaphores are zinc homeostatic metallophores required for colonization of *Mycobacterium tuberculosis*. *Proceedings of the National Academy of Sciences* **119**, e2110293119 (2022).

172. Jog, E. *et al.* Inhibiting de novo lipogenesis identifies a therapeutic vulnerability in therapy-resistant colorectal cancer. *Redox Biology* **79**, 103458 (2025).

173. Kapoor, Y. *et al.* Wag31, a membrane tether, is crucial for lipid homeostasis in mycobacteria. *eLife* **14**, (2025).

174. Shambhavi, S. *et al.* Emergence of Dip2-mediated Specific DAG-based PKC Signalling Axis in Eukaryotes. *eLife* **14**, (2025).

Rights for reusing data from publications:

1. *Chemical Reviews (Chapter 1)*

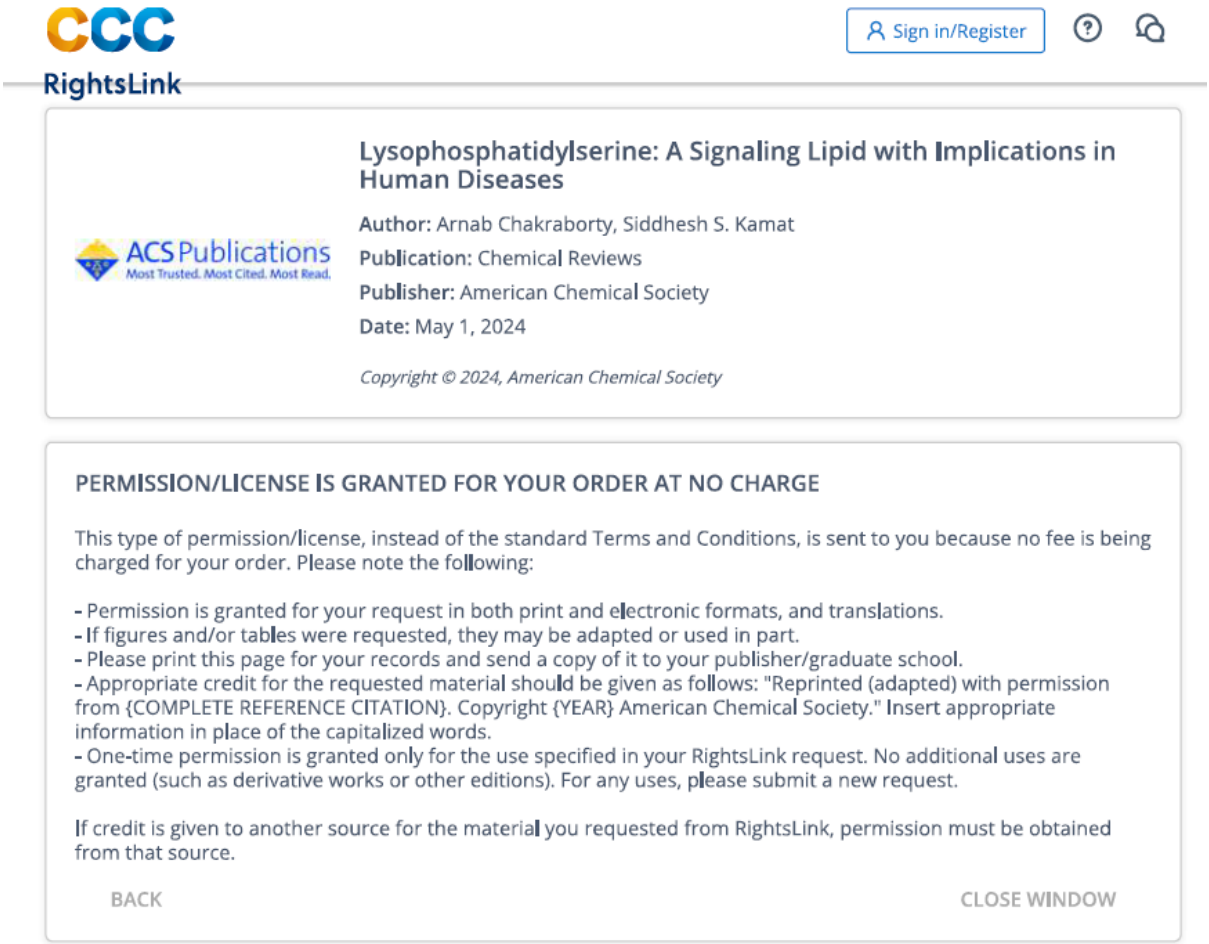

2. *Journal of Biological Chemistry (Chapter 3)*

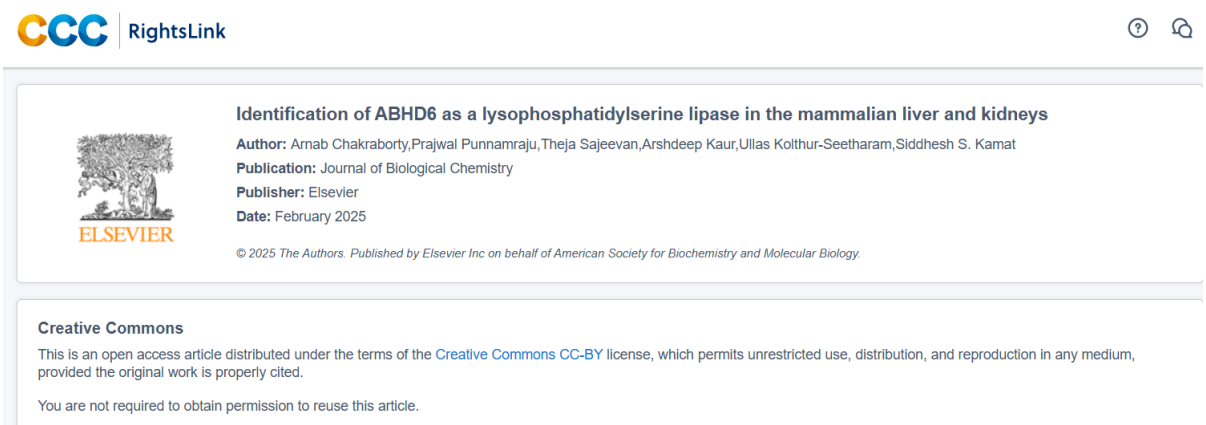

VITA

Name	Arnab Chakraborty
Address	Department of Biology
	IISER Pune, Dr. Homi Bhabha road
	Ward no. 8, NCL Colony
	Pune, Maharashtra 411008
Email	arnab.neil@gmail.com
	chakraborty.arnab@students.iiserpune.ac.in
Education	B.E. (Hons) Chemical Engineering (2013-2018) – BITS Pilani
	M.Sc. (Hons) Biological Sciences (2013-2018) – BITS Pilani
	Ph.D. Biology (2019-2025) – IISER Pune
Personal website	https://arnabneil.wixsite.com/website